

國立臺灣大學醫學院暨工學院醫學工程學研究所



博士論文

Graduate Institute of Biomedical Engineering
College of Medicine and College of Engineering
National Taiwan University
Doctoral Dissertation

奈米碳管結合低電壓電穿孔之藥物釋放平台於癌症治療應用

Combining the Single-Walled Carbon Nanotubes with
Low Voltage Electrical Stimulation for Effective Cancer
Therapy

李佩芝

Pei-Chi Lee

指導教授：謝銘鈞 博士

Advisor: Ming-Jium Shieh, Ph.D.

中華民國 105 年 6 月

June 2016



國立臺灣大學博士學位論文
口試委員會審定書

奈米碳管結合低電壓電穿孔之藥物釋放平台於癌症治療應用
Combining the Single-Walled Carbon Nanotubes with Low Voltage Electrical Stimulation for Effective Cancer Therapy

本論文係李佩芝君 (D98548001) 在國立臺灣大學醫學工程學研究所所完成之碩(博)士學位論文，於民國 105 年 5 月 13 日承下列考試委員審查通過及口試及格，特此證明

口試委員：

謝銘鈞

(簽名)

(指導教授)

林孝燦

林仁博

陳文翹

賴秉利

陳三元

楊禎岫

程次文

陳中明

(簽名)

系主任、所長

誌謝

感謝指導教授謝銘鈞醫師，在研究生涯中給予充分的自由與資源，在適當的時機給予支持與鼓勵，謝謝您。

感謝口試委員林峯輝老師、林文澧老師、陳三元老師、楊禎明老師、鍾次文老師、陳文翔醫師、以及賴秉杉老師，在口試時給予珍貴的建議，使研究最後能趨近於完善。

謝謝郁智與心怡在行政與實驗室大小事物上，都給予充分的幫助，無條件的犧牲與付出，謝謝你們。

最後，謝謝家人的默默支持與陪伴，沒有這分安定的力量，我是無法完成的。

李佩芝 2016, 7

中文摘要



本研究將奈米碳管視為奈米電極，分散於細胞外液中，在施予電壓的情況下，透過奈米碳管良好的導電性以及場致發射能力，可於碳管尖端處放大電場效應，降低電穿孔(electroporation)所需之電壓，有效刺激細胞膜改變其通透性 (electro-permeability)，令小分子與奈米粒子皆能達到高效能傳輸，大量累積於癌細胞與腫瘤。在細胞實驗中，我們證明了奈米碳管結合低電壓能在細胞膜上產生可恢復性 (reversible)之孔洞，克服了傳統電穿孔所需之高電壓對細胞所造成不可恢復性 (irreversible)孔洞的導致細胞死亡之障礙，增加細胞存活率並使小分子能有效的傳遞。在動物實驗中，我們給予老鼠尾靜脈注射奈米碳管電極液後，於腫瘤位置進行低電壓刺激，有效的增加了血管的通透性，使奈米粒子從血管穿透到癌細胞組織中，增強高滲透長滯留效應 (enhanced permeability and retention effect)。於癌症治療中，我們分別使用了光熱治療與化療兩種癌症療法，其結果顯示皆能有效的達到癌細胞毒殺以及腫瘤抑制之效果。綜合上述，我們證明此藥物傳輸平台不僅可用於傳統電脈衝化療(electro-chemotherapy)，結合奈米碳管的光學性質與熱傳導性，可適用於多樣化的癌症治療中。

關鍵字：奈米碳管；場致發射能力；電穿孔；高滲透長滯留效應；癌症治療

Abstract



Effective delivery of biomolecules or functional nanoparticles into target sites has always been the primary objective for cancer therapy. We demonstrated that by combining single-walled carbon nanotubes (SWNTs) with low-voltage (LV) electrical stimulation, biomolecule delivery can be effectively enhanced through reversible electroporation (EP). Clear pore formation in the cell membrane is observed due to LV (50 V) pulse electrical stimulation amplified by SWNTs. The cell morphology remains intact and high cell viability is retained. This modality of SWNT + LV pulses can effectively transfer both small molecules and macromolecules into cells through reversible EP. This drug delivery system we established could combine with various cancer treatments, such as phototherapy and chemotherapy. The results of animal studies also suggest that treatment with LV pulses alone cannot increase vascular permeability in tumors unless after the injection of SWNTs. The nanoparticles can cross the permeable vasculature, which enhances their accumulation in the tumor tissue. Therefore, in cancer treatment, both SWNT + LV pulse treatment followed by the injection of LIPO-DOX® and SWNT/DOX + LV pulse treatment can increase tumor inhibition and delay tumor growth. This novel treatment modality applied in a human cancer xenograft model can provide a safe and effective therapy using various nanomedicines in cancer treatment.

Keywords: cancer therapy; single-walled carbon nanotube; electroporation; tumor;

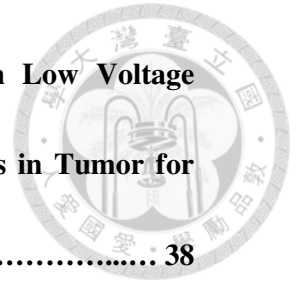
nanomedicine



Contents



中文摘要.....	I
Abstract	II
Contents	IV
List of figures	VI
Chapter 1. Introduction.....	1
Chapter 2. Materials and methods.....	5
Chapter 3. Results and discussions.....	20
Part I. Enhanced cell electro-permeabilisation combined with phototherapy to kill cancer cells by using single-walled carbon nanotube	20
3.1.1 Functionalization and characterization of SWNT-PEG/VNc.....	20
3.1.2 Photodynamic and Photothermal Properties of SWNT-PEG/VNc.....	22
3.1.3 Enhanced cellular uptake by the combination of LV pulses with SWNT	24
3.1.4 SWNT-PEG/VNc mediated Electro-Phototherapy efficiently kills cancer cells...	25
Part II. Effect of the LV stimulation on Cell Membrane Poration Enhanced by the Single-Walled Carbon Nanotubes.....	28
3.2.1 SWNTs combined with LV pulses induced cell electroporation	28
3.2.2 Reversibility of cell electroporation	32
3.2.3. The change of membrane potential in HT-29 cells after EP	34



Part III. Combining the Single-Walled Carbon Nanotubes with Low Voltage Electrical Stimulation to Improve Accumulation of Nanomedicines in Tumor for Effective Cancer Therapy.	38
3.3.1. EPR effect improvement by the increased electrical stimulation through SWNTs.....	38
3.3.2. In vivo studies of ECT.....	41
Chapter 4. Conclusions.....	46
Reference	47
Figures	58

List of figures



Scheme 1. Synthetic scheme for the fabrication of SWNT/PEG-VNc	58
Fig 1. Elemental analysis of SWNT and oxidized SWNT	59
Fig. 2. (A) Difference in fluorescence emission after mixing THA stock solution with raw SWNT or oxidized SWNT. (B) Fluorescent spectra of THA in the presence of raw SWNT and oxidized SWNT	60
Fig. 3. Zeta potential distribution of SWNT-COOH and SWNT-PEG were analyzed by DLS.	61
Fig. 4. ¹ H-NMR spectrum of SWNT-PEG. The arrow indicates the characteristic peak of PEG at approximately 3.5 ppm	62
Fig. 5. (A) VNc suspended in water, DMF and DMSO. (B) SWNT-PEG/VNc suspended in water	63
Fig. 6. TEM image of SWNT-PEG/VNc. The length of SWNT-PEG/VNc deduced from TEM image was approximately 188.64 nm	64
Fig. 7. HRTEM of SWNT-PEG and SWNT-PEG/VNc.....	65
Fig. 8. Representative EDX spectra of SWNT-PEG/VNc	66
Fig. 9. X-ray diffraction analysis of SWNT, SWNT-PEG/VNc and VNc	67
Fig. 10. UV-visible absorbance spectra of VNc (blue), SWNT-PEG/VNc (red), and SWNT-PEG (black)	68

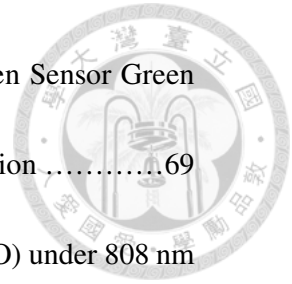


Fig. 11. Singlet oxygen generation of VNc in DMSO by Singlet Oxygen Sensor Green reagent. The sample was exposed to irradiation (808 nm) for $^1\text{O}_2$ generation69

Fig. 12. The thermal curves and of PBS and VNc (1, 2, 5 $\mu\text{g/ml}$ in DMSO) under 808 nm laser irradiation at 1.3 W/cm^2 for 5 min 70

Fig. 13. The thermal curves and of PBS and SWNT-PEG/VNc under 808 nm laser irradiation at 1.3 W/cm^2 for 3 min 71

Fig. 14. PI signals of HT-29 cells detected by flow cytometry. We used pulsing buffer with (PI/SWNT/LV and PI/SWNT/HV group) or without SWNT (PI/HV and PI/LV group) during the pulsation 72

Fig. 15. The data of histogram correspond to (**Fig. 14**) 73

Fig. 16. The cellular uptake of SWNT-PEG/VNc treated to HT-29 cells. (A) No EP group. (B) EP group. HV (1600 V, 10 ms, 3 pulses); LV (50 V, 40 ms, 100 pulses) 74

Fig. 17. Cell viability of HT-29 cells treated with SWNT-PEG and SWNT-PEG/VNc for 24 h 75

Fig. 18. Apoptosis and necrosis assay of the cells detected by fluorescence microscopy after incubation with SWNT-PEG and SWNT-PEG/VNc for 24 h with laser irradiation. (scale bar = $100 \mu\text{m}$) 76

Fig. 19. Cell viability of HT-29 cells after incubation with SWNT-PEG and SWNT-PEG/VNc for 24 h with or without laser irradiation 77

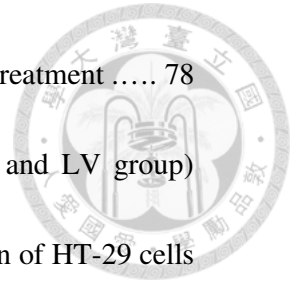


Fig. 20. The comparison of cell viability of HT-29 cells under different treatment 78

Fig. 21. (A) Pulsing buffer with (LV/SWNT group) or without (HV and LV group)

SWNT during the pulsation. The fluorescence of the PI signal expression of HT-29 cells

at 5, 15, and 60 min after transfecting with PI dye under HV (1600 V, 10 ms, 3 pulses)

and LV (50 V, 40 ms, 100 pulses) electro-pulses (scale bar = 100 μ m). (B) The integrated

optical density (IOD) of the PI signal expression from the fluorescence image (A)79

Fig. 22. Fluorescence micrographs captured from movie at 40 min of HV and LV/SWNT

groups after being transfected with the PI dye (Gray scale) (scale bar = 25 μ m) 80

Fig. 23. Concept of electric stimulation enhancement by CNTs. After giving the LV

pulses, the electric stimulation is amplified by CNTs at their tips so that the cell

electroporation could occur, and the delivery efficiency of biomolecules could

be enhanced81

Fig. 24. High magnification of field emission electron micrographs in the near-membrane

region following *in vitro* cellular exposure to no-treatment, LV, and LV combined with

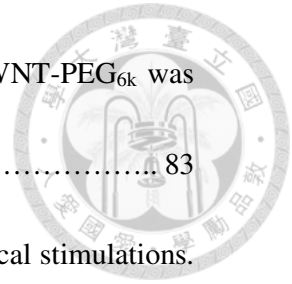
SWNT pulsing buffer. Green arrows demonstrated SWNT-like structures around the pore

in the surface of the cell membrane. The red star indicated the SWNT-like structures

appearing proximal in the pore 82

Fig. 25. (A) TEM image of SWNT-PEG_{6k}. High magnification of the TEM images

showed that the diameter of SWNT-PEG_{6k} was approximately 20 nm. (B) Size



distribution of SWNT-PEG_{6k} was deduced from (B). The length of SWNT-PEG_{6k} was approximately 187.36 nm. 83

Fig. 26. Cell viability after treatment with different intensities of electrical stimulations.

The HT-29 cells were transfected with the PI dye under HV (1600 V, 10 ms, 3 pulses) and LV (50 V, 40 ms, 100 pulses) pulses. At 24 h after EP, the cell viability was assessed by staining with calcein AM. (SWNT pulsing buffer = LV/SWNT group, pulsing buffer without SWNT = HV and LV group). Live cells appeared to be green (calcein AM), cellular uptake with PI appeared to be red, and the merged images appeared to be yellow (scale bar = 50 μ m) 84

Fig. 27. Apoptosis and necrosis assay of the cells detected by flow cytometry after different EP conditions (Control; 50 V, 40 ms, 100 pulses; 100 V, 40 ms, 50 pulses; 50 V, 40 ms, 10 pulses; 700 V, 20 ms, 3 pulses; 1300 V, 20 ms, 3 pulses; 1600 V, 10 ms, 3 pulses) 85

Fig. 28. The data of histogram correspond to (B). The results showed the obvious escalation of necrotic cells when the applied voltage was increased. 86

Fig. 29. Cell viability of HT-29 cells exposed to LV (50 V, 40 ms, 100 pulses) and HV (1600 V, 10 ms, 3 pulses) pulses by using SWNT pulsing buffer and commercial T-buffer[®]..... 87

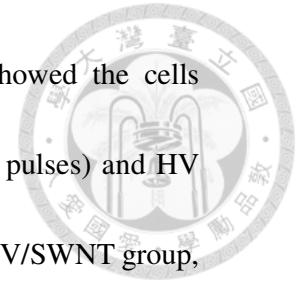


Fig. 30. Investigation of cell morphology. (A) The SEM images showed the cells following fixation immediately after receiving LV (50 V, 40 ms, 100 pulses) and HV (1600 V, 10 ms, 3 pulses) electric stimulation (SWNT pulsing buffer = LV/SWNT group, pulsing buffer without SWNT = HV and LV group)..... 88

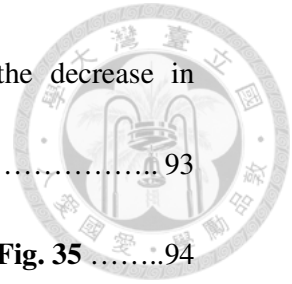
Fig. 31. Dot plot representations of flow cytometry data showed the cell size and granularity after the same EP condition from **Fig. 30**..... 89

Fig. 32. Dot plot data from flow cytometry showing the morphology change of cells after different EP conditions. Compared to the control (no EP) group, the cells treated by HV (1300V * 20 ms * 3 pulses and 1600 V * 10 ms * 3 pulses) stimulation revealed that the cell size (FSC-H) decreased while the cell granularity (SSC-H) increased 90

Fig. 33. The SEM images showed the cells following fixation at 0, 5, 15, and 60 min after receiving HV (1600 V, 10 ms, 3 pulses) electric stimulation 91

Fig. 34. Scanning electron microscope images of the cells. Cell membrane appearances at 1 and 60 min after exposing to LV/SWNT electrical stimulation. Pores were easily identified within the surface of cells at 1 min after EP. However, the pore numbers were decreased at 60 min after EP. Green arrows showed the pores distributed numerously on the cell membrane 92

Fig. 35. Investigation of the transmembrane potential of HT-29 cells by the membrane potential probe. (A) Fluorescence images showed DIOC₆-highlighted changes in the



membrane potential immediately after EP. White arrows showed the decrease in fluorescence intensity (scale bar = 50 μm) 93

Fig. 36. Flow cytometry of HT-29 cells. Conditions were the same as in **Fig. 35** 94

Fig. 37. Membrane potential monitored by JC-1 dye at 5, 30, 60, and 120 min after EP.

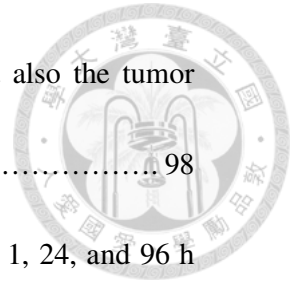
The results showed the same fields of view of cells, before and after electro-pulsation.

The loss of orange J-aggregate fluorescence and cytoplasmic diffusion of green monomer fluorescence occurred after the exposure of electro-stimulation in the HV and LV/SWNT groups (scale bar = 50 μm). 95

Fig. 38. HT-29 cells transfected with minicircle DNA encoding GFP by using transfection reagent or exposing to LV (50 V, 40 ms, 100 pulses) and HV (1600 V, 10 ms, 3 pulses) pulses. Histogram data analysis by flow cytometry showed the fluorescence intensity of GFP expressed in HT-29 cells at 48 h after transfection (SWNT pulsing buffer = LV/SWNT group, pulsing buffer without SWNT = HV and LV group). 96

Fig. 39. PI dye transferred into cells at 3 h after EP. Fluorescence images: LysoTracker (green), PI (red), and Merge (yellow). High magnification showing the different modes of entrance of PI for HV compared with the LV/SWNT group (Scale bar = 100 μm) 97

Fig. 40. EPR effect enhancement following low-intensity electric stimulation enlarged due to CNTs. The accumulation of nanoparticles in the tumor tissue occurred due to not



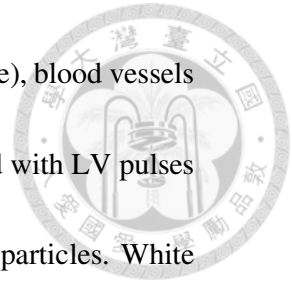
only the original intercellular space between the endothelial cells but also the tumor vascular permeability increased by the electric stimulation effect. 98

Fig. 41. (A) *In vivo* IVIS images of the mice bearing HT-29 tumors at 1, 24, and 96 h after injection with nanoparticles, respectively. Accumulation of nanoparticles in the tumors was different between the different EP conditions. The treatment methods demonstrated are from (A) (HV = 700 V, 20 ms, 3 pulses, LV = 50 V, 40 ms, 10 pulses). (B) *Ex vivo* imaging of nanoparticles in the heart, liver, spleen, lung, kidney, and tumor of mice at 96 h after the same treatments as in (A). 99

Fig. 42. Comparison of the tumor surface (right side tumor) after treating with different EP conditions. The mice with the SWNT post-injection treated with LV pulse stimulation (LV/SWNT) showed no harmful effect of the tumor. However, an obvious ablation was observed on the tumor treated with HV pulses (HV). (The red arrow indicated the tumor treated by HV after 1 h with severe blood stasis). 100

Fig. 43. Different regions of tumors were imaged using fluorescence microscopy for 10 min post-injection. Nanoparticles (red), tumor cells (Hoechst, blue). (Scale bar = 100 μ m). 101

Fig. 44. (A) Typical intravital micrograph of tumors treated without electro-stimulation after injecting nanoparticles. The nanoparticles were completely filled inside the tumor vessels at 10 min after injection. At 60 min, the nanoparticles aggregated along the tumor



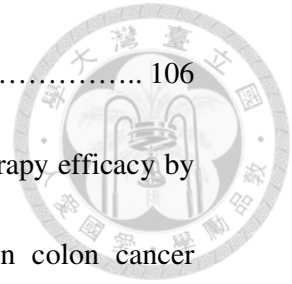
vessels without obvious appearance in the tumor tissue. Tumor cells (blue), blood vessels (green), and nanoparticles (red) (scale bar = 100 μm). (B) Tumor treated with LV pulses after SWNT injection, followed by intravenous administration of nanoparticles. White arrows indicated the leakage of nanoparticles into the tumor interstitial tissue at 60 min after EP. Tumor cells (blue), blood vessels (green), and nanoparticles (red) (scale bar = 100 μm). 102

Fig. 45. Comparison of LV/SWNT with LV groups by enhancement of nanoparticle accumulation. Tumor sections were extracted at 3 h after administering nanoparticle injection. (A) The tumor treated with SWNT post-injection showed an apparent aggregation of nanoparticles in the tumor region. Nanoparticles (red), tumor cell (Hoechst, blue). (Scale bar = 50 μm). (B) The tumor treated without SWNT showed less aggregation of nanoparticles compared to (A). Nanoparticles (red), tumor cell (Hoechst, blue). (Scale bar = 50 μm). 103

Fig. 46. SWNT-PEG was loaded with doxorubicin non-covalently by π - π stacking.... 104

Fig. 47. Particle size and zeta potential analyses of SWNT-COOH, SWNT-PEG, and SWNT/DOX by DLS. SWNT with much more modification showed a larger size. Zeta potentials of the SWNT showed that SWNT-PEG had negative charges. Loading DOX increased the zeta potentials of SWNT-PEG. 105

Fig. 48. UV-visible absorbance spectra of SWNT/DOX (blue), DOX (red), and SWNT-



PEG (black). The drug loading efficiency was 56.4%..... 106

Fig. 49. SWNT combined with LV pulses for improving the tumor therapy efficacy by nanomedicine. Schematic representation of ECT in a HT-29 human colon cancer xenograft model. 107

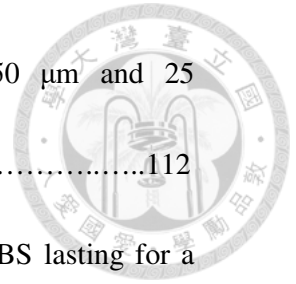
Fig. 50. Body weights of all the groups showed no notable changes. 108

Fig. 51. Tumor volume ratio of HT-29-bearing mice among the various groups. Animals that received a combination of pulses and nanomedicine showed significant tumor growth suppression (SWNT/DOX + EP vs SWNT/DOX, $*p < 0.05$; SWNT + EP + LIPO-DOX vs LIPO-DOX, $*p < 0.05$). 109

Fig. 52. Photographs of dissected tumors. Measurement of tumor weight for each group after 36 days. The effective EP combined with nanomedicine revealed a high reduction in the tumor weights (SWNT/DOX + EP vs SWNT/DOX, $**p < 0.01$; SWNT+ EP + LIPO-DOX vs LIPO-DOX, $*p < 0.05$). 110

Fig. 53. Hematoxylin and eosin (H&E) staining of organs of HT-29 tumor xenograft-bearing mice treated with PBS (control), LIPO-DOX, SWNT/DOX, and SWNT + EP + LIPO-DOX. Scale bar = 50 μ m. 111

Fig. 54. H&E-stained images revealed severe damage in the tumor tissues of SWNT/DOX + EP and SWNT + EP + LIPO-DOX groups. No notable damage was



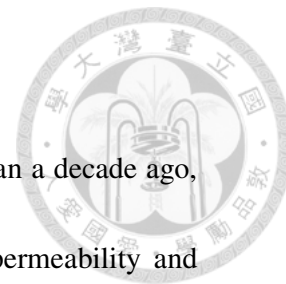
observed in the PBS and SWNT + EP groups. Scale bar = 50 μm and 25 μm112

Fig. 55. Photograph of SWNT-PEG and SWNT/DOX suspended in PBS lasting for a month. The solutions were stored at 4°C. 113

Fig. 56. Images of livers extracted from mice at 1 and 8 weeks after injecting with PBS (control), SWNT, and SWNT/DOX. 114

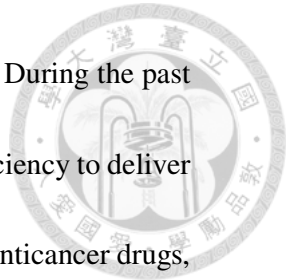
Fig. 57. Hematoxylin and eosin (H&E)-stained images of livers extracted from mice injected at 1, 6, and 8 weeks after injecting with PBS (control), SWNT, and SWNT/DOX. Black arrows showed the aggregation of SWNT/DOX. Scale bar = 50 μm115

Chapter 1. Introduction



Nanoparticles were introduced to biomedical engineering more than a decade ago, particularly for tumor drug delivery [1–4]. Owing to the enhanced permeability and retention (EPR) effect, nanovectors could carry the antitumor reagent to the blood vessels in the tumor and possibly leak into the tumor tissue through the intercellular space between the endothelial cells [3–5]. Although the antitumor drug could reach the target region because of the accumulation of nanoparticles in the tumor, the concentration of the drug in the tumor tissue remains poor because of the size of nanoparticles and their circulation time [6]. In this study, we propose an improvement in the EPR effect by electrical stimulation.

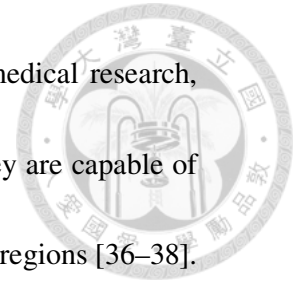
Electroporation (EP) is an efficient physical method of transporting biomolecules or nanoparticles into the cells because of its local electric field at the target tissue [7–9]. Application of a strong electrical stimulation results in an increased transmembrane potential that could in turn result in the formation of pores in the cell membrane. These reversible pores could last for a specific time, during which the cells could be repaired [10], and the biomolecules could diffuse or drift by the strong electrophoretic force into the target region [11,12]. Due to its effective transfection ability in the treatment of various types of tumors, this method is commonly used for cancer therapies including gene therapy and targeted electrochemotherapy (ECT) [13–22].



Clinical trials using ECT have been approved since the 1990s [23]. During the past few decades, this technology was greatly improved owing to its high efficiency to deliver chemical therapeutics or small molecules into the tumors. Among these anticancer drugs, bleomycin, cisplatin, and doxorubicin are promising drugs that can be applied in combination with EP [24]. These anticancer agents can be administered by intravenous (IV) or intratumoral injections and usually have a dosage limitation because of the high biotoxicity. Therefore, it is very important to note the adverse effects caused by these drugs, including pulmonary fibrosis, nephrotoxicity, and neurotoxicity [25,26]. Using EP could effectively lower the dosage and decrease the side effects. Moreover, the incorporation of a nanovector could overcome the limitation of the anticancer agent's poor solubility in aqueous solutions. However, effective EP usually requires high voltages (HVs), which could result in irreversible EP and tissue ablation [27,28]. Here, we report the application of a single-walled carbon nanotube (SWNT) pulsing buffer, which can be combined with low external static electric fields. Using this method, the delivery of nanoparticles could be effectively enhanced by reversible EP. Moreover, the conventional ECT limitation could be overcome.

Considering their unique physical properties, carbon nanotubes (CNTs) have various applications in biomedical nanotechnology including photothermal therapy, near infrared imaging, and photoacoustic imaging [29–35]. However, there remains few applications

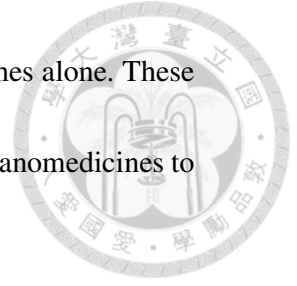
for the field emission capability of CNTs that can be applied in biomedical research, particularly in tumor models. Due to the high aspect ratio of CNTs, they are capable of enhancing the electric field at their tips and creating localized high-field regions [36–38].



This well-known phenomenon has been broadly used in field emission applications in which CNTs act as an electron field emitter [39]. Moreover, in vitro electropermeabilization studies, which are based on CNTs, have revealed that they could amplify the external electric field, thereby inducing pore formation in the cell membrane [40–43]. When the cells were exposed to electric field inside the microfluid chip embedded with CNTs, it led to leakage of the intracellular components, and a low voltage (LV) was sufficient for the electrical stimulation [42]. Wang et al demonstrated that the MWNT-enhanced EP effect via significantly lower electric fields had the potential for tumor cell ablation in vitro [43].

In the present study, we employed SWNTs as nanoelectrodes dispersed in the pulsing buffer around the cellular environment during electro-stimulation in order to lower the EP voltages and reduce cell mortality. Using an animal model, we also demonstrated that this method enhanced the EPR effect, thereby improving the delivery of nanoparticles that permeate from the blood vessel to the tumor tissue. Moreover, we presented evidence that SWNTs and liposomal nanovector with doxorubicin (SWNT/DOX and LIPO-DOX[®]) can be used as nanomedicines with SWNT + EP, which

showed improvement in tumor inhibition as compared with nanomedicines alone. These results suggest that the new modality can be applied to various types of nanomedicines to improve antitumor therapy efficacy.



Chapter 2. Materials and methods



Part I

Oxidative Shortening of SWNT

Raw SWNT was purchased from Golden Innovation Business Co., Ltd (Taipei, Taiwan). SWNT was oxidized by exposure to a strong acid solution (H_2SO_4 : $\text{HNO}_3 = 3:1$) for 24 h. After purification, oxSWNT was refluxed in 4 M HNO_3 at 80°C for 48 h to shorten the length. After washing, the resultant suspension was then diluted with 250 mL of water, and the oxSWNT was collected on a 100-nm pore membrane filter (Millipore) and washed with deionized water. The obtained oxSWNT was further resuspended in water and centrifuged at $4000 \times g$ for 30 min to remove the residuals. The collected oxSWNT was lyophilized to dryness at room temperature.

oxSWNT-PEG

The oxSWNT was dissolved in phosphate-buffered saline (PBS) ($\text{pH} = 7.2$) and sonicated for 30 min. 1-Ethyl-3-(3-dimethylaminopropyl) carbodiimide hydrochloride (Sigma-Aldrich) and sulfo-NHS (N-hydroxysulfosuccinimide) (Sigma-Aldrich) were added to the SWNT solution and stirred at room temperature for 1 h. This was followed by treatment with poly (ethylene glycol) bis (3-aminopropyl) terminated (MW = 6000) (Sigma-Aldrich) for 72 h with stirring at room temperature. Unbonded excess materials

were removed by filter tubes (100 kDa AmiconYM-50, Millipore), centrifuged at 4000 rpm for 30 min, and washed thoroughly with water.

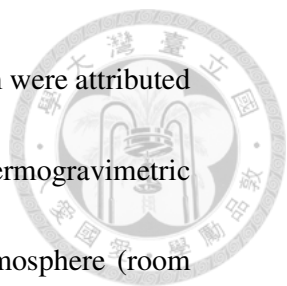


oxSWNT-PEG/VNc

oxSWNT-PEG (10mg) was dissolved in DMF and sonicated for 1 h. The VNc was added and the resulting blackish green solution was further sonicated for 30 min. This was followed by room temperature stirring for 48 h. The solid was washed with ethanol with repeated centrifugation until the solution was free of any green color. The resulting oxSWNT-PEG/VNc was freeze-dried.

Characterization.

The O amount of oxSWNT was evaluated by Element ANALYZER (Thermo Flash 2000). Size distribution was deduced by TEM (Hitachi H-7650) images. High-magnification images of SWNT were obtained from FEG-TEM (Philips Tecnai F30 Field Emission Gun Transmission Microscope). The difference of zeta potential between oxSWNT and SWNT-PEG was measured by Zetasizer (Malvern-zetasizer 3000hs, Malvern, UK). To identify the phase structure of the SWNT-PEG/VNc, the dry sample powder was observed by an X-ray powder diffraction instrument (PANalytical; X' Pert PRO) with CuK α radiation (40 mV, 40kV). Scanning angle was observed from 15° to 70° (step size = 0.02°). The covalent interactions between PEG and SWNT were evaluated by ¹H-NMR spectroscopy. The SWNT-PEG was thoroughly suspended in D₂O. The



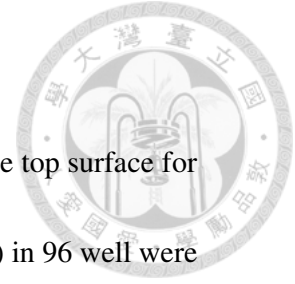
characteristic peak of 5 ppm was the D₂O solvent peak and 3.4 – 3.6 ppm were attributed to the PEG. Thermal decomposition temperature was measured by thermogravimetric analysis (TGA) (TA Instrument 5100-Dynamic Q500) in air or N₂ atmosphere (room temperature to 800°C, 10°C/min). For the diffraction pattern analysis, SWNT-PEG/VNc was observed by HRTEM/EDS (Philips/FEI Tecnai 20 G2 S-Twin Transmission Electron Microscope including EDX Spectroscopy, CCD Camera with Diffpack program).

Spectrochemical titration

An ethanolic solution of THA was added to small amount (2 mg) of SWNT, and the mixture is allowed to stir at room temperature for 1 h [63]. After centrifugation SWNT have been removed and the solution filtered on a 0.45 µm pore filter. The absorbance intensity (590 nm) was determined by a micro-plate reader (Gemini EM; Molecular Devices, Germany).

Singlet oxygen production of VNc

To measure the production of ¹O₂ by VNc, the sensing probe singlet oxygen sensor green (Molecular Probes Inc., Leiden, The Netherlands) was used. In brief, singlet oxygen sensor green and VNc (5 µg/ml) were dissolved in DMSO in 96 well. The corresponding well were treated with irradiation (808 nm, 340 mW) for 30, 60, 90, 120 s. The fluorescence intensity was determined by a micro-plate reader (Gemini EM; Molecular Devices, Germany) excitation/emission of 488/524 nm.



Photothermal Effects.

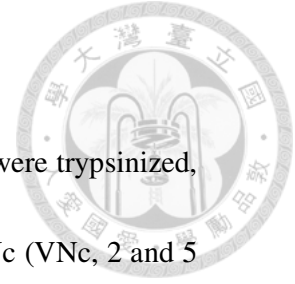
SWNT-PEG/VNc dispersion (PBS) in 96 well were irradiated at the top surface for 3 min with 808 nm (power, 1.3 W) diode laser. VNc dispersion (DMSO) in 96 well were irradiated at the top surface for 5 min with 808 nm (power, 1.3 W) diode laser. Temperature was measured by a thermocouple thermometer.

Cell culture

HT-29 cells (human colon adenocarcinoma cell lines) were obtained from the American Type Culture Collection (ATCC). Cells were routinely cultured in flasks containing Dulbecco's Modified Eagle's medium (DMEM, Invitrogen) supplemented with 10% fetal bovine serum (FBS, Invitrogen), 100 U/ml penicillin, and 100 µg/ml streptomycin (Invitrogen). Cells were incubated at 37°C in a humidified atmosphere with 5% CO₂.

Propidium iodide dye delivery

For cell permeabilization in 100 µl of pulsing buffer, HT-29 cells were trypsinized, centrifuged for 5 min at 1500 rpm, and resuspended in buffer T[®] or SWNT buffer (10⁶ cells/ml) mixed with propidium iodide (PI, 0.5 µg/ml). After EP, the cells were seeded into 24-well plates. Cells with pore formation were identified by the cellular uptake of the PI dye with flow cytometry. The EP parameters were LV (100 pulses at 50 V, pulse duration = 40 ms) and HV (3 pulses at 1600 V, pulse duration = 10 ms).



Cellular uptake of SWNT-PEG/VNc

For cell permeabilization in 100 μ l of pulsing buffer, HT-29 cells were trypsinized, centrifuged for 5 min at 1500 rpm, and resuspended in SWNT-PEG/VNc (VNc, 2 and 5 μ g/ml). After EP, the cells were seeded into 24-well plates. The cellular uptake of the SWNT-PEG/VNc was evaluated with flow cytometry. The EP parameters were LV (100 pulses at 50 V, pulse duration = 40 ms) and HV (3 pulses at 1600 V, pulse duration = 10 ms).

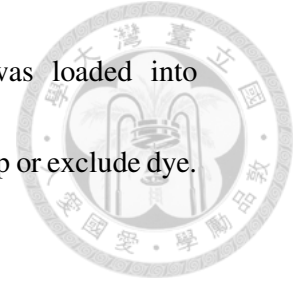
MTT assay

HT-29 cells were first seeded onto 96-well plates at a density of 8000 cells per well and cultured. After 24 h, cells were incubated in media containing with VNc (0.1- 50 μ g/ml) for 24 h. Cell viability was determined using an MTT assay and a scanning multi-well ELISA reader (Microplate Readers Sunrise, TECAN Group ltd, Switzerland). The fraction of live cells was calculated by dividing the mean optical density obtained from treated cells by the mean optical density from untreated control cells.

Trypan blue assay (Dye exclusion assay)

HT-29 cells were seeded onto 24-well plates at a density of 5×10^4 cells per well and incubated for 24 h. After 24 h, cells were incubated in media containing with SWNT-PEG (1, 5, 10, 20 and 50 μ g/ml) and SWNT-PEG/VNc (1, 5, 10, 20 and 50 μ g/ml). After 24 h, the cells were washed by PBS twice and trypsinized. 10 μ l of cell suspension was simply

mixed with 10 μ l of trypan-blue dye. The cell sample solution was loaded into hemacytometer then visually examined to determine whether cells take up or exclude dye.



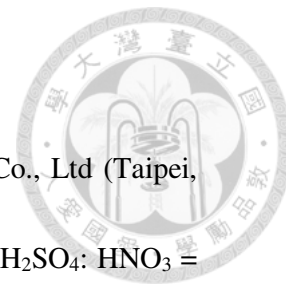
Phototherapy in vitro

HT-29 cells were seeded onto 24-well plates at a density of 5×10^4 cells per well and incubated for 24 h. After 24 h, cells were incubated in media containing with SWNT-PEG (20 μ g/ml) and SWNT-PEG/VNc (SWNT 20 μ g/ml and VNc 2 μ g/ml) for 24 h. After incubation, the cell changed with fresh medium and laser with a wavelength of 808 nm (1.3 W) was used to irradiate the cells for 3 min. After irradiation, we incubated the cells for 24 h. The cell viability was estimated by using a trypan blue assay. Besides, the cells were also stained with FITC Annexin V/Dead Cell Apoptosis Kit (Invitrogen) to evaluate the mortality attributed to phototherapy. All the results were collected by flow cytometry.

Electro- Phototherapy in vitro

For cell permeabilization in 100 μ l of pulsing buffer, HT-29 cells were trypsinized, centrifuged for 5 min at 1500 rpm, and resuspended in SWNT-PEG/VNc (VNc, 2, 5 μ g/ml). After EP, the cells were seeded into 24-well plates. After incubation, the cell changed with fresh medium and laser with a wavelength of 808 nm (1.3 W) was used to irradiate the cells for 3 min. After irradiation, we incubated the cells for 24 h. The cell viability was estimated by using a trypan blue assay.

Part II-III



Preparation of SWNT pulsing buffer

Raw SWNTs were purchased from Golden Innovation Business Co., Ltd (Taipei, Taiwan). SWNTs were oxidized by exposure to a strong acid solution (H_2SO_4 : HNO_3 = 3:1) for 24 h. After purification, oxSWNTs were refluxed in 4 M HNO_3 at 80°C for 48 h to shorten the length. After washing, the resultant suspension was then diluted with 250 mL of water, and the oxSWNTs were collected on a 100-nm pore membrane filter (Millipore) and washed with deionized water. The obtained oxSWNTs were further resuspended in water and centrifuged at $4000 \times g$ for 30 min to remove the residuals. The collected oxSWNTs were lyophilized to dryness at room temperature. The resulting particles were dissolved in phosphate-buffered saline (PBS) ($\text{pH} = 7.2$) and sonicated for 30 min. 1-Ethyl-3-(3-dimethylaminopropyl) carbodiimide hydrochloride (Sigma-Aldrich) and sulfo-NHS (N-hydroxysulfosuccinimide) (Sigma-Aldrich) were added to the SWNTs and stirred at room temperature for 1 h. This was followed by treatment with poly(ethylene glycol) bis(3-aminopropyl) terminated (MW = 6000) (Sigma-Aldrich) for 72 h with stirring at room temperature. Unbonded excess materials were removed by filter tubes (100 kDa AmiconYM-50, Millipore), centrifuged at 4000 rpm for 30 min, and washed thoroughly with water. Next, the SWNT-PEG_{6k} (20 $\mu\text{g}/\text{ml}$) was suspended in PBS with 0.01% Pluronic F127 (Sigma-Aldrich) as an SWNT pulsing buffer for cell electropermeabilization. The size distribution was deduced by TEM (Hitachi H-7650)

images. High-magnification images of SWNTs were obtained from FEG-TEM (Philips Tecnai F30 Field Emission Gun Transmission Microscope).



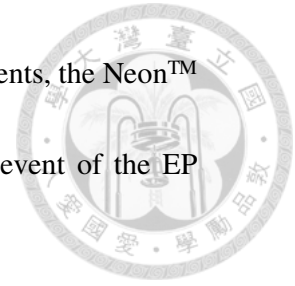
DOX loading on PEGylated SWNTs

SWNT-PEG was loaded with doxorubicin non-covalently by π - π stacking and hydrophobic interactions according to the aromatic structure of DOX [44]. We mixed DOX with PEGylated SWNTs (weight ratio = 1:10) in PBS (pH = 7.4) overnight. Unabsorbed excess DOX was removed by filter tubes (100 kDa AmiconYM-50, Millipore), centrifuged at 4000 rpm for 30 min, and washed thoroughly with water until the filtrate was no longer red. The formed SWNT/DOX complex was characterized by a UV-vis spectrophotometer (SpectraMax Microplate Readers, Molecular Devices, USA). The particle size and zeta potential were analyzed by Zetasizer Nano-ZS90 (Malvern Instruments Ltd, UK).

EP systems

We used two types of commercial EP systems in our investigation: suspension and attachment types. Two tests were performed to investigate the repeatability combined with SWNT pulsing buffer. We used the NeonTM Transfection System (MP-100, InvitrogenTM, Life Technology) and a NeonTM 100 μ l kit (InvitrogenTM, Life Technology) for the cell-suspended permeabilization. The attachment type used was a BEX electroporator (Tokiwa Science, Tokyo, Japan) with electrodes (LF650S7, LF647P2X5)

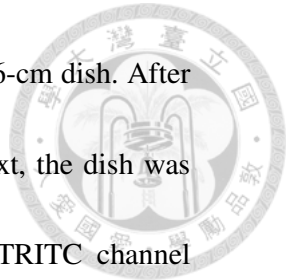
for both the *in vitro* and *in vivo* experiments. For all the *in vitro* experiments, the Neon™ Transfection System was used, excluding the JC-1 and the real-time event of the EP experiments.



Propidium iodide dye delivery

HT-29 cells (human colon adenocarcinoma cell lines) were obtained from the American Type Culture Collection (ATCC). Cells were routinely cultured in flasks containing Dulbecco's Modified Eagle's medium (DMEM, Invitrogen) supplemented with 10% fetal bovine serum (FBS, Invitrogen), 100 U/ml penicillin, and 100 µg/ml streptomycin (Invitrogen). Cells were incubated at 37°C in a humidified atmosphere with 5% CO₂. For cell permeabilization in 100 µl of pulsing buffer, HT-29 cells were trypsinized, centrifuged for 5 min at 1500 rpm, and resuspended in buffer T® or SWNT buffer (10⁶ cells/ml) mixed with propidium iodide (PI, 0.5 µg/ml). At 5, 15, and 60 min after EP, the cells were seeded into 24-well plates. Cells with pore formation were identified by the cellular uptake of the PI dye with the subsequent fluorescent signal immediately. The EP parameters were LV (100 pulses at 50 V, pulse duration = 40 ms) and HV (3 pulses at 1600 V, pulse duration = 10 ms). The PI signal expression in HT-29 cells was quantified by calculating the integrated optical density (IOD) using the Image Pro Plus software (Media Cybernetics, Silver Spring, MD).

Real-time observation of cell electroporation



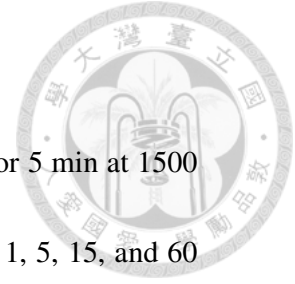
To monitor the real-time event of EP, the cells were seeded into a 6-cm dish. After 24 h, the medium was changed with pulsing buffer mixed with PI. Next, the dish was placed under a fluorescence microscope (Olympus IX71) using the TRITC channel (Excitation filter: HQ535, Emission filter: HQ610). Before and after electro-stimulation, the images were captured (1.53–1.84 image/s) for 40 min by the camera (Olympus U-CMAD3). The results are demonstrated in Movie S1 and S2.

Cell viability

HT-29 cells were trypsinized, centrifuged for 5 min at 1500 rpm, and resuspended in buffer T[®] buffer or SWNT pulsing buffer (10^6 cells/ml) mixed with 0.5 μ g/ml PI. At 60 min after EP, the cells were seeded into plates and changed with the fresh medium. After 24 h, the cells were stained with Calcein AM (Sigma-Aldrich) to observe the cell viability. Cells with pore formation were identified by the fluorescent signal of PI.

Apoptosis and necrosis assay

HT-29 cells were trypsinized, centrifuged for 5 min at 1500 rpm, and resuspended in T[®] buffer (10^6 cells/ml). At 24 h after different EP conditions (no treatment, 50 V*40 ms*100 pulses, 100 V*40 ms*50 pulses, 50 V*40 ms*10 pulses, 700 V*20 ms*3 pulses, 1300 V*20 ms*3 pulses, 1600 V*10 ms*3 pulses), the cells were stained with FITC Annexin V/Dead Cell Apoptosis Kit (Invitrogen) to evaluate the mortality attributed to EP. All the results were collected by flow cytometry.



SEM

After incubating for 24 h, the cells were trypsinized, centrifuged for 5 min at 1500 rpm, and resuspended in buffer T[®] or SWNT buffer (10^7 cells/ ml). At 1, 5, 15, and 60 min after LV and HV stimulation, the cells were fixed in 5% glutaraldehyde immediately for 2 days at 4°C and then rinsed three times with PBS. The fixed cells were dehydrated in serial concentrations of ethanol. After critical point drying, according to the manufacturer's directions, the cover slips were sputter-coated with gold and viewed by the field-emission scanning electron microscope (FE-SEM, Hitachi S-4800).

DIOC₆ and JC-1 staining

To investigate the membrane potential change after EP, cells were trypsinized and stained with DIOC₆ (5 µg/ml) (Invitrogen) in suspension. After incubating for 15 min at 37°C, the cells were washed and changed with the pulsing buffer. Then, the cells were treated by stimulation with LV, HV, and LV/SWNT. After EP, cells were seeded back to the 12-cm wells followed by fluorescence microscopy and observed in FITC channel (Excitation filter: HQ480, Emission filter: HQ535). In addition, the fluorescence intensities were detected by flow cytometry (BD, Bioscience). The alterations in the cell membrane potential were also assessed by JC-1 (Invitrogen). The cells were seeded in a dish and incubated at 37°C with 5% CO₂. After 24 h, the cells were stained with JC-1 (5 µg/ml) for 15 min, followed by washing and then changed with the pulsing buffer. Next,

the cells were treated by stimulation with LV, HV, and LV/SWNT. After EP, cells were observed at 5, 30, 60, and 120 min in the FITC channel (Excitation filter: HQ480, Emission filter: HQ535) and TRITC channel (Excitation filter: HQ535, Emission filter: HQ610).

GFP expression

To evaluate the transfection efficiency, HT-29 cells were transfected with minicircle DNA encoding GFP protein (CMV-GFP-T2A-Luciferase, SBI). HT-29 cells were seeded in a 12-well plate. After 24 h, cells were trypsinized and resuspended (10^7 cells/ml) in the pulsing buffer A (SWNT 20 μ g/ml and minicircle DNA 10 μ g/ml mixed with 0.01% F127 in PBS) for the LV/SWNT stimulation group and pulsing buffer B (minicircle DNA 1 μ g in buffer T[®]) for the LV and HV stimulation group. After EP, cells were seeded back to the 12-cm wells. For the transfection reagent group, Lipofactamine[®] (Invitrogen) was used and DNA–lipid complex was added to the cells. After 48 h, all the transfected cells were analyzed by flow cytometry (BD Bioscience).

EP protocol: in vivo study

All the animal experiments were performed using the BEX electroporator. The animals were kept under isoflurane/air anesthesia for the entire procedure. We used HV (3 pulses at 700 V, pulse duration = 20 ms) and LV (10 pulses at 50 V, pulse duration = 40 ms) pulses as our EP conditions to evaluate the effect of electro-stimulation *in vivo*.

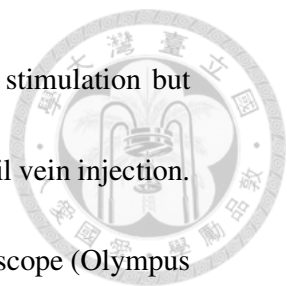


IVIS imaging

We examined the ability of SWNT + LV pulses to enhance nanoparticle delivery. FluoSphere[®] (Ex.580/Em.605, Molecular probe, Invitrogen) beads, approximately 100 nm in diameter, were used as aqueous suspensions containing 2% solids. The animals were divided into three groups. In the LV/SWNT group, to evaluate the SWNT effect combined with LV pulses, SWNT-PEG_{6k} (300 µg/mouse) in PBS with 0.01% Pluronic F127 was intravenously injected and electropulsation was applied on the right tumor immediately after the injection of FluoSpheres[®] (500 µl/mice). The HV and LV group without SWNT post-injection were administered only the nanoparticle injection. Then, the mice were imaged using IVIS Lumina II with an excitation wavelength of 570 nm at 1, 24, and 96 h post-injection. Next, various tissues, including the heart, liver, spleen, lung, kidney, and tumor, were extracted from the mice at 96 h post-injection. Finally, the tissues were imaged using IVIS Lumina II with an excitation wavelength of 570 nm.

Intravital microscopy

Mice were injected with Hoechst (Sigma-Aldrich, 33258) for labeling the cancer cells and FITC-dextran (Sigma-Aldrich) for labeling the tumor vessels. The animals were divided into two groups. In one group, to evaluate the SWNT effect combined with LV, SWNT-PEG_{6k} (300 µg/mouse) in PBS with 0.01% Pluronic F127 was intravenously injected and electropulsation was applied on the tumor immediately after the injection of



FluoSphere® (100 µl/mice). The other group lacked of the LV/SWNT stimulation but followed the same procedure. All the substances were administered by tail vein injection. The mice were placed on the platform underneath the fluorescence microscope (Olympus IX71), with the tumor lying on the cover slip next to the objective lens. The tumor cells were observed by DAPI filter (Excitation filter: D350, Emission filter: D460/50 m). The tumor vessels were observed by the FITC filter (Excitation filter: HQ480, Emission filter: HQ535), and the nanoparticles were observed by the TRITC filter (Excitation filter: HQ535, Emission filter: HQ610/75 m). The real-time images were captured by a camera (Olympus U-CMAD3) and processed using a software (PictureFrame™ 2.2, Optronics).

Electrochemotherapy by nanomedicine in vivo

Female BALB/c athymic nude mice aged 4–5 weeks were purchased from the National Laboratory Animal Center (Taipei, Taiwan). All the *in vivo* studies were approved by the National Taiwan University College of Medicine and the College of Public Health Institutional Animal Care and Use Committee (IACUC). HT-29 cells were subcutaneously injected in the flank of mice (10^7 cells/mice). When the tumor reached a mean volume of 100 mm^3 (approximately 16 days after the injection), the mice were randomly divided into PBS, SWNT, SWNT/DOX, LIPO-DOX (TTY Biopharm Company Limited, Taiwan), SWNT/DOX + EP, and SWNT + EP + LIPO-DOX groups (n = 5/group). The animals of the SWNT/DOX + EP group were injected with

SWNT/DOX (SWNT 7.14 mg/kg, DOX 4 mg/kg), followed by LV pulses (50 V, 40 ms, 10 pulses) immediately. Animals of the SWNT + EP + LIPO-DOX group were injected with SWNT (7.14 mg/kg), followed by LV pulses (50 V, 40 ms, 10 pulses) immediately.

Immediately after the pulses, LIPO-DOX (4 mg/kg) was administered. The other groups were administered only tail vein injections of PBS, SWNT (7.14 mg/kg), SWNT/DOX (SWNT 7.14 mg/kg, DOX 4 mg/kg), and LIPO-DOX (4 mg/kg) without electro-pulses.

All the injections were IV and all the groups were administered three times at 1, 4, and 8 days. Tumor volumes and body weight were measured twice a week for 36 days. The tumor sizes were calculated by the formula: volume = length \times width²/2. The mice were sacrificed after 36 days, and the tumors were extracted to weight. Tissues from the tumors were dissected from the HT-29 tumor-bearing mice at 24 h after treatment and fixed with 4% formaldehyde solution at room temperature for 48 h. Hematoxylin and eosin (H&E) staining was performed, and the tissues were observed under bright field microscopy (Olympus).

Statistical analysis

All the data were expressed as mean \pm SD. ANOVA was used to determine the significant differences in tumor volume in multiple groups. The significant difference between the comparison of EP (+) and EP (-) group was analyzed by the Student's t-test. Asterisks * and ** indicate significance with p values of < 0.05 and < 0.01, respectively.

Chapter 3. Results and discussions



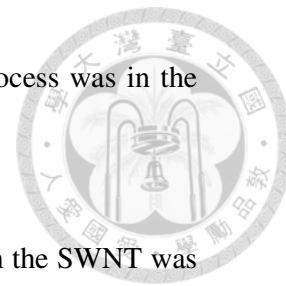
Part 1. Enhanced Cell Electro-permeabilisation Combined with Phototherapy to Kill Cancer Cells by Using Single-walled Carbon Nanotube

In part 1, SWNT showed the promising ability to be a nanoelectrode to enhance the LV stimulation for using in EP treatment and lead to effective drug delivery. We loaded near infrared (NIR) dye vanadium naphthalocyanine (VNc, PDT agent) onto SWNT-PEG (PHT agent) to achieve double photodynamic therapy (PDT) and photohyperthermia (PHT) cancer phototherapy system. The HT-29 cells could be killed effectively during the phototherapy after the EP treatment.

3.1.1 Functionalization and characterization of SWNT-PEG/VNc

SWNT-PEG/VNc was prepared according to the process in **Scheme 1**. Briefly, the raw SWNT was oxidized by the acid mixture of H₂SO₄ and HNO₃ (1:3 by volume). After 24 h, for shortening the oxSWNT, oxSWNT in HNO₃ was reflux under 80°C during 48 h. The short oxSWNT with carboxyl group was covalently binding to the PEG (MW = 6000) via EDC/NHS for 24 h. After purification, the SWNT-PEG and VNc were added into the DMF and sonicated for 30 min to obtain the well dispersion. After stirring 48 h, DMF was evaporated, the membrane formed onto the glass bottle. We used DDW water to dissolve the membrane into the greenish solution. The solution was then dialysis for

a week to obtain the purified SWNT-PEG/VNc. The more detailed process was in the **Materials and Methods** section.



In **Fig. 1** by the element analyzer, the weight percent of oxygen on the SWNT was increased from 1.83% to 11.90% after acidic process. The result showed that the carboxyl groups were successfully generated after acid treatment. The amount of COOH was quantity by the positive dye THA, which could absorb on the acid site (COO⁻) of oxSWNT due to the electrostatic force [63]. When THA mixed with oxSWNT, the fluorophores were taken up by the oxSWNT and the blue color of solution would obviously decreased (**Fig. 2A**). After removing oxSWNT by filtration, residue THA was calculate by absorbance spectrum, the signal was significantly decreased compared to the raw SWNT showed the amount of COOH group was 0.24 umol per mg of oxSWNT (**Fig. 2B**). The surface charge of oxSWNT was -43.1 mV due to the COO⁻ (**Fig. 3**). After binding with the PEG, the increased potential (-43.1 mV to -14 mV) of SWNT-PEG showed the formation of the CONH bond. The covalent bonds between PEG and oxSWNT were also confirmed by NMR peak at 3.5 ppm indicate attachment of PEG (**Fig. 4**).

Next, we used NIR dye VNc as our photosensitizer. VNc was hydrophobic and had the well dispersion in the solvent such as DMSO or DMF (**Fig. 5A**). After attaching to SWNT-PEG, SWNT-PEG/VNc had well suspension in water (**Fig. 5B**). The length of

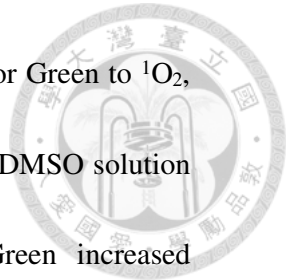
SWNT-PEG /VNc approached to ~188.64 nm was calculated from the TEM image (**Fig.**

6). The structure images of SWNT-PEG and SWNT-PEG/VNc were obtained from the high resolution TEM (**Fig.7**). Compared to the image of SWNT-PEG, SWNT-PEG/VNc showed the aggregation of VNc molecules attached to the SWNT-PEG surface.

Furthermore, to investigate the relation of VNc with SWNT-PEG, the aggregation on the SWNT-PEG/VNc was investigated by the energy-dispersive x-ray (EDX) spectrometer. The EDX elemental spectrum images indicated that C, N, O and V were present throughout the entire aggregation. The peaks corresponding to C (0.27 eV), N (0.39 eV), O (0.52 eV), and V (4.94 eV) were visible (**Fig. 8**). The C, N, O atoms could from SWNT, PEG and VNc, but the V atom was only from the VNc. The result confirmed that VNc was attached with SWNT. We also used X-ray diffraction (XRD) analysis of dried SWNT, SWNT-PEG/VNc and VNc. There showed the peak from the SWNT at 25 angle, but there was no peak from the VNc crystalline either SWNT-PEG/VNc (**Fig. 9**).

3.1.2 Photodynamic and Photothermal Properties of SWNT-PEG/VNc

Absorption spectrum of the aqueous solution of SWNT-PEG/VNc showed absorption peak at 808 nm, which were characteristic of VNc. The data also indicated the VNc remained properties absorb the NIR at 808 nm (**Fig. 10**). The amount of attached VNc calculated from absorption spectrum was 10%. To test properties of VNc as an agent for photodynamic therapy (PDT), production of singlet oxygen ($^1\text{O}_2$) was evaluated. After



treatment with laser diode (808 nm), the result of Singlet Oxygen Sensor Green to $^1\text{O}_2$, which was induced by photochemical reaction of the VNc plus light in DMSO solution (**Fig.11**). The fluorescence intensity of Singlet Oxygen Sensor Green increased significantly in VNc with the increasing time. (**Fig. 11**). Thus, VNc within the developed SWNT nanoparticles is capable of an efficient $^1\text{O}_2$ generation to act as a PDT agent. The previous studies have demonstrated that VNc is a suitable photosensitizer because of its high quantum yield. Olena *et al* showed that the quantum yield of SiNc-loaded nanoparticles ($\Phi_F = 11.8$) was much higher than indocyanine green (ICG) ($\Phi_F = 2.7\%$) were excited at 750 nm [63]. We also monitor the temperature evaluation of VNc with irradiation at a power density of 1.3 W/cm^2 for 5 min, but there showed no obvious increased temperature (**Fig. 12**).

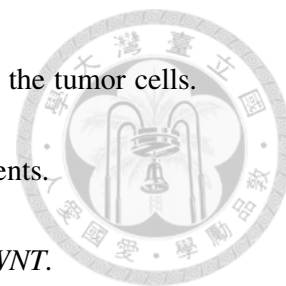
SWNT also exhibit strong optical absorption in the broad NIR offer unique advantages for photothermal cancer therapy [29]. To confirm the photothermal effect, we monitored the temperature of PBS solutions with dispersed SWNT-PEG/VNc and exposure under 808 nm laser at a power density of 1.3 W/cm^2 . A temperature elevation of approximately 23°C resulted from 3 min NIR irradiation on 20 $\mu\text{g/ml}$ SWNT-PEG/VNc. The results indicated that SWNT possessed a strong capacity of light-heat conversion under NIR laser irradiation. The SWNT-PEG/VNc solution showed a rapid increase of temperature when exposed to the laser within a short time (**Fig. 13**). It is

known the hyperthermia treatment that heating to 40–43°C can destroy the tumor cells.

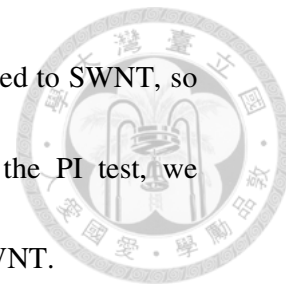
Therefore, it appears that SWNT-PEG/VNc is suitable to act as PHT agents.

3.1.3 Enhanced cellular uptake by the combination of LV pulses with SWNT.

Since the effective treatment of phototherapy is highly depend on the amount of photosensitizer delivered into cancer cells, we used low voltage stimulation to enhance the cellular uptake due to the pore formation in the cell membrane. We expected that SWNT-PEG/VNc would be readily taken up by HT-29 cells after EP. For pore formation testing, we used PI dye to identify the cell electro-permeabilization. We used pulsing buffer with (PI/SWNT/LV and PI/SWNT/HV group) or without SWNT (PI/HV and PI/LV group) during the pulsation to assess the ability of SWNT to induce pore formation in the cell membrane by enhancing the LV electrical stimulation. In **Fig. 14**, the PI signal was increasing obviously in the cells at 24 h after giving HV pulses (50 V, 40 ms, 10 pulses), but the signal between the PI/SWNT/HV (63.50%) and PI/HV (70.48%) group showed no obviously difference. This is because the high voltage stimulation could induce aggressive electric field, the irreversible pore formed in the cell membrane and lead to cell death. Compare PI (16.28%) with PI/LV (17.39%) groups, the PI signal showed no obviously increase by the LV pulses (1600 V, 10 ms, 3 pulses), the result indicate the LV stimulation was not enough to induce the cell electroporation. But in the PI/SWNT/LV group by using the SWNT pulsing buffer, the PI signal increase from



17.39% to 31.34% indicating the enhanced LV stimulation was attributed to SWNT, so that cell electroporation could be induced (**Fig. 15**). According to the PI test, we demonstrated that the enhanced LV stimulation was attributed to the SWNT.

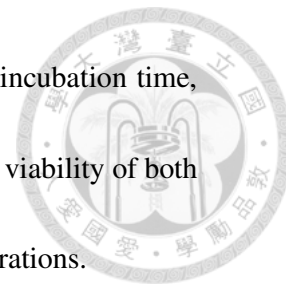


Next, to investigate the cellular uptake of SWNT-PEG/VNc, we separated the HT-29 cells into EP and no EP groups. For the no EP group, HT-29 cells were incubated in medium containing SWNT-PEG/VNc (20-50 ug/ml, 2-5 ug/ml) for 24 h without any electro-stimulation (**Fig. 16A**). For the EP group, HT-29 cells trypsinized, and resuspended in SWNT-PEG/VNc solution (20 ug/ml, 2 ug/ml). The cell exposure to the HV and LV pulses and then incubated for 24 h. After incubation, VNc fluorescence in cells was detected by flow cytometry. In **Fig. 16A**, the measurements revealed that only 15.32% and 19.31% of the cells took up SWNT-PEG/VNc. But for the EP group, the measurements revealed that 31.03 % (LV) and 47.43 % (HV) of the cells took up SWNT-PEG/VNc, a much larger percentage than for the no EP group (**Fig. 16B**). The result indicated that SWNT combined with LV stimulation could increase the cellular uptake effectively.

3.1.4 SWNT-PEG/VNc mediated Electro-Phototherapy efficiently kills cancer cells.

The most concern issue towards the medical applications of functionalized SWNT is their impact on cell viability. For this reason, the cytotoxicity of the SWNT was evaluated. The HT-29 cells were incubated with SWNT-PEG and SWNT-PEG/VNc at

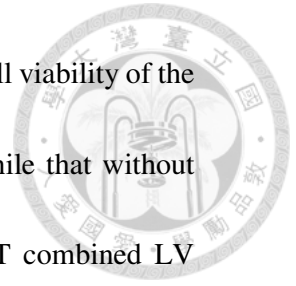
concentrations ranging from 5 to 50 ug/ml for 24 h. At the end of the incubation time, cells were collected, the results displayed in **Fig. 17** showed that the cell viability of both SWNT/PEG and SWNT-PEG/VNc was preserved at increasing concentrations.



To test the double phototherapy, we incubated HT-29 cells with SWNT-PEG and SWNT-PEG/Nc for 24 h, then 808 nm laser was used to irradiate the cells for 3 min. In **Fig. 18 and 19**, cell cytotoxicity assay demonstrated that combined with NIR irradiation (808 nm, 1.3 W/cm²) induced stronger cytotoxicity compared with either SWNT or NIR light irradiation alone. But compare SWNT-PEG/Nc (60.64%) to SWNT-PEG (58.44%), the cell viability show no obvious difference indicated that the effective treatment may attribute to the SWNT due to the photothermal effect.

Then, we combined the electro-stimulation with the phototherapy to kill the HT-29 cells. We separated the cells into laser and without laser groups. Both groups were treated with LV, HV, SWNT-PEG/Nc, SWNT-PEG/Nc + LV and SWNT-PEG/Nc + HV. Without laser irradiation, the photothermal effect could not be induced so that no cell death was founded except the cell treated with HV pulses (HV, SWNT-PEG/Nc + HV). For the laser group, cells exposure to the LV pulses showed no obvious harmful effect, the cells viability could remained 88.58%. Compare to the LV pulses, the cells treated with HV pulses showed the decreased cell viability (15.76%). The result revealed that HV pulses could induce irreversible pore formation on the cell membrane and cause cell

death. Compare SWNT-PEG/Nc + LV to SWNT-PEG/Nc groups, the cell viability of the cells with electro-stimulation before laser irradiation was 27.17 %, while that without electro-stimulation was approximately 54.89 %. Therefore, the SWNT combined LV pulses before phototherapy could cause an obvious increase in toxicity.



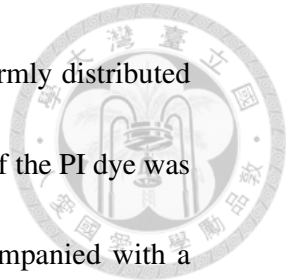
Part II. Effect of the LV stimulation on Cell Membrane Poration Enhanced by the SWNT



Effective delivery of biomolecules or functional nanoparticles into target sites has always been the primary objective for cancer therapy. In Part II, we demonstrated that by combining single-walled carbon nanotubes (SWNTs) with low-voltage (LV) electrical stimulation, biomolecule delivery can be effectively enhanced through reversible electroporation (EP). Clear pore formation in the cell membrane is observed due to LV (50 V) pulse electrical stimulation amplified by SWNTs. The cell morphology remains intact and high cell viability is retained. This modality of SWNT + LV pulses can effectively transfer both small molecules and macromolecules into cells through reversible EP.

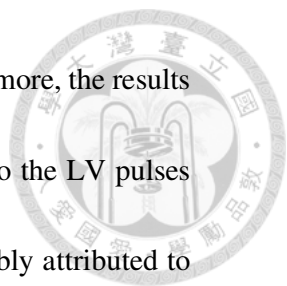
3.2.1 SWNTs combined with LV pulses induced cell electropermeabilization

We used a pulsing buffer with (LV/SWNT group) or without SWNTs (HV and LV group) during the pulsation to assess the ability of SWNTs to induce pore formation in the cell membrane by enhancing the LV electrical stimulation. In addition, we used PI to identify cell electropermeabilization. PI fluorescence was observed in the cells at 5 min after HV (1600 V, 10 ms, 3 pulses) pulses, and the signal increased at 15 min (**Fig. 21A**). However, at 60 min, the IOD was not significantly increased (**Fig. 21B**). In real-time observation, acceleration of the signal appeared in the cells after HV pulses, the cell



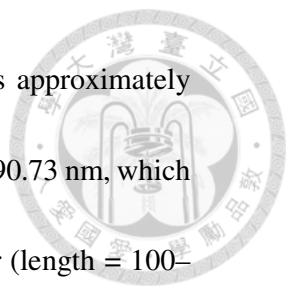
cytoplasm was immediately brightened, and the fluorescence was uniformly distributed throughout the cell (**Movie S1, Fig. 22**). This result indicated that most of the PI dye was introduced into the cells at the beginning of EP. PI transfer was accompanied with a significant driving force due to the HV pulses. As time progressed, diffusion became the primary process for PI delivery. However, no PI signal was observed in the cells during the whole observation period after the cells were exposed to LV pulses (50 V, 40 ms, 100 pulses) (**Fig. 21A and B**). This is because the external electric field could not increase the transmembrane potential to the threshold value due to which the cell membrane could not be ruptured, resulting in the failure of EP. The required electric field pulse amplitude is usually in the range of 10^3 – 10^4 V/cm to raise the transmembrane potential to 0.5–1.0 V, which can result in EP [45]. The effective pulses used for inducing cell permeabilization are usually >1000 V [46].

Although there was no PI signal observed at 5 min after LV pulses in the cells of the LV/SWNT group, as the incubation time increased, the PI signal started to escalate (at 15 min) (**Fig. 21A**). At 60 min, the IOD had no obvious difference between the HV and LV/SWNT groups (**Fig. 21B**). In the real-time video, PI appeared slowly as the time increased, and the signal was finally smeared around in the cell membrane during the 40 min observation period (**Movie S2, Fig. 22**). Compared with the HV group, PI was introduced into the cells without any obvious driving force in the LV/SWNT group, and



the cellular uptake was totally attributed to the passive diffusion. Furthermore, the results suggested that cell electropermeabilization is not induced by exposure to the LV pulses unless the SWNT pulsing buffer is used. The pore formation was probably attributed to the amplified electric field by SWNTs (**Fig. 23**). Rojas-Chapana *et al* had demonstrated that the activation of CNTs was due to the “lightening rod” effect that occurred when CNTs in a region of electric field caused a strong field enhancement at the tips [38]. The cells with the CNTs attached to the surface and a stream of nanoparticles entered the cell along with the CNTs [38]. Besides, the interaction in the region between the CNT tips and cell membrane exit due to the electrostatic force could pull CNTs off the cell membranes by rotation [41].

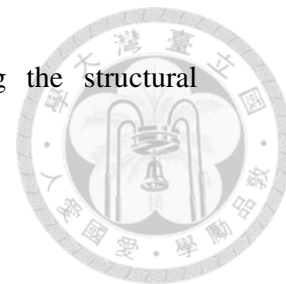
Therefore, we used high-magnification images obtained from a field emission scanning electron microscope (FE-SEM) to investigate the surface of the cell membrane after giving pulses immediately. In the LV group, we could not find pore formation in the cell membrane; the surface was flat and similar to that of the no-treatment group (**Fig. 24**, no-treatment and LV group). In the SWNT group, aggregated SWNT-like structures were visible; a large fraction of the tubular structures attached to the surface without any appearance of pores (**Fig. 24**, SWNT). However, in the LV/SWNT group, we not only observed the SWNT-like structures within the cells but the apparent pores in the surface could also be found easily and with the tubular structures nearby (**Fig. 24**, LV/SWNT,



indicated by green arrows). The length of these tubular structures was approximately 162.01 nm ($n = 22$) and the range of the length was between 103.52 and 290.73 nm, which were consistent with the SWNT-PEG that we used in the pulsing buffer (length = 100–300 nm, diameter = 20 nm) (**Fig. 25A and B**); the group treated without SWNTs demonstrated no obvious tubular structures on the surface, indicating that the structures were SWNTs. No obvious pore formation was observed after LV stimulation without SWNTs, suggesting that the LV pulse effect was amplified by the SWNT. CNTs possess unique electrical properties that potentially make them ideal field emitters [39]. Their small tips with high aspect ratios (>1000) allow for a large electric field enhancement near the tip. Due to the aspect ratio of SWNTs ($L/D =$ approximately 7.5–10), the field enhancement factor at their tip could reach 22.5–35 to amplify the low electric field [38].

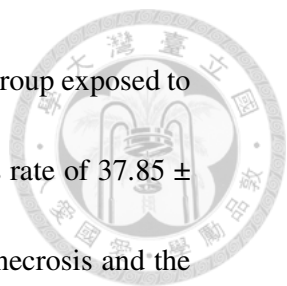
In our study, some SWNTs even appeared proximal in the pore, revealing that EP occurred with the involvement of SWNTs (**Fig. 24**, red star). These results prove that the SWNTs interacted with the cell membrane during the EP process and the pore formation could be induced under the LV pulses. Furthermore, we could observe the tubular structure bent, which was because the SWNTs were processed with a strong oxidation. Although the deformation of the SWNT usually occurs on the defect site, which is the five- or seven-membered rings in the carbon network by the initial formation [47], the strong oxidation could also lead to the severe defect on the side wall of the SWNT.

Different defects make for various chemical structures, including the structural deformations caused by bending or twisting of the nanotubes [48].



3.2.2 Reversibility of cell electroporation

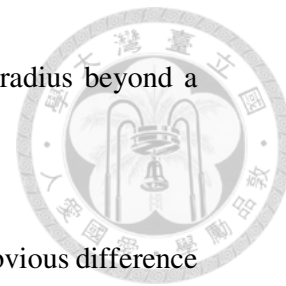
At 24 h of incubation, the cells treated with the LV pulses in combination with SWNT pulsing buffer (LV/SWNT group) demonstrated a strong PI fluorescence (**Fig. 26**). However, the cells treated with the LV pulses only (LV group) showed no obvious signal. Both groups treated with LV electrical stimulation remained viable and showed a green fluorescence and high cell density. Meanwhile, the cells treated with HV pulses also demonstrated a red fluorescence, but the adhesive HT-29 cells no longer adhered after 24 h and the cells were washed off. These results revealed that HV pulses could induce irreversible pore formation on the cell membrane and cause cell death. We also used the apoptosis/necrosis assay to evaluate the cell viability at 24 h after treatment with different voltages of electro-stimulation, and it was observed that the survival rates of the cells gradually decreased with increasing voltage (Necrotic cell: 1300 V vs control, $**p < 0.01$; 1600 V vs control, $**p < 0.01$) (**Fig. 27 and Fig. 28**). The apoptosis and necrosis rate of the cells exposed to the electric pulses of 50 V (40 ms, 100 pulses) showed no obvious differences from that of the control group, and the survival rate remained at $89.6 \pm 0.42\%$. We also confirmed the cell viability of the LV group combined with SWNTs that showed no obvious cell death, suggesting that the method was a suitable treatment *in*



vitro (**Fig. 29**). The lowest survival rate of the cells was observed in the group exposed to the electric pulses of 1600 V (10 ms, 3 pulses), and an obvious necrosis rate of $37.85 \pm 0.39\%$ was observed, which indicated that the HV stimulation induced necrosis and the survival rate was only $57.2 \pm 0.56\%$.

The SEM images showed that the shape of the HT-29 cells without treatment was spherical with a relatively smooth surface (**Fig. 30**, no-treatment). Both the LV and LV/SWNT groups showed similar cell shapes, with no significant difference as compared with the control group (**Fig. 30**, LV and LV/SWNT). In the HV group, severe structural damage of the cell membranes was observed (**Fig. 30**, HV). Flow cytometry after EP showed a decrease in the FSC signal and an increase in the SSC signal in the cells stimulated by HV, which may be attributed to the significant cell debris and the necrotic cells (**Fig. 31**, **Fig. 32**). Irregular outlines and broken surfaces of the cell membranes were observed immediately after the application of HV pulses (**Fig. 33**). Some substance seemed to excrete out of the cell because of the ruptured membrane. The cells became flat, and the boundary of the cells was hard to define. At 5, 15, and 60 min after EP, as time progressed, the cells recovered to a relatively spherical surface (**Fig. 33**). However, we could observe obvious micropores on the surface, which were not re-sealed. The cell viability assay results (**Fig. 27**) also showed that the HV pulses could induce necrosis in the cells and lead to permanent damage. This is because the pores created due to larger

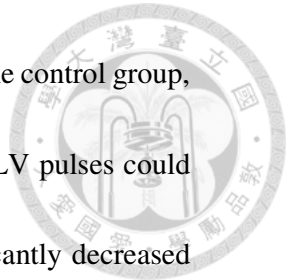
transmembrane potentials could expand more rapidly and exceed the radius beyond a limit so that the irreversible EP could occur [49].



In the LV/SWNT group, because of the smooth boundary with no obvious difference from that in the no-treatment group (**Fig. 30**), we used the high magnification image to observe the reversibility of pore formation. Pores obviously appeared at the region near the membrane at 1 min after EP; however, the number of pores reduced at 60 min (**Fig. 34**). Unlike the HV group, the enhanced electric field due to SWNTs may occur in the local region between the SWNT tips and the cell membrane, which could avoid the unnecessary exposure of the cells to high electric field environment and increase cell viability. Moreover, the pore formation may be due to the SWNT spearing or stripping by the electrostatic force, which could be prevented from the larger transmembrane potential, thereby causing the irreversible EP [41].

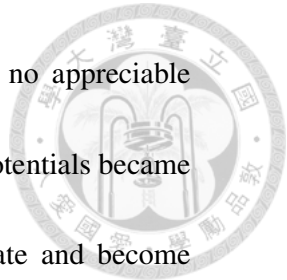
3.2.3. The change of membrane potential in HT-29 cells after EP

We labeled the cells with DIOC₆ to detect the membrane potential after providing electrical stimulation. The lipophilic cationic dye DIOC₆ usually accumulates abundantly in the mitochondria and cell membrane due to the negative membrane potential. When the transmembrane potential becomes more positive, the dye could no longer aggregate near the membrane. The dye diffuses laterally within the cell membrane, resulting in a reduction of fluorescence. **Fig. 35** showed the apparent fluorescence observed when the



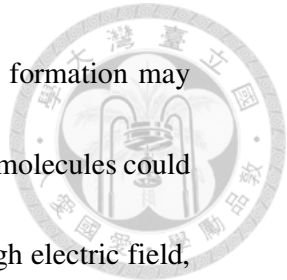
dye was incorporated into the membrane of the control cells. Similar to the control group, the obvious fluorescence observed in the LV group suggested that the LV pulses could not depolarize the cell membrane and induce EP. However, the significantly decreased fluorescence of the HV group revealed the drastic change in the membrane potential due to the intense electric field (**Fig. 35**, HV, indicated by white arrows). The LV/SWNT group also showed reduced fluorescence in the cells, indicating that the LV pulses could increase the transmembrane potential by the amplified electric field due to SWNTs (**Fig. 35**, LV/SWNT, indicated by white arrows). Flow cytometry revealed the left shift of the DIOC₆ fluorescence peak of the HV and LV/SWNT groups, which indicated the loss of DIOC₆ in which the depolarization was induced by the effective EP (**Fig. 36**).

Furthermore, we used another cationic carbocyanine dye JC-1 to detect the change in the membrane potential at different time points after EP. **Fig. 37** showed the same field of view of the cells before and after electrical stimulation. Before EP, the cells were stained with both orange and green fluorescence. Most of the dyes that formed orange fluorescence J-aggregates (emission maximum at approximately 590 nm) accumulated at the cell membrane and were distributed throughout the cytoplasm in the granular structures due to the hyperpolarized membrane potential. After EP, the HV pulses induced a marked loss of orange J-aggregate fluorescence in the cells and the green monomer fluorescence (emission maximum at approximately 529 nm) increased. However, the



fluorescence of the cells exposed to LV without SWNT pulsing had no appreciable change. In the LV/SWNT group, with the effective EP, the membrane potentials became more positive so that the cationic JC-1 dyes could no longer aggregate and become monomers, resulting in an increase in the green fluorescence. These results indicated that although the mechanism of the SWNT in enhancing the cell electropermeabilization was not completely clear, SWNT amplified the electric field under the LV pulses and led to the effective EP.

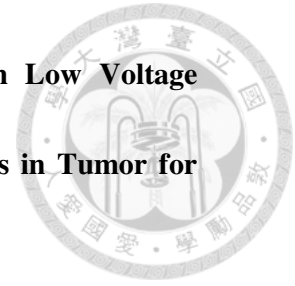
Subsequently, we transfected the HT-29 cells with a minicircle DNA encoding GFP fluorescence to investigate the transfection efficiency of the HV, LV, and LV/SWNT groups. The HV pulses resulted in an increased higher level of GFP expression than that of the commercial transfection reagent (Lipofectamine[®], Invitrogen) (**Fig. 38**). Although the transfection efficiency of the LV/SWNT group was lower than that of the HV and transfection reagent groups, the level of fluorescence intensity was higher than that observed by using LV alone. These results showed that a higher intensity of electric field could lead to more effective transfection efficiency. Therefore, we tried to determine the difference in cell electropermeabilization induced by the HV pulses and SWNT-amplified LV pulses. In **Fig. 39**, the PI signal at 3 h after HV stimulation was localized at the cell nucleus, which implied that under the HV pulses, the small molecules could possibly migrate into the nucleus during the short time period. However, the PI signal of the



LV/SWNT group was dispersed only broadly into the cytoplasm. Pore formation may initially be induced in the cells exposed to the electric pulses, and the biomolecules could possibly enter the cell interior through diffusion. Meanwhile, under a high electric field, the shock wave induced by the HV pulses could lead to an electrophoretic force that accelerated the migration of charge molecules including DNA [50]. The higher electric field could also result in convection in the fluid environment so that the fluid-dissolved molecules could possibly flow into the cell [51, 52]. Furthermore, the sufficient intensity of electric field can cause transmembrane voltages at the organelles, thus inducing the large and long organelle channels, which could explain the PI signals in the organelle [53].

EP is usually considered a reversible mechanism for introducing molecules into the cells. However, most of the effective transfection usually accompanies the higher voltage stimulation combined with short time duration and less number of pulses to achieve adequate cellular uptake. The HV pulses could break down the lipid bilayer of the membrane to rupture it directly or create micropores in the surface, leading to cell death [54]. These events are inappropriate for the delivery of biomolecules into cells. Therefore, the LV pulses combined with SWNT-facilitated delivery of different types of molecules would be more suitable for the application of ECT. We then tried to examine this new modality using animal models.

**Part III. Combining the Single-Walled Carbon Nanotubes with Low Voltage
Electrical Stimulation to Improve Accumulation of Nanomedicines in Tumor for
Effective Cancer Therapy**



In Part III, the results of animal studies suggest that treatment with LV pulses alone cannot increase vascular permeability in tumors unless after the injection of SWNTs. The nanoparticles can cross the permeable vasculature, which enhances their accumulation in the tumor tissue. Therefore, in cancer treatment, both SWNT + LV pulse treatment followed by the injection of LIPO-DOX® and SWNT/DOX + LV pulse treatment can increase tumor inhibition and delay tumor growth.

3.3.1. EPR effect improvement by the increased electrical stimulation through SWNTs

To investigate whether the accumulation of nanoparticles was enhanced in the tumor by LV pulses combined with SWNTs, we used the red fluorescence FluoSpheres® beads (ex/em: 580/605 nm, Invitrogen) as our nanoparticles, with a mean diameter of approximately 100 nm. HT-29 xenograft model (human colon cancer) was performed beneath the skin. Animals bearing bilateral HT-29 tumors were separated into three groups. The LV/SWNT group of mice was administered IV injection with SWNTs, followed by LV pulses to the right side tumors. The HV and LV groups of mice were administered only HV and LV pulses on the right side tumors. The left side tumors were

received no pulses and were assigned as control. All the groups were administered with IV injections with nanoparticles after giving the pulses (**Fig. 40**).



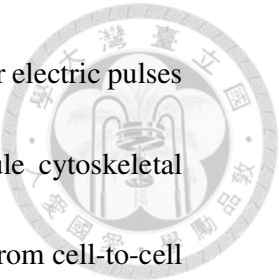
Fig. 41A showed the spread of the fluorescence signals in the HV group throughout the body and without any selectivity at 1 h post-injection. At 24 h, the accumulation of nanoparticles was observed in the HV-treated tumor (right), but the uptake in the control tumor (left) was hard to detect. At 96 h, the nanoparticles showed a high tumor (right) selectivity. However, we could also observe tumor ablation at 1 h after giving the pulses, which meant that HV pulses related EP was irreversible and such an intense electric stimulation caused the tissue destruction (**Fig. 42**). In the LV/SWNT group, the signals in the tumor also showed the similar result to that of the HV group and the accumulation of nanoparticles in the LV/SWNT-treated tumor (right) revealed high retention at 96 h. Besides, the tumors showed no obvious damage after giving the pulses, suggesting that this new modality causes only the enhancement of vascular permeability without harming the tissue. However, in the LV group without the SWNT injection, the fluorescence intensity in the tumors showed a similar level between the LV-treated and control tumors (**Fig. 41A**). These results indicated that the permeability of tumor blood vessels could not be enhanced by the LV pulses alone, unless we increased the electrical stimulation (HV pulses) or performed the SWNT injection. At 96 h after treatment, the harvested tumors subjected to *ex vivo* imaging revealed similar results, the tumor that received the pulses

showed an increased uptake of nanoparticles compared to the control tumors, indicating that the accumulation could be attributed to the EP (**Fig. 41B**).



Furthermore, we used intravital microscopy to monitor nanoparticle accumulation in the tumor tissue. We could observe that the influx of the nanoparticle occurred completely in the tumor vessels at 10 min after injection (**Fig. 43 and Fig. 44A**). At 60 min, the fluorescence signals decreased to few spots and aggregated along the vessels, and we could not observe any apparent signals in the tumor tissue (**Fig. 44A**). However, in the LV/SWNT-treated tumor, we could observe not only the red spots in the vessel but also the obvious red fluorescence in the tumor bed. These results indicated that the SWNT-amplified LV pulses could enhance the permeability of the vessel, so that the nanoparticles could leak rapidly into the tumor tissue (**Fig. 44B**). Moreover, by extracting the LV-treated tumor with or without SWNT injection at 3 h after treatment, we observed that the tumor with only LV pulses had no apparent accumulation of nanoparticles (**Fig. 45B**). The SWNT-treated tumor showed more obvious red signal among the tumor tissues (**Fig. 45A**). These results of animal studies showed that the SWNTs increased the LV stimulation effect, and the EPR effect could be enhanced without harming the tissue.

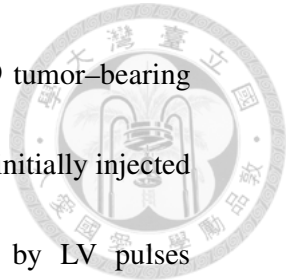
Although the reversible permeabilization of tumor cell membrane due to EP is the basic mechanism of the antitumor effectiveness of ECT, the direct effect of electric pulses applied to the tumor was also found to enhance tumor vascular permeability via the EP



occurring on the endothelial cells [55]. The endothelial permeability under electric pulses could be enhanced by the disruption of microfilament and microtubule cytoskeletal networks, loss of contractility, and loss of vascular endothelial cadherin from cell-to-cell junctions immediately after EP [56]. Therefore, SWNTs play a role as a “nanoelectrode” that could enhance the local electric field effect at the tumor vessel. The strong electrostatic force could pull SWNT off the endothelial cell membrane during the rotation [41], and the structure of cell membrane deformed under the enhanced LV pulses. Consequently, the requirement of HV would be unnecessary, and the side effect in the irreversible EP of tissue ablation that may create serious problems including cardiac arrhythmias and uncontrolled muscle contractions could be avoided [57]. Moreover, SWNTs could play a role as a nanovector to deliver the chemo-drug into the target site. We injected SWNT-based nanomedicine into mice via the tail vein and then gave the pulses to the tumor. The nanomedicine could leak into the tumor tissue due to the increased vascular permeability. This resulted in the enhancement of both the EPR effect and effective ECT.

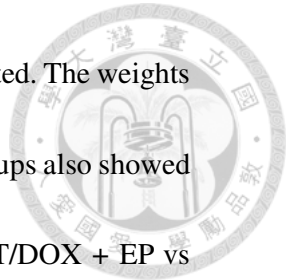
3.3.2. *In vivo studies of ECT*

To examine whether the therapeutic efficacy of nanomedicine was enhanced by SWNT combined with LV pulses, both commercial liposomal doxorubicin (LIPO-DOX[®], TTY Biopharm Company Limited, Taiwan) and SWNT/DOX complex (see Materials and



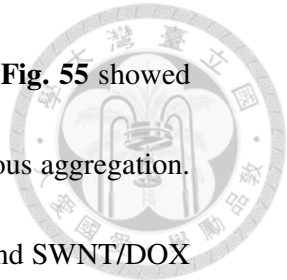
Methods and **Fig. 46-48**) were used in this study. Six groups of HT-29 tumor-bearing mice were used for the experiments. The SWNT/DOX + EP group were initially injected with SWNT/DOX (SWNT 7.14 mg/kg, DOX 4 mg/kg), followed by LV pulses immediately. Another EP group of SWNT + EP + LIPO-DOX was initially injected with SWNT (7.14 mg/kg), followed by LV pulses immediately. Right after the pulses, LIPO-DOX (4 mg/kg) was administered intravenously (**Fig. 49**). The other groups were injected with phosphate-buffered saline (PBS), SWNT (7.14 mg/kg), SWNT/DOX (SWNT 7.14 mg/kg, DOX 4 mg/kg), and LIPO-DOX (4 mg/kg) without electro-pulses. The treatments were administered three times in all the groups.

The significant difference in the tumor volume between groups was determined. The results indicated that the SWNT + EP + LIPO-DOX (* $p = 0.023 < 0.05$), LIPO-DOX (* $p = 0.033 < 0.05$), and SWNT/DOX + EP (* $p = 0.027 < 0.05$) groups were found to be more effective in tumor inhibition compared with the control group. On the other hand, there was no significant difference in SWNT ($p = 0.168$) and SWNT/DOX ($p = 0.109$) groups when compared with the control group, indicating that the tumors in these groups were not efficiently inhibited. It was noted that in comparison to EP (+) and EP (-) groups, the group treated with EP showed better tumor inhibition (**Fig. 51**) (SWNT/DOX + EP vs SWNT/DOX, * $p < 0.05$; SWNT + EP + LIPO-DOX vs LIPO-DOX, * $p < 0.05$). No significant changes in body weight were observed during the experiments (**Fig. 50**). At



day 36, after three times of IV injection, the extracted tumors were weighted. The weights of tumor tissues of SWNT/DOX + EP and SWNT+ EP + LIPO-DOX groups also showed obvious inhibition compared with the group treated without EP (SWNT/DOX + EP vs SWNT/DOX, $**p < 0.01$; SWNT+ EP + LIPO-DOX vs LIPO-DOX, $*p < 0.05$) (**Fig. 52**). However, no significant tumor inhibition was observed in the PBS and SWNT groups. H&E staining of animal tissues from all the groups did not exhibit any obvious damage (**Fig. 53**). Moreover, H&E staining showed comparable tumor tissue necrosis in the animals treated with nanomedicine combined with EP (SWNT/DOX + EP and SWNT + EP + LIPO-DOX); however, no tumor cell damage was observed in the PBS (control) and SWNT + EP groups (**Fig. 54**). These results demonstrated that the tumor inhibition was attributed to doxorubicin instead of SWNT + EP. The effect induced by SWNT + EP was only the increase in the vessel permeability to enhance the accumulation of nanoparticles in the tumors.

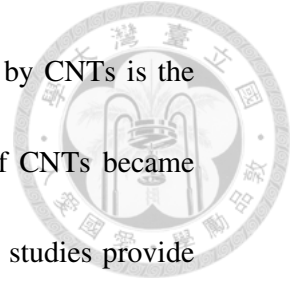
Although SWNT is a promising nanomaterial in biomedical application, its safety remains major concern. The aggregation of SWNTs could be a limitation of their biological application and lead to toxicity. To solve this problem, the modification of SWNTs with PEG is important for using SWNTs *in vivo*. The well dispersion of SWNTs could be achieved; moreover, the circulation time of SWNTs in the animals could be increased [58]. Therefore, we modified the SWNTs by oxidation and pegylation processes



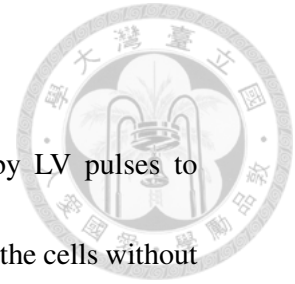
to shorten the size and to keep SWNTs well suspended in the solution. **Fig. 55** showed that SWNT and SWNT/DOX remained stable for a month without obvious aggregation. We also extracted the livers at 1 and 8 weeks after injection of SWNT and SWNT/DOX to investigate the accumulation and clearance of SWNT nanoparticles. The livers of mice injected with SWNT or SWNT/DOX showed dark color compared with the control (maroon) (**Fig. 56**). However, at 8-week post-injection, the dark color faded away over time, and SWNT could hardly be detected via H&E staining (**Fig. 57**).

Many studies have proposed that SWNT is a biodegradable material [58-60]. A long-term *in vivo* investigation found SWNT in the feces and bladder, which implied that SWNT could possibly be excreted via the biliary and renal pathways, and no obvious toxicity was observed via necropsy, histology, and blood chemistry examinations at 3 months after SWNT injection [58]. Recently, several *in vitro* studies have demonstrated that peroxidases, including human myeloperoxidase (hMPO), eosinophil peroxidase (EPO), and lactoperoxidase (LPO), can induce CNT degradation [59,60]. Kagan *et al* used molecular modeling to demonstrate the interactions between the basic amino acids of hMPO with the carboxyl group of the CNTs. These findings suggest that CNTs are biodegraded and do not generate an inflammatory response when aspirated into the lungs of mice [59]. Moreover, Elgrabli *et al* demonstrated that macrophages employed several oxidative mechanisms to degrade CNTs, including NOX₂ complex activation, superoxide

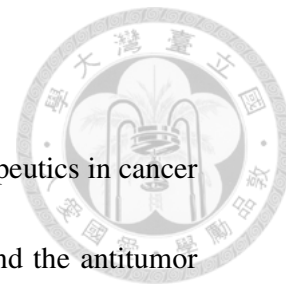
production, and hydroxyl radical attack. The primary species attacked by CNTs is the $\text{OH}\cdot$ produced by the NOX_2 complex in the phagosomes. The wall of CNTs became thinner via tearing and perforation due to chemical defects [60]. These studies provide sufficient information for the development of SWNTs by which they could be considered as safer biomaterials.



Chapter 4. Conclusions

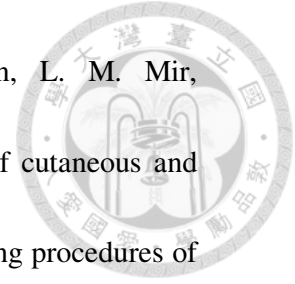


We demonstrated that SWNTs can amplify electro-stimulation by LV pulses to achieve cell EP, by which various sizes of molecules can be delivered to the cells without harmful effects. Although the HV pulses could induce pore formation in both the cell membrane and cell organelles, thereby enhancing the transfection efficiency to a greater degree than that by LV/SWNT stimulation, the cell mortality will increase significantly. Moreover, in animal studies, we demonstrated the combination of SWNT and LV pulses could enhance the EPR effect, and thus increase the accumulation of nanoparticles in the tumor. We also confirmed that SWNT pre-injection, followed by exposure to LV pulses, could enhance ECT in various nanoparticle drugs. In clinical research, several ECT studies have confirmed the valid antitumor effect on patients with malignant melanoma, basal cell carcinoma, and other superficial tumors [19]. Besides, bipolar electrodes combined with our new modality could also be applied in conventional endoscopy to open through the working channel of the endoscope, ensuring that the tip–tissue distance remains constant as the device performs EP [61,62]. This new platform has the potential to be used for both superficial and deep-seated cancer treatment precisely and safely in the future.



Reference

- [1] Y. Matsumura, H. Maeda, A new concept for macromolecular therapeutics in cancer chemotherapy: mechanism of tumor-tropic accumulation of proteins and the antitumor agent smancs, *Cancer Res.* 46 (1986) 6387–6392.
- [2] H. Maeda, Tumor-selective delivery of macromolecular drugs via the EPR effect: background and future prospects, *Bioconjugate Chem.* 21 (2010) 797–802.
- [3] S. Lee, H. Koo, J.H. Na, S.J. Han, H.S. Min, S.J. Lee, S.H. Kim, S.H. Yun, S.Y. Jeong, I.C. Kwon, K. Choi, K. Kim, Chemical Tumor-targeting of nanoparticles based on metabolic glycoengineering and click chemistry, *ACS Nano* 8 (2014) 2048-2063.
- [4] Y. Zhong, F. Meng, C. Deng, Z. Zhong, Ligand-directed active tumor-targeting polymeric nanoparticles for cancer chemotherapy, *Biomacromolecules* 15 (2014) 1955-1969.
- [5] K. Sano, T. Nakajima, P.L. Choyke, H.Kobayashi, Markedly enhanced permeability and retention effects induced by photo-immunotherapy of tumors, *ACS Nano* 7 (2013) 717-724.
- [6] T. Stylianopoulos, EPR-effect: utilizing size-dependent nanoparticle delivery to solid tumors, *Ther. Deliv.* 4 (2013) 421-423.
- [7] M. Marty, G. Sersa, J.R. Garbay, J. Gehl, C. G. Collins, M. Snoj, V. Billard, P. F. Geertsen, J. O. Larkin, D. Miklavcic, I. Pavlovic, S. M. Paulin-Kosir, M. Cemazar, N.



Morsli, D. M. Soden, Z. Rudolf, C. Robert, G. C. O'Sullivan, L. M. Mir,
Electrochemotherapy - an easy, highly effective and safe treatment of cutaneous and
subcutaneous metastases: results of ESOPE (european standard operating procedures of
electrochemotherapy) Study, E.J.C. Supplements. 4 (2006) 3–13.

[8] D. Miklavčič, G. Serša, E. Breclj, J. Gehl, D. Soden, G. Bianchi, P. Ruggieri, C.R.
Rossi, L.G. Campana, T. Jarm, Electrochemotherapy: technological advancements for
efficient electroporation-based treatment of internal tumors, Med. Biol. Eng. Comput. 50
(2012) 1213–1225.

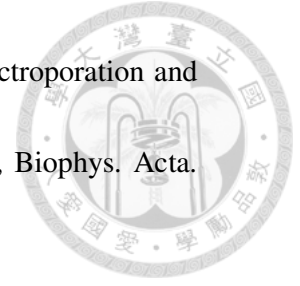
[9] J. Gehl, Electroporation: theory and methods, perspectives for drug delivery, gene
therapy and research, Acta. Physiol. Scand. 177 (2003) 437-447.

[10] S. Gintautas, Pore disappearance in a cell after electroporation: theoretical simulation
and comparison with experiments, Biophys. J. 73 (1997) 1299-1309.

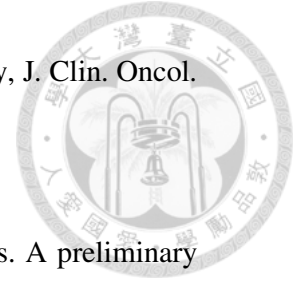
[11] J. Lekner, Electroporation in cancer therapy without insertion of electrodes, Phys.
Med. Biol. 59 (2014) 6031-6042.

[12] E. Neumann, S. Kakorin, K. Toensing, Fundamentals of electroporative delivery of
drugs and genes, Bioelectrochem. Bioenerg. 48 (1999) 3-16.

[13] E. Neumann, R. M. Schaefer, Y. Wang, P. H. Hofschneider, Gene transfer into
mouse lyoma cells by electroporation in high electric fields, EMBO J. 1 (1982) 841–845.



- [14] A. V. Titomirov, S. Sukharev, E. Kistanova, Biochim. In vivo electroporation and stable transformation of skin cells of newborn mice by plasmid DNA, *Biophys. Acta.* 1088 (1991) 131–134.
- [15] M. Cemazar, M. Golzio, G. Sersa, P. Hojman, S. Kranjc, S. Mesojednik, M. P. Rols, J. Teissie, Control by pulse parameters of DNA electrotransfer into solid tumors in mice, *Gene. Ther.* 16 (2009) 635–644.
- [16] L. C. Heller, R. Heller, In vivo electroporation for gene therapy, *Hum. Gene. Ther.* 17 (2006) 890–897.
- [17] G. J. Prud'homme, Y. Glinka, A. S. Khan, R. Draghia-Akli, Electroporation-enhanced nonviral gene transfer for the prevention or treatment of immunological, endocrine and neoplastic diseases, *Curr. Gene. Ther.* 6 (2006) 243–273.
- [18] L. G. Camapana, S. Mocellin, M. Basso, O. Puccetti, G. L. De Salvo, S. V. Chiarion, A. Vecchiato, L. Corti, C. R. Rossi, D. Nitti, Bleomycin-based electrochemotherapy: clinical outcome from a single institution's experience with 52 patients, *Ann. Surg. Oncol.* 16 (2009) 191-199.
- [19] J. Gehl, G. Serša, J. R. Garbay, D. Soden, Z. Rudolf, M. Marty, G. C. O'Sullivan, P. F. Geertsen, L. M. Mir, Results of the ESOPE (european standard operating procedures on electrochemotherapy) study: efficient, highly tolerable and simple palliative treatment



of cutaneous and subcutaneous metastases from cancers of any histology, *J. Clin. Oncol.* 24 (Suppl) (2006) s8047.

[20] M. P. Rols, Y. Tamzali, J. Teissié, Electrochemotherapy of horses. A preliminary clinical report, *Bioelectrochemistry* 55 (2002) 101-105.

[21] S. Satkauskas, D. Batiuskaite, D. S. Salomskaite, M. S. Venklauskas, Effectiveness of tumor electrochemotherapy as a function of electric pulse strength and duration, *Bioelectrochemistry* 65 (2005) 105-111.

[22] U. Pliquett, R. Elez, A. Piiper, E. Neumann, Electroporation of subcutaneous mouse tumors by rectangular and trapezium high voltage pulses, *Bioelectrochemistry* 62 (2004) 83-93.

[23] M. Belehradec, C. Domenge, B. Luboinski, S. Orłowski, J. J. Belehradec, L.M. Mir, Electrochemotherapy, a new antitumor treatment. First clinical phase i-ii trial, *Cancer* 72 (1993) 3694-3700.

[24] G. Schmidt, B. I Juhasz, E.F. Solomayer, D.Herr, Electrochemotherapy in breast cancer: a review of references, *Geburtshilfe Frauenheilkd* 74 (2014) 557-562.

[25] M. Lluis, J. Gehl, G. Sersa, C. G. Collins, J. R. Garbay, V. Billard, P. F. Geertsen, Z. Rudolf, G. C. O'Sullivan, M. Martyet, Standard operating procedures of the electrochemotherapy: instructions for the use of bleomycin or cisplatin administered



either systemically or locally and electric pulses delivered by the cliniporator™ by means of invasive or non-invasive electrodes, *E.J.C.* 4 (Suppl) (2006)14–25.

[26] G. Sersa, D. Miklavcic, Electrochemotherapy of tumours, *J. Vis. Exp.* 22 (2008) 1038.

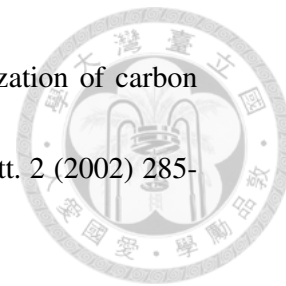
[27] V. Kasivisvanathan, A. Thapar, Y. Oskrochi, J. Picard, E. L. S. Leen, Irreversible electroporation for focal ablation at the porta hepatis, *Cardiovasc. Intervent. Radiol.* 35 (2012) 1531-1534.

[28] A. T. Esser, K. C. Smith, T. R. Gowrishankar, J. C. Weaver, Towards solid tumor treatment by irreversible electroporation: intrinsic redistribution of fields and currents in tissue, *Technol. Cancer. Res. Treat.* 6 (2007) 261–274.

[29] N. W. Kam, M. O'Connell, J. A. Wisdom, H. Dai, Carbon nanotubes as multifunctional biological transporters and near-infrared agents for selective cancer cell destruction, *Proc. Natl. Acad. Sci. U.S.A.* 102 (2005) 11600-11605.

[30] A. M. Smith, M. C. Mancini, S. Nie, Bioimaging: second window for in vivo imaging, *Nat. Nanotechnol.* 4 (2009) 710-711.

[31] A. D. L. Zerda, C. Zavaleta, S. Keren, S. Vaithilingam, S. Bodapati, Z. Liu, J. Levi, B. R. Smith, T. J. Ma, O. Oralkan, Z. Cheng, X. Chen, H. Dai, B. T. Khuri-Yakub, S. S. Gambhir, Carbon nanotubes as photoacoustic molecular imaging agents in living mice, *Nat. Nanotechnol.* 3 (2008) 557-562.



[32] M. Shim, N. W. S. Kam, R. J. Chen, Y. Li, H. Dai, Functionalization of carbon nanotubes for biocompatibility and biomolecular recognition, *Nano. Lett.* 2 (2002) 285-288.

[33] J. E. Podesta, K. T. Al-Jamal, M. A. Herrero, B. Tian, H. Ali-Boucetta, V. Hegde, A. Bianco, M. Prato, K. Kostarelos, Antitumor activity and prolonged survival by carbon-nanotube-mediated therapeutic siRNA silencing in a human lung xenograft model, *Small* 5 (2009) 1176-118.

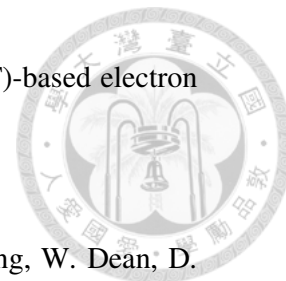
[34] L. Lacerda, S. Raffa, M. Prato, A. Bianco, K. Kostarelos, Cell-penetrating CNTs for delivery of therapeutics, *Nano Today* 2 (2007) 38-43.

[35] P. C. Lee, Y. C. Chiou, J. M. Wong, C. L. Peng, M. J. Shieh, Targeting colorectal cancer cells with single-walled carbon nanotubes conjugated to anticancer agent SN-38 and EGFR antibody, *Biomaterials* 34 (2013) 8756-8765.

[36] R. Saito, G. Dresselhaus, M. S. Dresselhaus, *Physical properties of carbon nanotube*, Imperial College Press. London, 2010, pp. 1-29.

[37] B. Kozinsky, N. Marzari, Static dielectric properties of carbon nanotubes from first principles, *Phys. Rev. Lett.* 96 (2006) 166801.

[38] C. J. A. Rojas, D. M. A. Correa, Z. Ren, K. Kempa, M. Giersig, Enhanced introduction of gold nanoparticles into vital acidithiobacillus ferrooxidans by carbon nanotube-based microwave electroporation, *Nano. Lett.* 4 (2004) 985-988.



[39] S. B. Grigory, V. E. Alexander, Theory of carbon nanotube (CNT)-based electron field emitters, *Nanomaterials* 3 (2013) 393-442.

[40] D. Cai, D. Blair, F. J. Dufort, M. R. Gumina, Z. Huang, G. Hong, W. Dean, D.

Canahan, K. Kempa, Z. F. Ren, T. C. Chiles, Interaction between carbon nanotubes and mammalian cells: characterization by flowcytometry and application, *Nanotechnology* 19 (2008) 1-10.

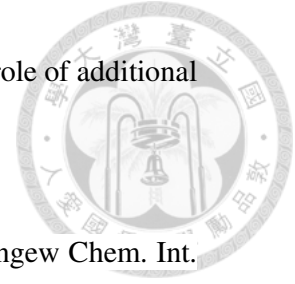
[41] V. Raffa, G. Ciofani, O. Vittorio, V. Pensabene, A. Cuschieri, Carbon nanotube-enhanced cell electropermeabilisation, *Bioelectrochemistry* 79 (2010) 136-141.

[42] M. Shahini, J. T. Yeow, Cell electroporation by CNT-featured microfluidic chip, *Lab. Chip.* 13 (2013) 2585-2590.

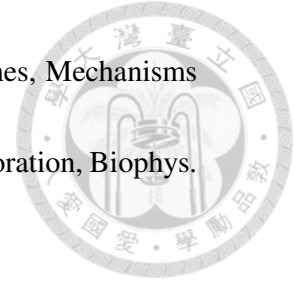
[43] L. Wang, D. Liu, R. Zhou, Z. Wang, A. Cuschieri, Tumour Cell Membrane Poration and Ablation by Pulsed Low-Intensity Electric Field with Carbon Nanotubes, *Int. J. Mol. Sci.* 16 (2015) 6890–6901.

[44] Z. Liu, A.C. Fan, K. Rakhra, S. Sherlock, A. Goodwin, X. Chen, Q. Yang, D.W. Felsher, H. Dai, Supramolecular stacking of doxorubicin on carbon nanotubes for in vivo cancer therapy. *Angew. Chem. Int. Ed. Engl.* 48 (2009) 7668-72.

[45] C. W. James, Electroporation: a general phenomenon for manipulating cells and tissues, *J. Cell Biochem.* 51 (1993) 426-435.



- [46] S. Cecilia, S. Alejandro, M. Felipe, O. Nahuel, M. Guillermo, The role of additional pulses in electroporation protocols, *Plos One* 9 (2014) e113413.
- [47] A. Hirsch, Functionalization of single-walled carbon nanotubes. *Angew Chem. Int. Ed. Engl.* 41 (2002) 1853-1859.
- [48] Z. Jin, Z. Hongling, Q. Quan, Y. Yanlian, L. Qingwen, L. Zhongfan, G. Xinyong, D. Zuliang, Effect of Chemical Oxidation on the Structure of Single-Walled Carbon Nanotubes, *J. Phys. Chem. B* 107(2003) 3712-3718
- [49] C. S. Kyle, C. N. John, K. Wanda, Model of creation and evolution of stable electropores for DNA delivery, *Biophys. J.* 86 (2004) 2813–2826.
- [50] M. E. Jean, P. Thomas, W. Luc, T. Justin, D. David, P. R. Marie, What is (still not) known of the mechanism by which electroporation mediates gene transfer and expression in cells and tissues, *Mol. Biotechnol.* 41 (2009) 286–295.
- [51] A. Z. David, W. Joshua, B. M. Henshaw, Y. Fan, Mechanistic analysis of electroporation-induced cellular uptake of macromolecule, *Exp. Biol. Med.* (Maywood) 233 (2008) 94–105.
- [52] S. Sandra, R. Paulius, Š. Ingrida, Č. Karolina, Š. Saulius, The dependence of efficiency of transmembrane molecular transfer using electroporation on medium viscosity, *J. Gene. Med.* 17 (2015) 80–86.



[53] T. E. Axel, C. S. Kyle, T. R. Gowrishankar, V. Zlatko, C. W. James, Mechanisms for the intracellular manipulation of organelles by conventional electroporation, *Biophys. J.* 98 (2010) 2506–2514.

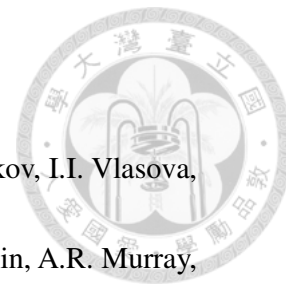
[54] P. C. Kevin, W. Farrah, N. Lelia, W. Brody, R. Murray, E. D. Damian, Irreversible electroporation of the pancreas in swine: a pilot study, *H. P. B. (Oxford)* 12 (2010) 348–351.

[55] G. Sersa, T. Jarm, T. Kotnik, A. Coer, M. Podkrajsek, M. Sentjurc, D. Miklavcic, M. Kadivec, S. Kranjc, A. Secerov, M. Cemazar, Vascular disrupting action of electroporation and electrochemotherapy with bleomycin in murine sarcoma, *Br. J. Cancer.* 98 (2008) 388-398.

[56] C. Kanthou, S. Kranjc, G. Sersa, G. Tozer, A. Zupanic, M. Cemazar, The endothelial cytoskeleton as a target of electroporation-based therapies, *Mol. Cancer Ther.* 5 (2006) 3145-3152.

[57] H.J. Scheffer, K. Nielsen, M.C. de Jong, A.A. van Tilborg, J.M. Vieveen, A.R. Bouwman, S. Meijer, C. van Kuijk, P.M. van den Tol, M.R. Meijerink, Irreversible electroporation for nonthermal tumor ablation in the clinical setting: A systematic review of safety and efficacy. *J. Vasc. Interv. Radiol.* 25 (2014) 997–1011.

[58] Z. Liu, C. Davis, W. Cai, L. He, X. Chen, H. Dai, Circulation and long-term fate of functionalized, biocompatible single-walled carbon nanotubes in mice probed by Raman



spectroscopy. *Proc. Natl. Acad. Sci. U. S. A.* 105 (2008) 1410-1415.

[59] V.E. Kagan, N.V. Konduru., W. Feng, B.L. Allen, J. Conroy, Y. Volkov, I.I. Vlasova, N.A. Belikova, N. Yanamala, A. Kapralov, Y.Y. Tyurina, J. Shi, E.R. Kisin, A.R. Murray,

J. Franks, D. Stolz, P. Gou, J. Klein-Seetharaman, B. Fadeel, A. Star, A.A. Shvedova,

Carbon nanotubes degraded by neutrophil myeloperoxidase induce less pulmonary inflammation, *Nat. Nanotechnol.* 5 (2010) 354-359.

[60] D. Elgrabli, W. Dachraoui, C. Ménard-Moyon, X.J. Liu, D. S. Bégin, Bégin-Colin,

A. Bianco, F. Gazeau, D. Alloyeau, Carbon Nanotube Degradation in Macrophages: Live

Nanoscale Monitoring and Understanding of Biological Pathway, *ACS Nano.* 9

(2015)10113-101124.

[61] W.R. Panje, N. Sadeghi, Endoscopic and electroporation therapy of paranasal sinus

tumors, *Am. J. Rhinol.* 14 (2000) 187-191.

[62] C. P. Swain, I. Lu, Endoscopic Mucosal Dissection in GI Malignancies. *Ann.*

Gastroenterol. 23 (2010) 172-179.

[62] O. Taratula, B. S. Doddapaneni, C. Schumann, X. Li, S. Bracha, M. Milovancev, A.

W. G. Alani, O. Taratula, Naphthalocyanine-Based Biodegradable Polymeric

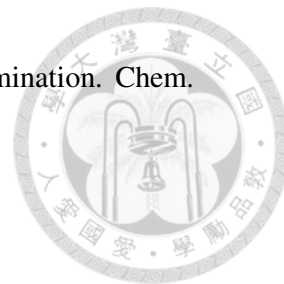
Nanoparticles for Image-Guided Combinatorial Phototherapy. *Chem. Mater.* 27 (2015)

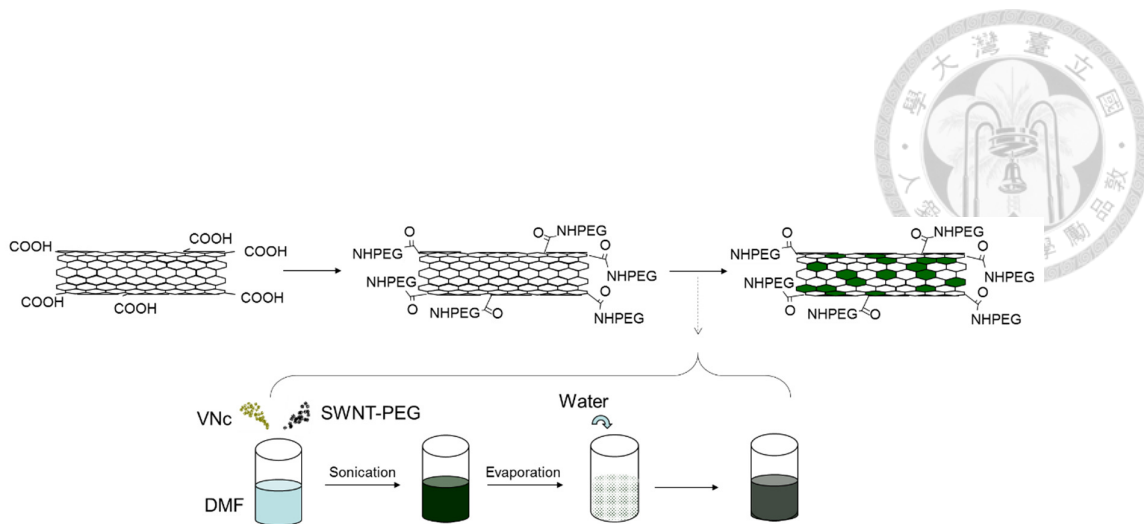
6155–6165.

[63] S. Visentin, N.Barbero, S. Musso, V. Mussi, C. Biale, R. Ploeger, G. Viscardi, A

Sensitive and Practical Fluorimetric Test for CNT Acidic Site Determination. Chem.

Commun. (Camb) 46 (2010) 1443-1445.





Scheme 1. Synthetic scheme for the fabrication of SWNT/PEG-VNc.

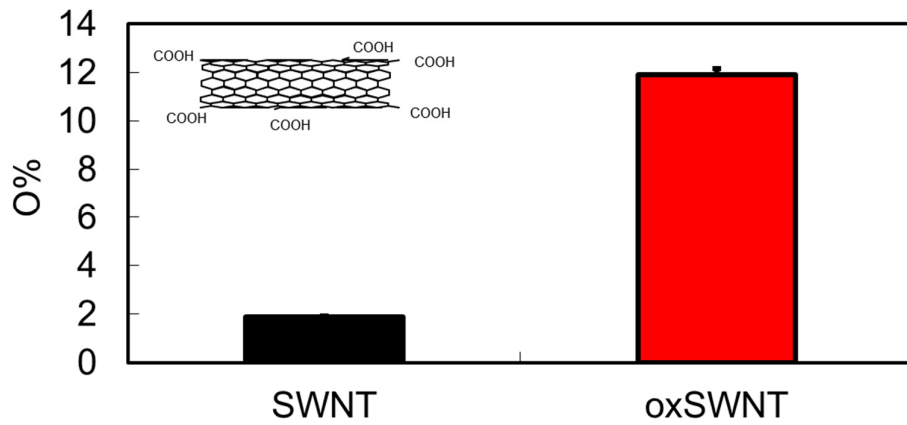


Fig 1. Elemental analysis of SWNT and oxidized SWNT.

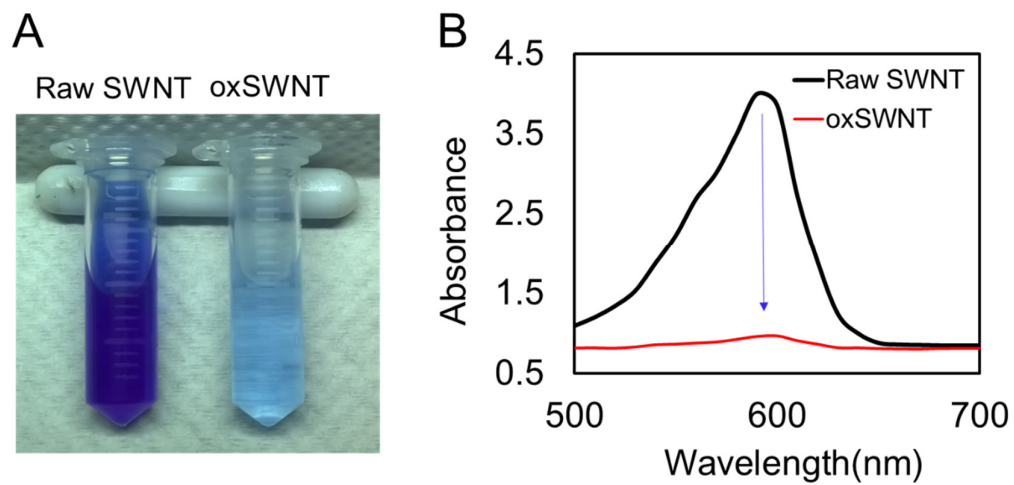


Fig. 2. (A) Difference in fluorescence emission after mixing THA stock solution with raw SWNT or oxidized SWNT. (B) Fluorescent spectra of THA in the presence of raw SWNT and oxidized SWNT

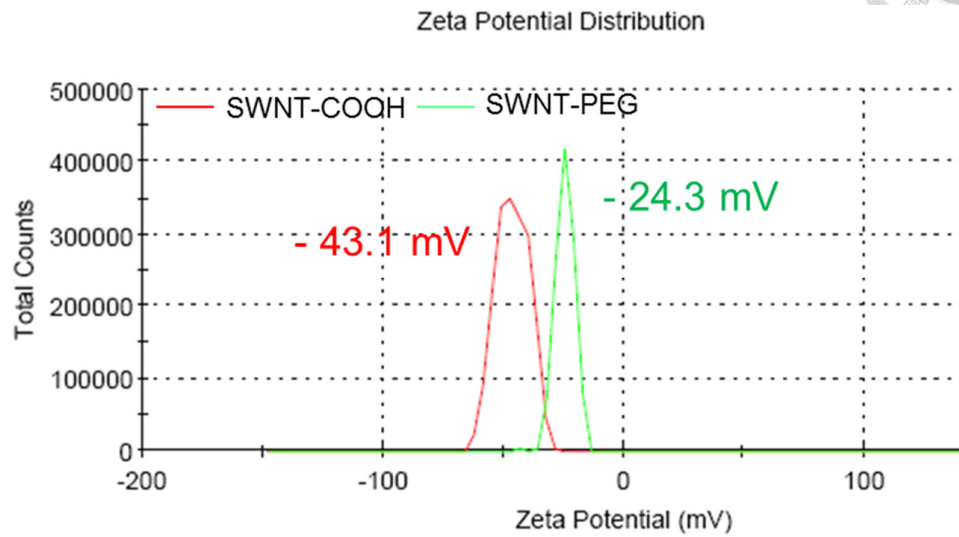


Fig. 3. Zeta potential distribution of SWNT-COOH and SWNT-PEG were analyzed by DLS.

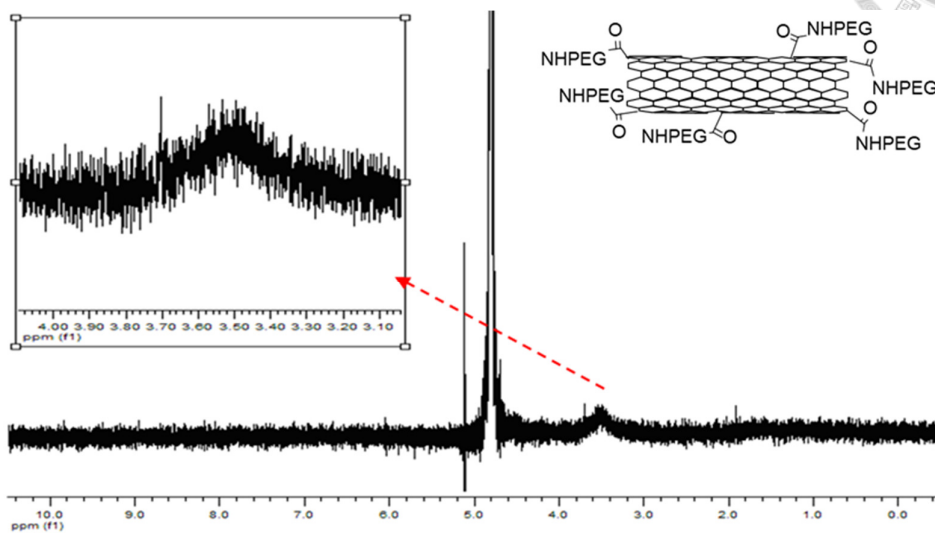


Fig. 4. ^1H -NMR spectrum of SWNT-PEG. The arrow indicates the characteristic peak of PEG at approximately 3.5 ppm.

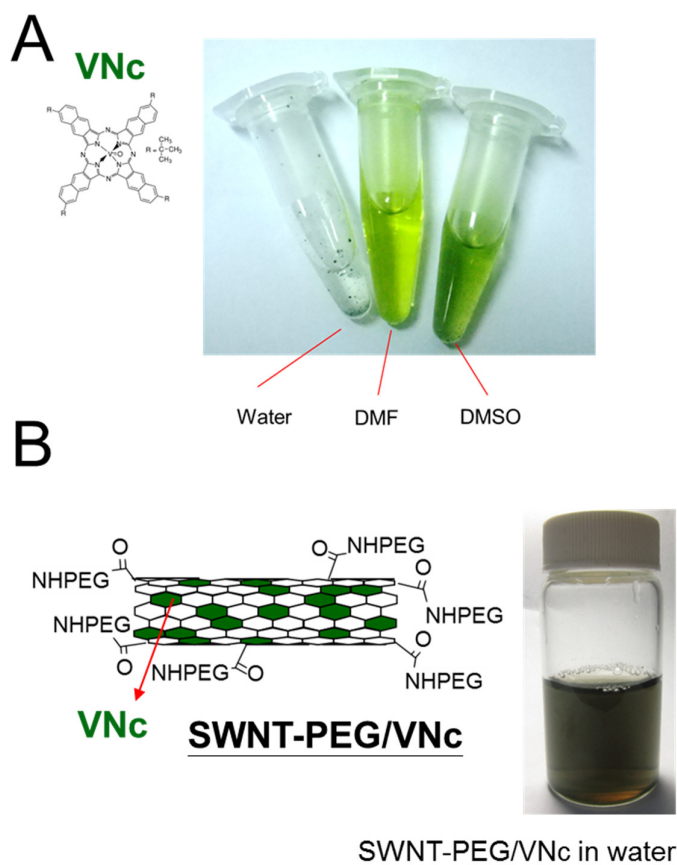


Fig. 5. (A) VNc suspended in water, DMF and DMSO. (B) SWNT-PEG/VNc suspended in water.

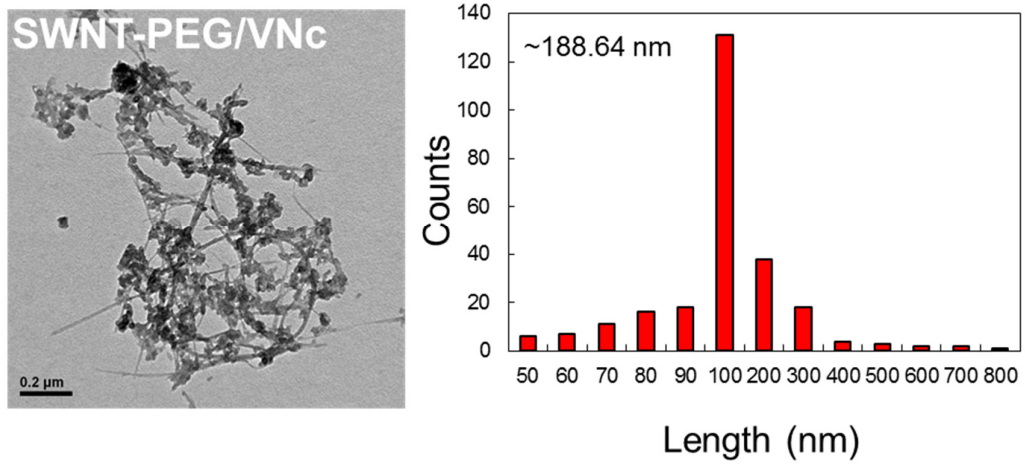


Fig. 6. TEM image of SWNT-PEG/VNc. The length of SWNT-PEG/VNc deduced from TEM image was approximately 188.64 nm.

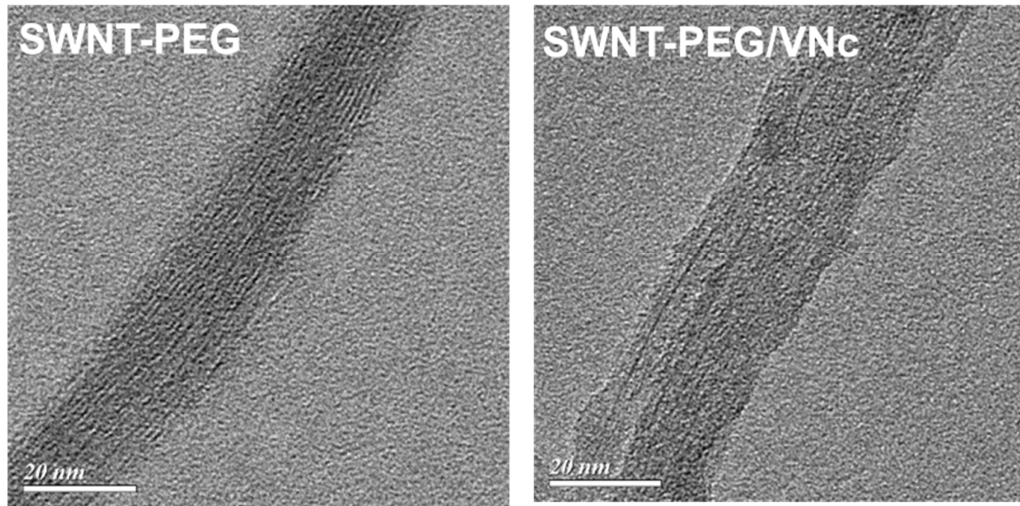


Fig. 7. HRTEM of SWNT-PEG and SWNT-PEG/VNc.

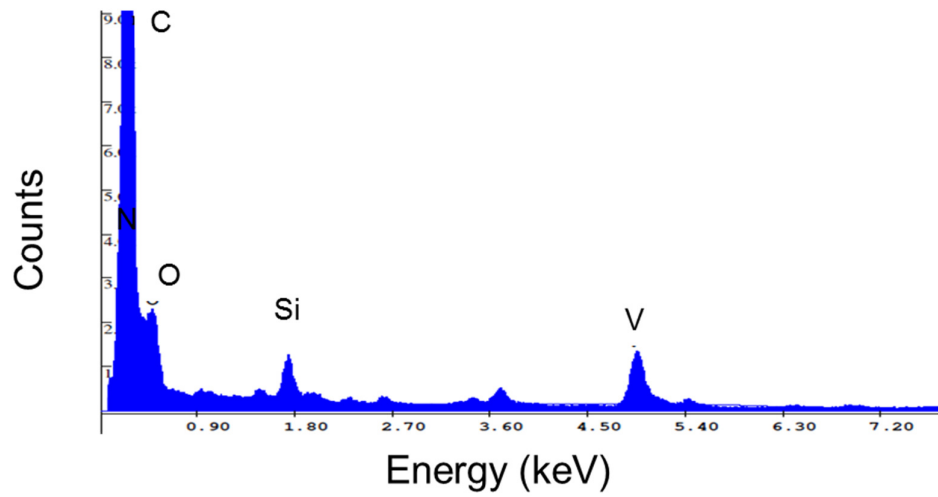


Fig. 8. Representative EDX spectra of SWNT-PEG/VNc.

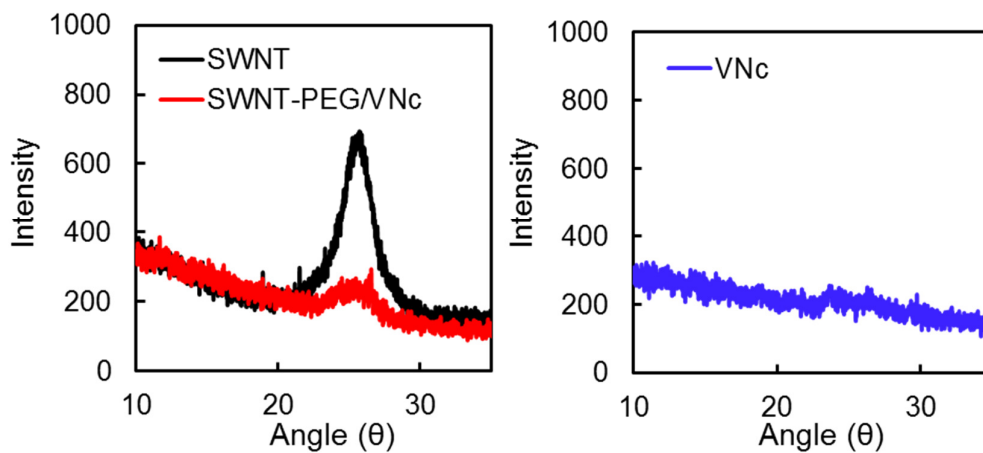


Fig. 9. X-ray diffraction analysis of SWNT, SWNT-PEG/VNc and VNc.

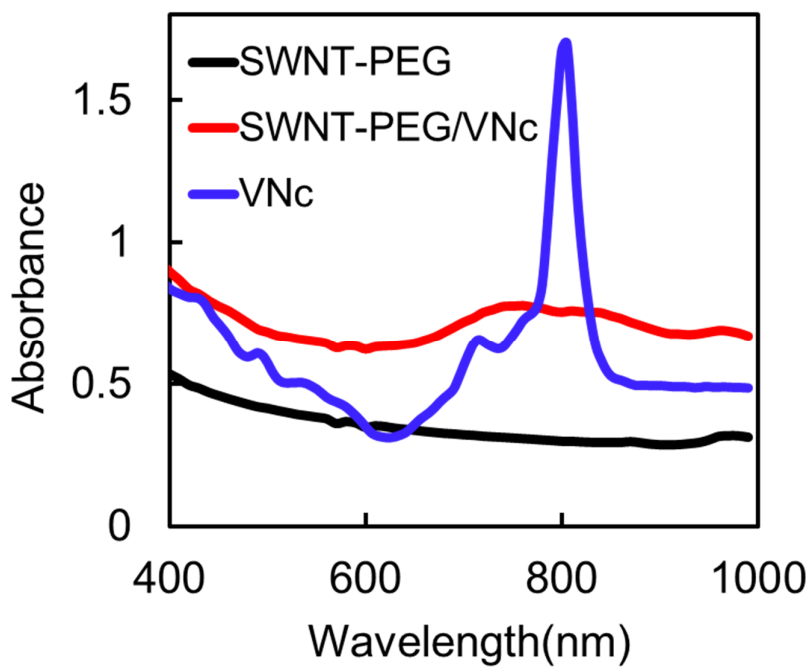


Fig. 10. UV-visible absorbance spectra of VNc (blue), SWNT-PEG/VNc (red), and SWNT-PEG (black).

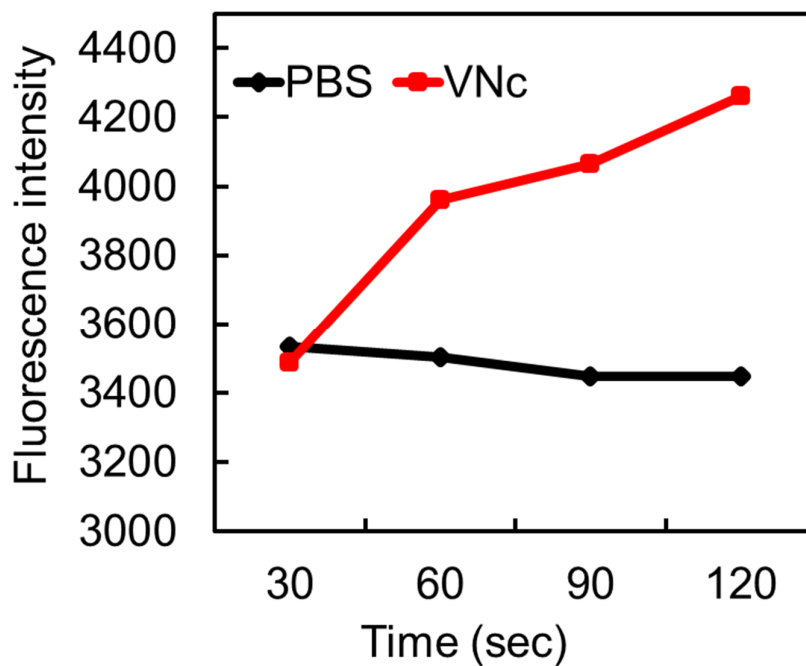


Fig. 11. Singlet oxygen generation of VNC in DMSO by Singlet Oxygen Sensor Green reagent. The sample was exposed to irradiation (808 nm) for $^1\text{O}_2$ generation

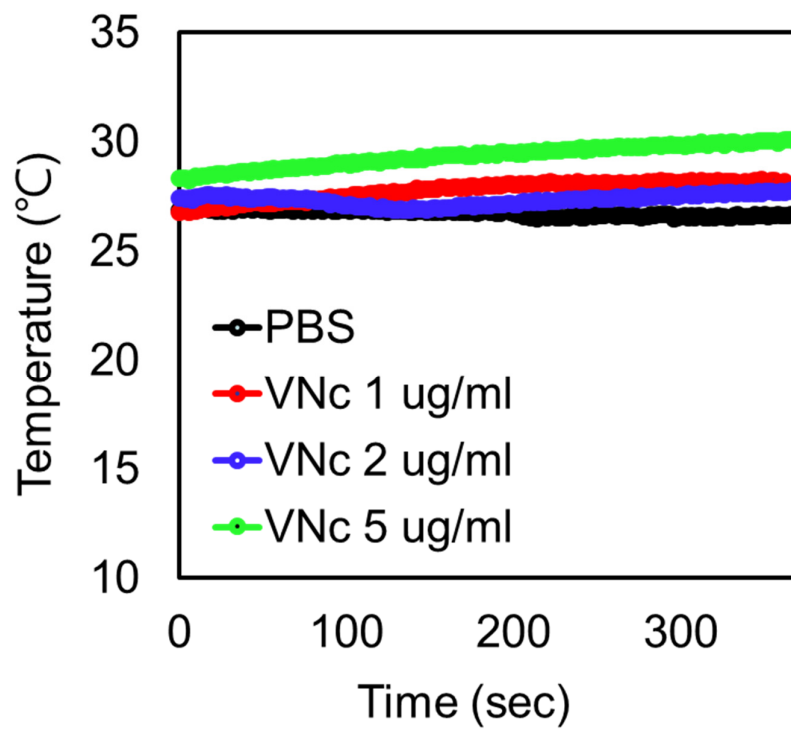
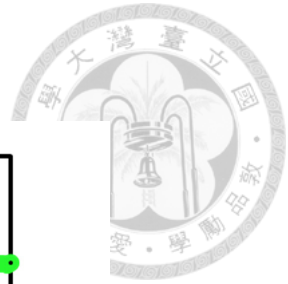


Fig. 12. The thermal curves and of PBS and VNC (1, 2, 5 $\mu\text{g/ml}$ in DMSO) under 808 nm laser irradiation at 1.3 W/cm^2 for 5 min.

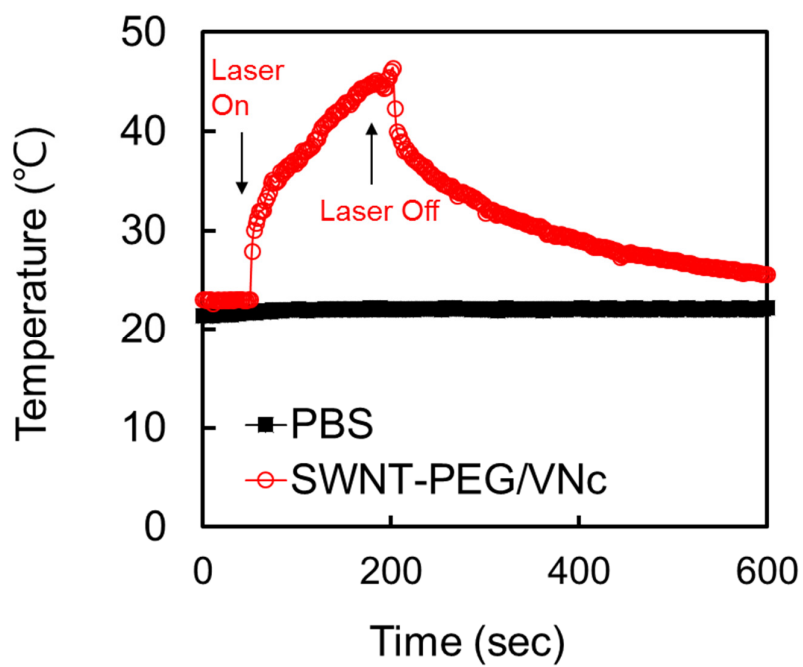


Fig. 13. The thermal curves and of PBS and SWNT-PEG/VNc under 808 nm laser irradiation at 1.3 W/cm² for 3 min.

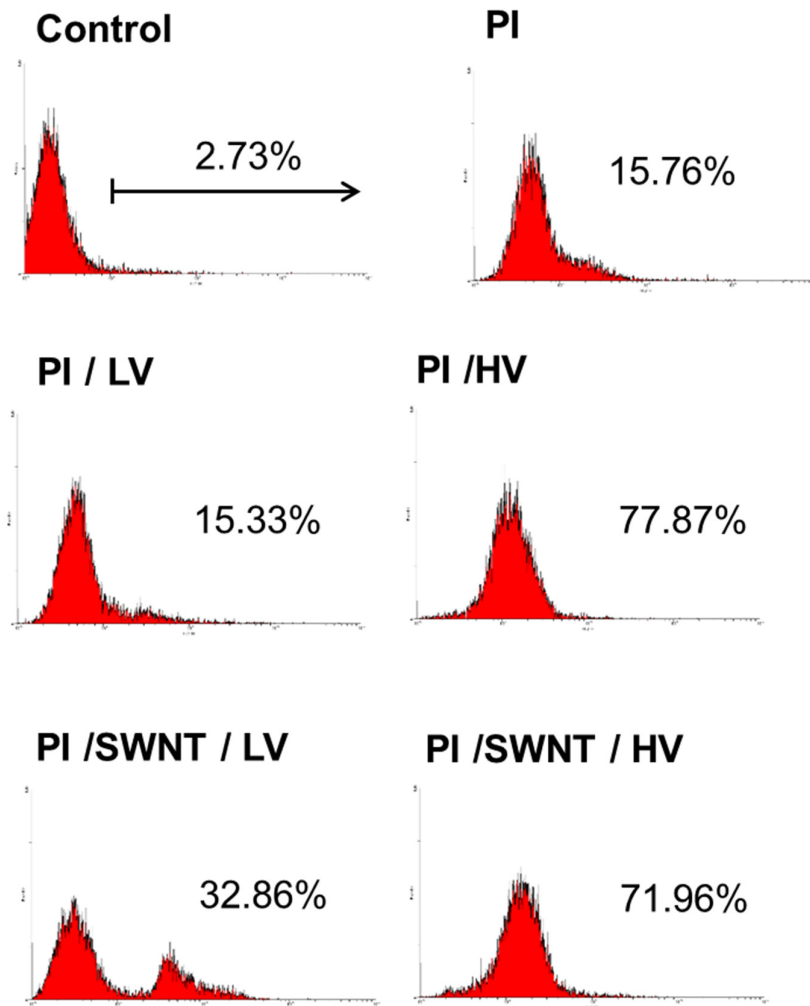


Fig. 14. PI signals of HT-29 cells detected by flow cytometry. We used pulsing buffer with (PI/SWNT/LV and PI/SWNT/HV group) or without SWNT (PI/HV and PI/LV group) during the pulsation.

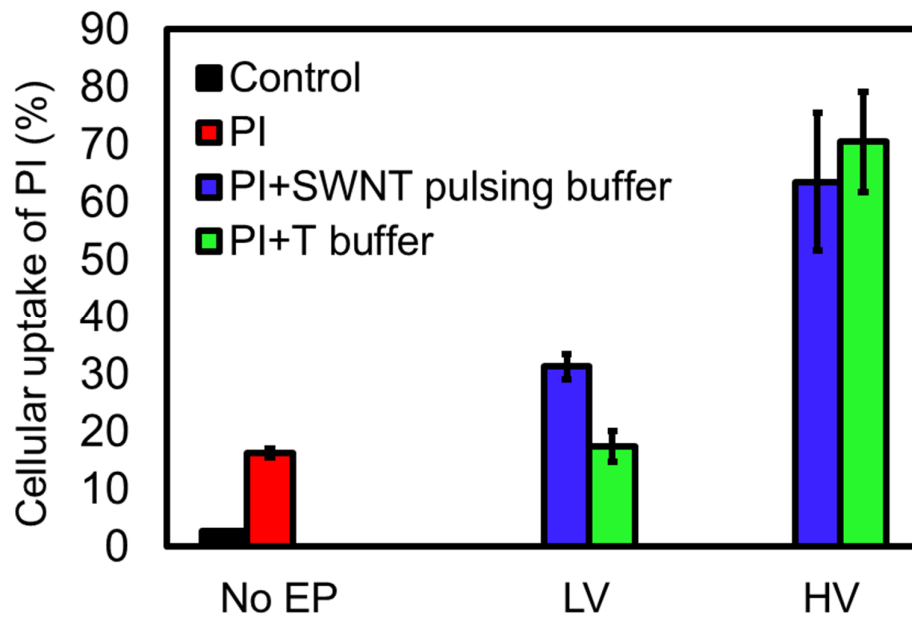
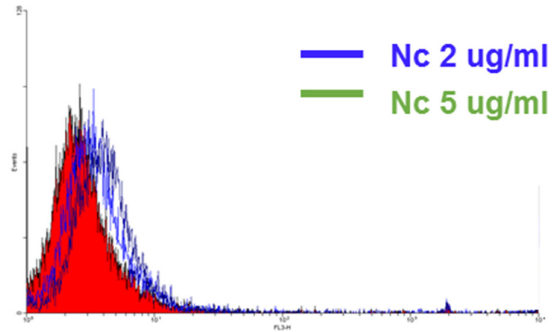


Fig. 15. The data of histogram correspond to (Fig. 14).



SWNT-PEG/VNc



SWNT-PEG/VNc + EP

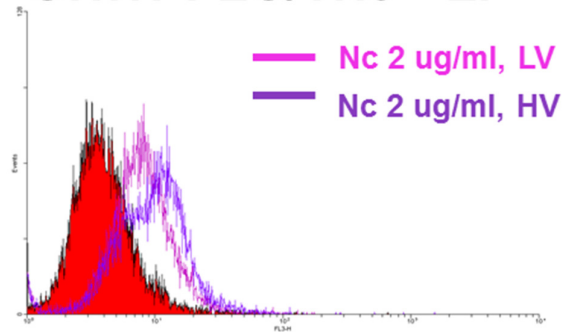


Fig. 16. The cellular uptake of SWNT-PEG/VNc treated to HT-29 cells. (A) No EP group.

(B) EP group. HV (1600 V, 10 ms, 3 pulses); LV (50 V, 40 ms, 100 pulses).

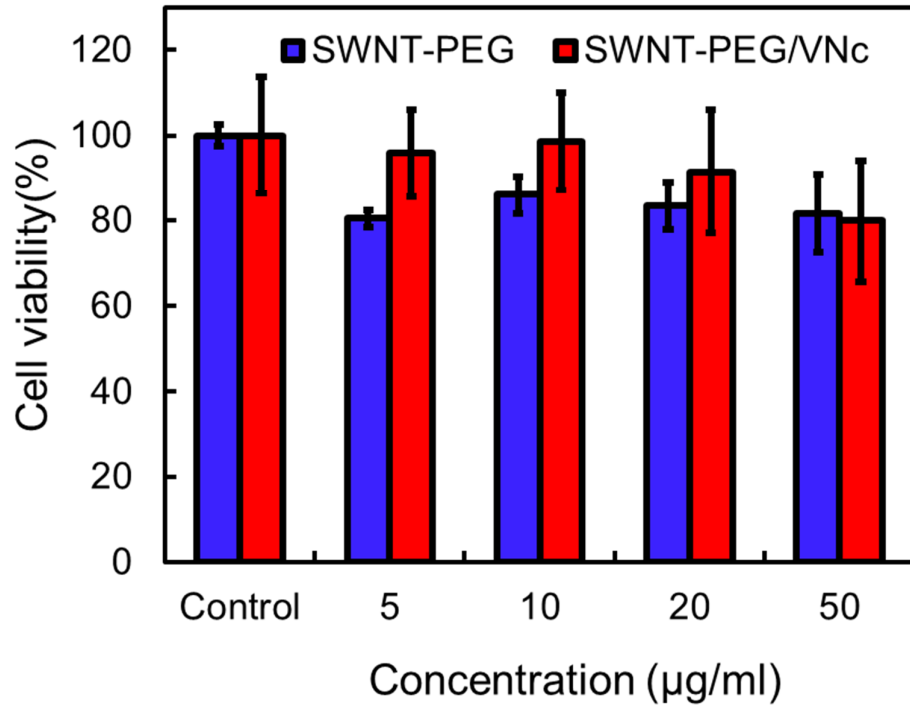


Fig. 17. Cell viability of HT-29 cells treated with SWNT-PEG and SWNT-PEG/VNc for 24 h.

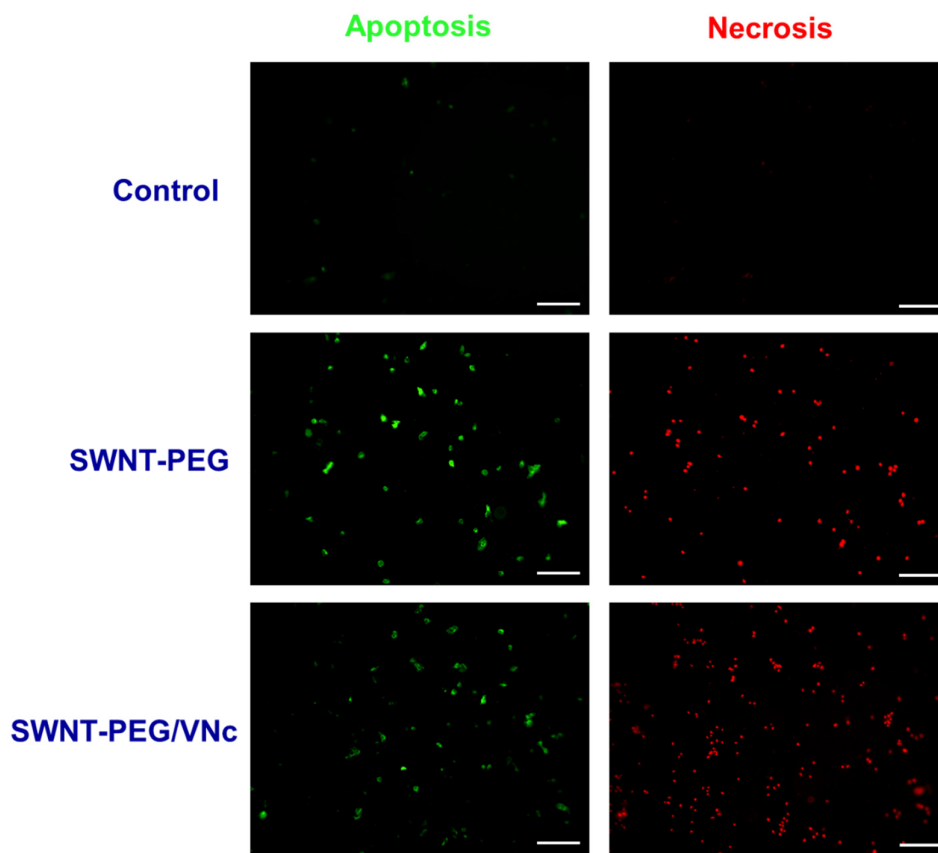


Fig. 18. Apoptosis and necrosis assay of the cells detected by fluorescence microscopy after incubation with SWNT-PEG and SWNT-PEG/VNc for 24 h with laser irradiation.

(scale bar = 100 μm)

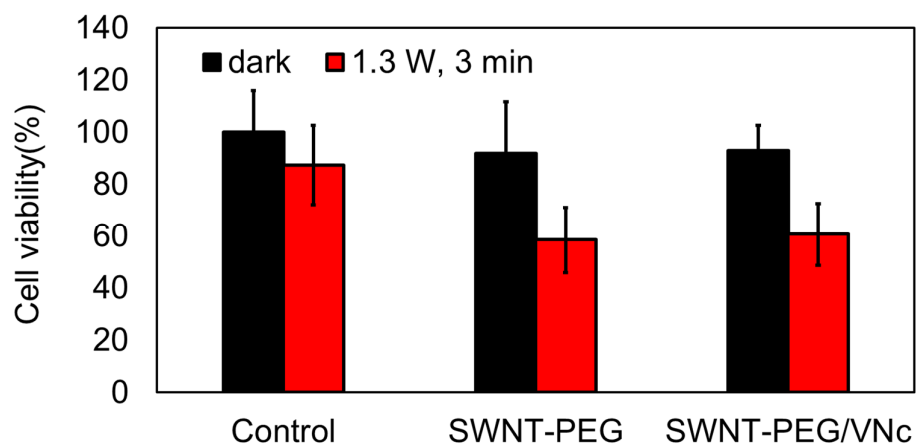


Fig. 19. Cell viability of HT-29 cells after incubation with SWNT-PEG and SWNT-PEG/VNc for 24 h with or without laser irradiation.

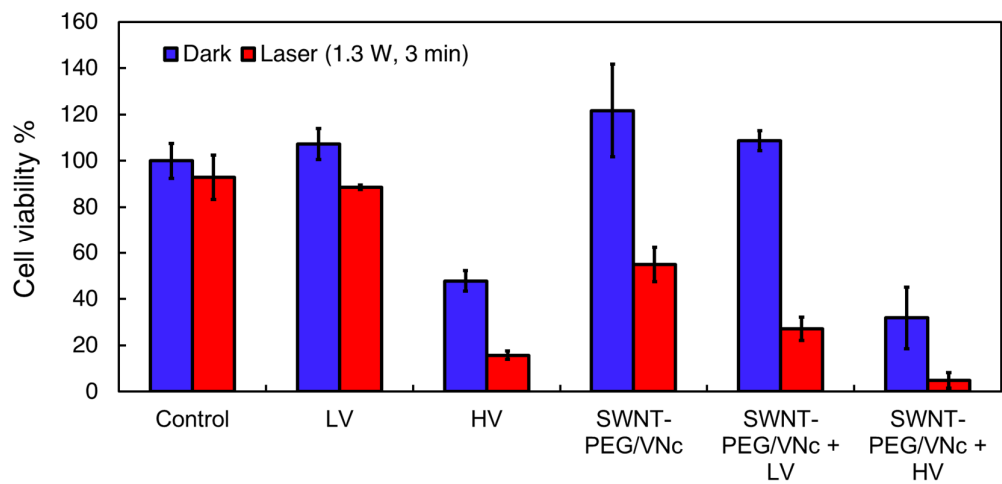


Fig. 20. The comparison of cell viability of HT-29 cells under different treatment.

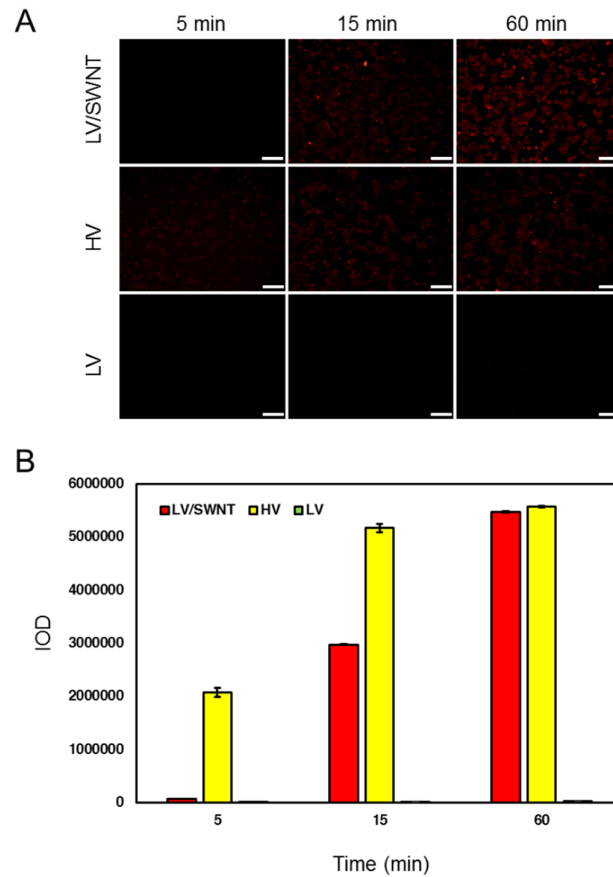


Fig. 21. (A) Pulsing buffer with (LV/SWNT group) or without (HV and LV group) SWNT during the pulsation. The fluorescence of the PI signal expression of HT-29 cells at 5, 15, and 60 min after transfecting with PI dye under HV (1600 V, 10 ms, 3 pulses) and LV (50 V, 40 ms, 100 pulses) electro-pulses (scale bar = 100 μ m). (B) The integrated optical density (IOD) of the PI signal expression from the fluorescence image (A)

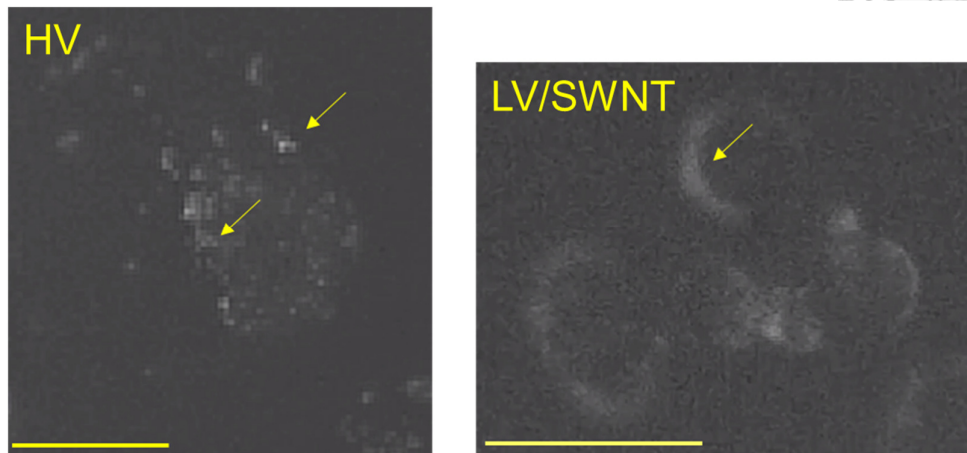


Fig. 22. Fluorescence micrographs captured from movie at 40 min of HV and LV/SWNT groups after being transfected with the PI dye (Gray scale) (scale bar = 25 μm).

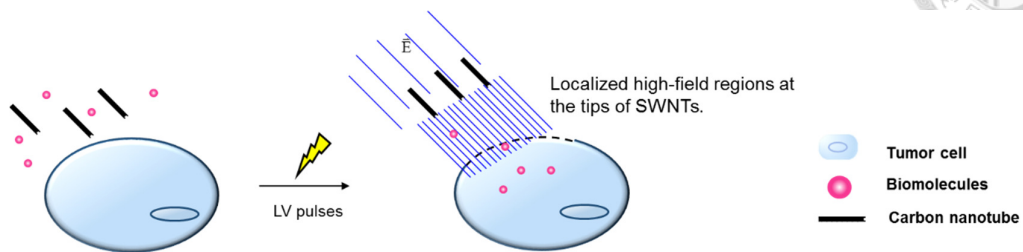


Fig. 23. Concept of electric stimulation enhancement by CNTs. After giving the LV pulses, the electric stimulation is amplified by CNTs at their tips so that the cell electropermeabilization could occur, and the delivery efficiency of biomolecules could be enhanced

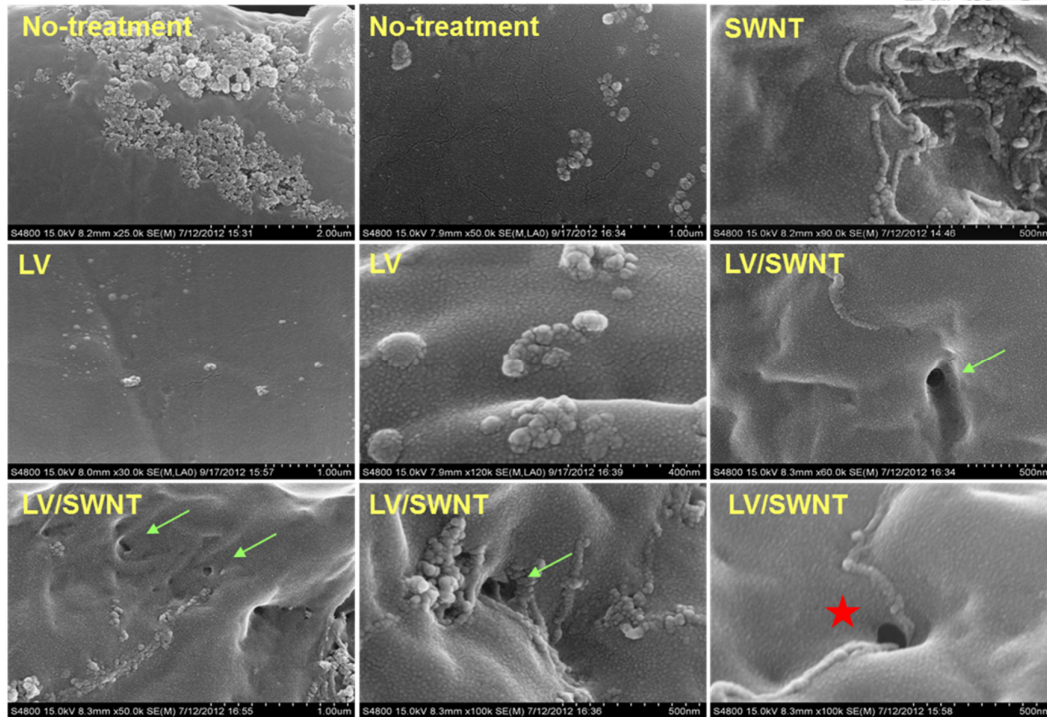


Fig. 24. High magnification of field emission electron micrographs in the near-membrane region following *in vitro* cellular exposure to no-treatment, LV, and LV combined with SWNT pulsing buffer. Green arrows demonstrated SWNT-like structures around the pore in the surface of the cell membrane. The red star indicated the SWNT-like structures appearing proximal in the pore.

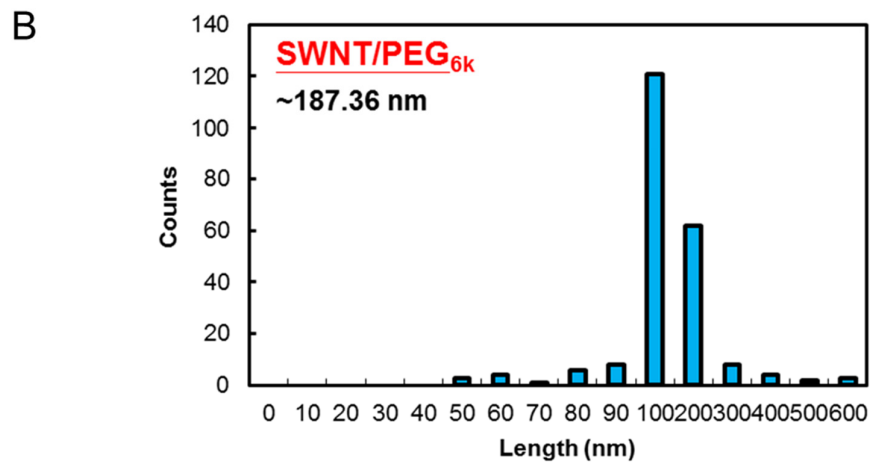
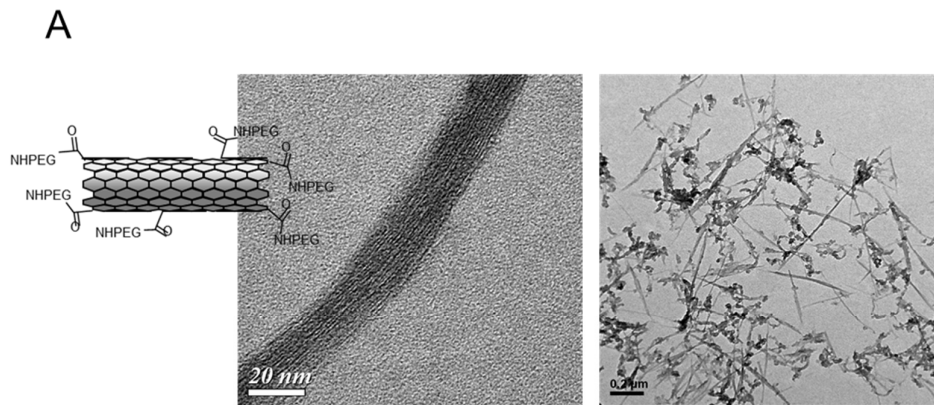


Fig. 25. (A) TEM image of SWNT-PEG_{6k}. High magnification of the TEM images showed that the diameter of SWNT-PEG_{6k} was approximately 20 nm. (B) Size distribution of SWNT-PEG_{6k} was deduced from (B). The length of SWNT-PEG_{6k} was approximately 187.36 nm.

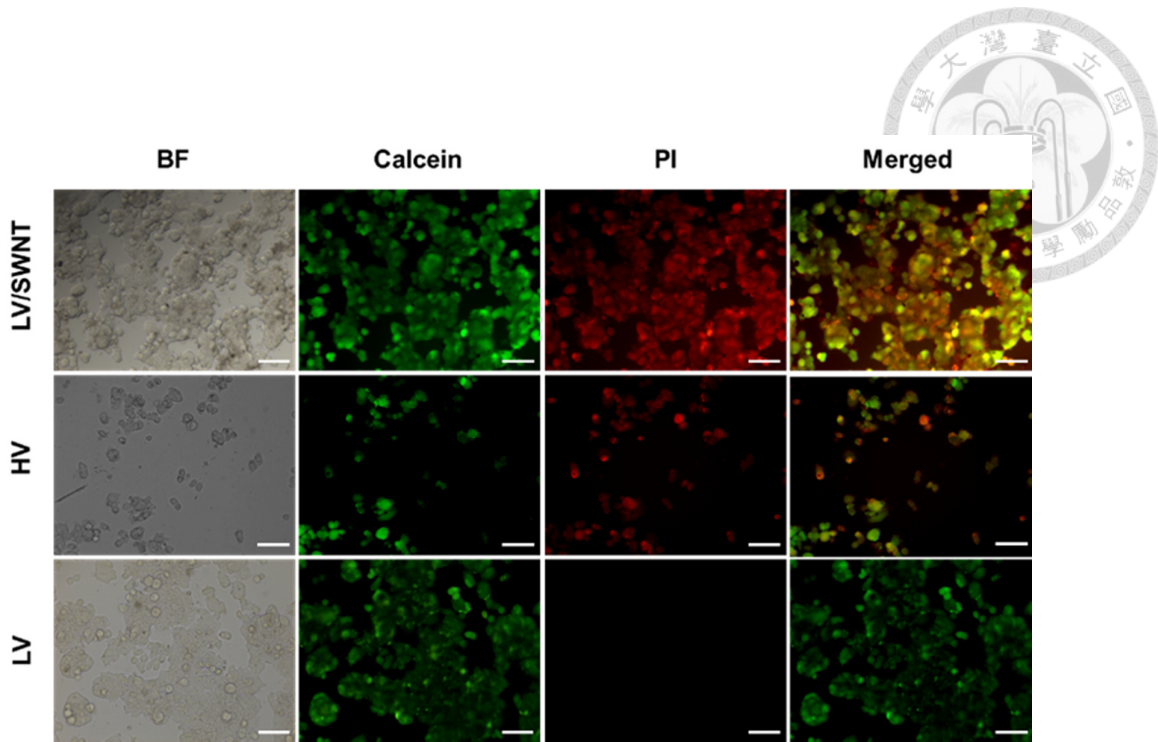


Fig. 26. Cell viability after treatment with different intensities of electrical stimulations.

The HT-29 cells were transfected with the PI dye under HV (1600 V, 10 ms, 3 pulses) and LV (50 V, 40 ms, 100 pulses) pulses. At 24 h after EP, the cell viability was assessed by staining with calcein AM. (SWNT pulsing buffer = LV/SWNT group, pulsing buffer without SWNT = HV and LV group). Live cells appeared to be green (calcein AM), cellular uptake with PI appeared to be red, and the merged images appeared to be yellow (scale bar = 50 μm).

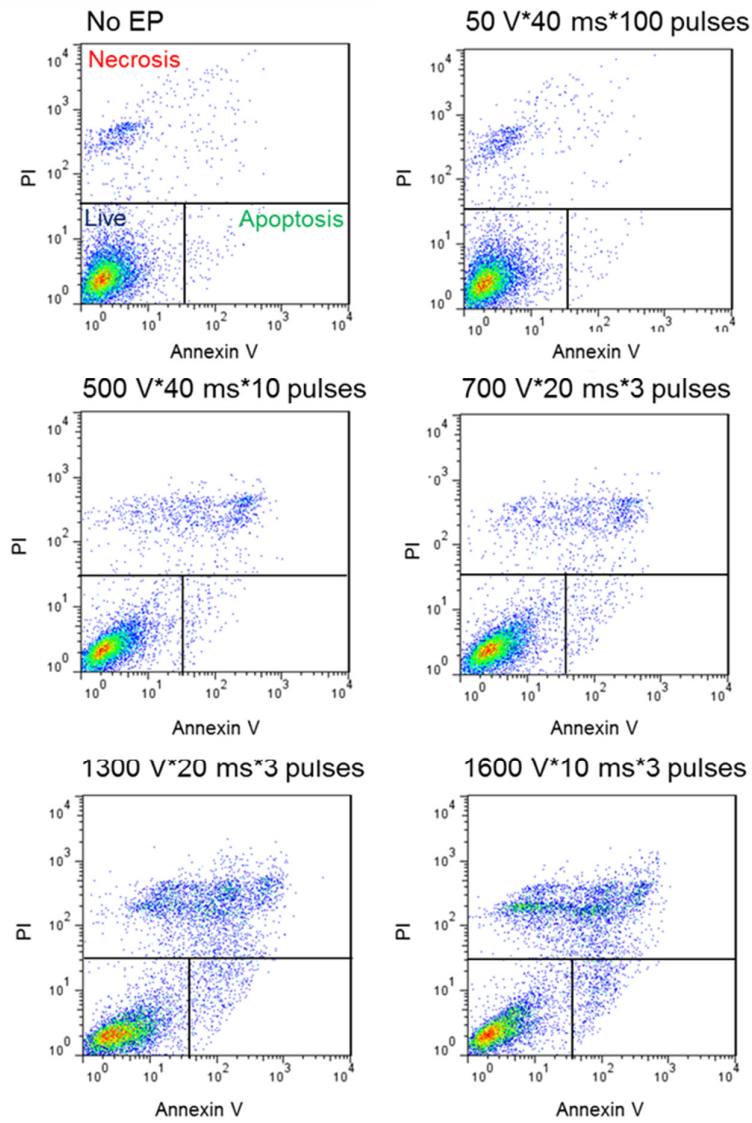


Fig. 27. Apoptosis and necrosis assay of the cells detected by flow cytometry after different EP conditions (Control; 50 V, 40 ms, 100 pulses; 100 V, 40 ms, 50 pulses; 50 V, 40 ms, 10 pulses; 700 V, 20 ms, 3 pulses; 1300 V, 20 ms, 3 pulses; 1600 V, 10 ms, 3 pulses).

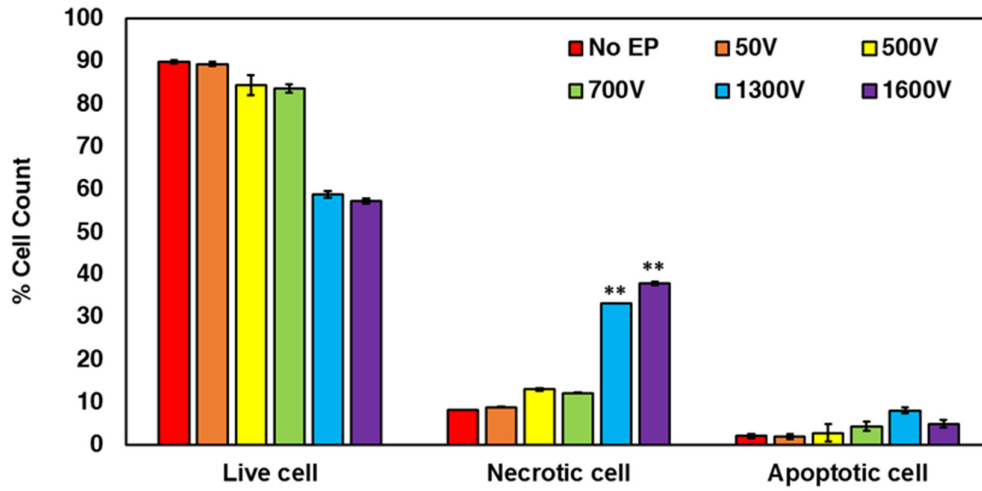


Fig. 28. The data of histogram correspond to (B). The results showed the obvious escalation of necrotic cells when the applied voltage was increased.

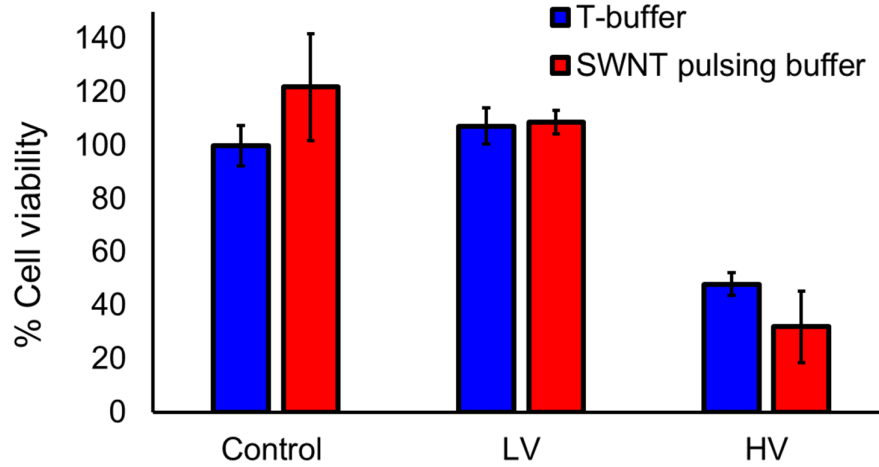


Fig. 29. Cell viability of HT-29 cells exposed to LV (50 V, 40 ms, 100 pulses) and HV (1600 V, 10 ms, 3 pulses) pulses by using SWNT pulsing buffer and commercial T-buffer®.

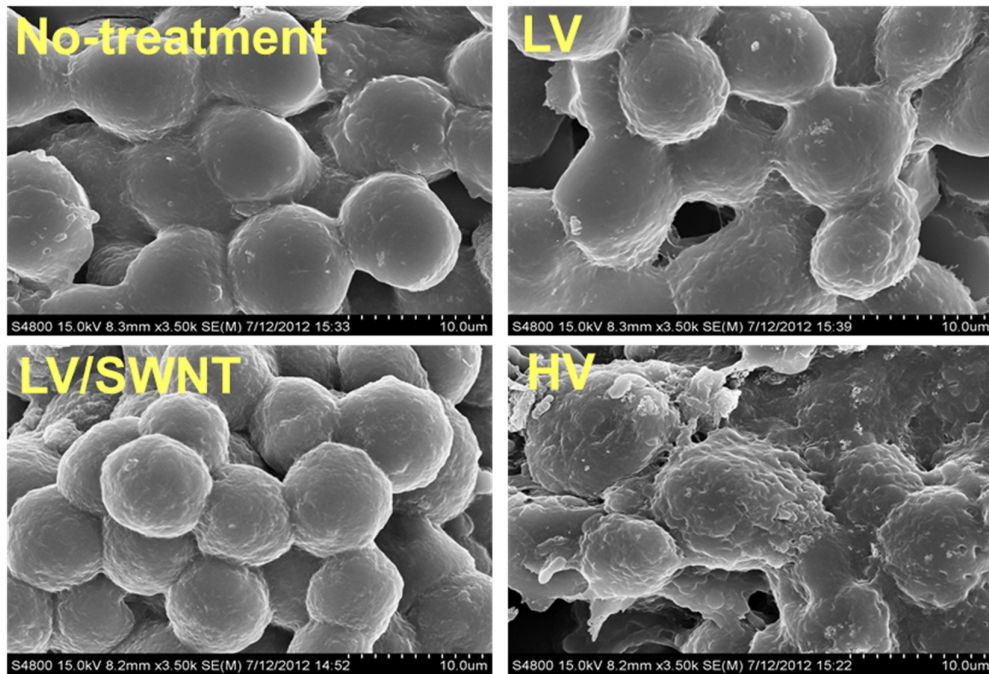
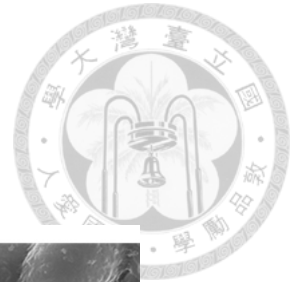


Fig. 30. Investigation of cell morphology. (A) The SEM images showed the cells following fixation immediately after receiving LV (50 V, 40 ms, 100 pulses) and HV (1600 V, 10 ms, 3 pulses) electric stimulation (SWNT pulsing buffer = LV/SWNT group, pulsing buffer without SWNT = HV and LV group).

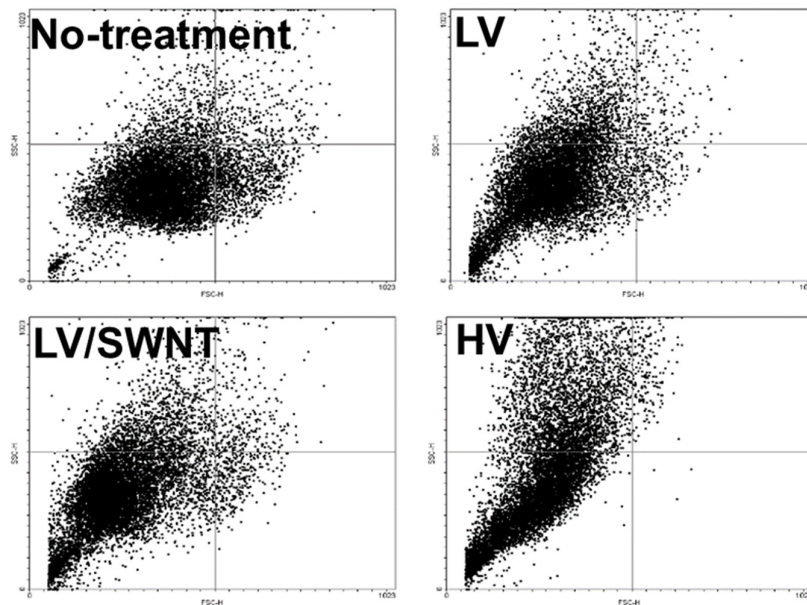


Fig. 31. Dot plot representations of flow cytometry data showed the cell size and granularity after the same EP condition from **Fig. 30**.

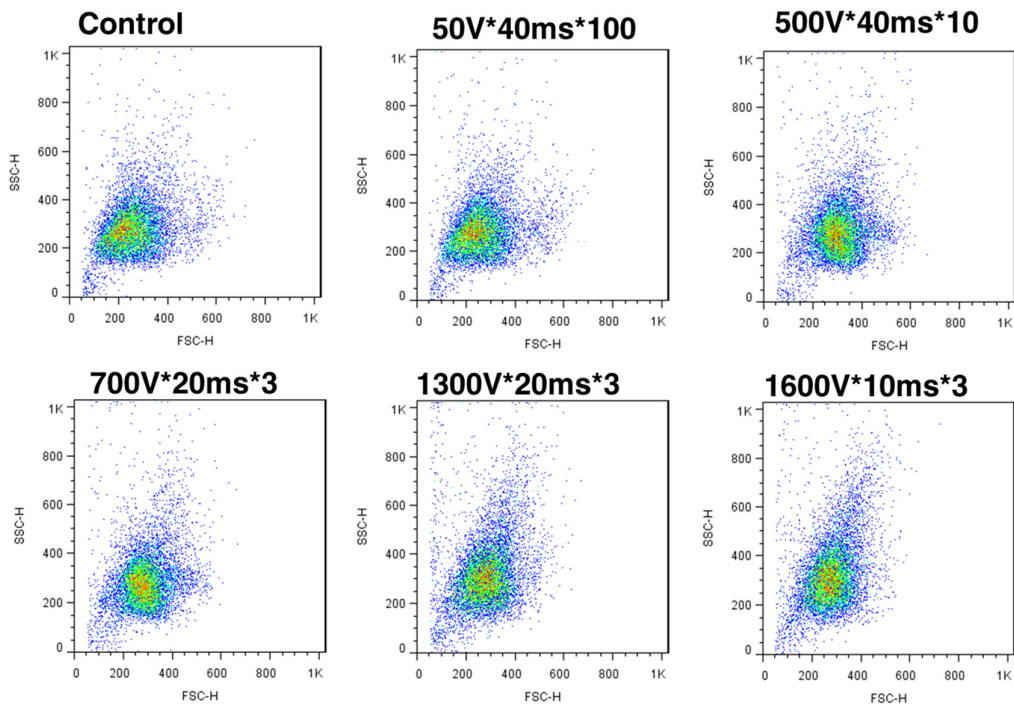
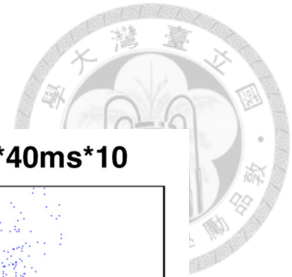


Fig. 32. Dot plot data from flow cytometry showing the morphology change of cells after different EP conditions. Compared to the control (no EP) group, the cells treated by HV (1300V * 20 ms * 3 pulses and 1600 V * 10 ms * 3 pulses) stimulation revealed that the cell size (FSC-H) decreased while the cell granularity (SSC-H) increased.

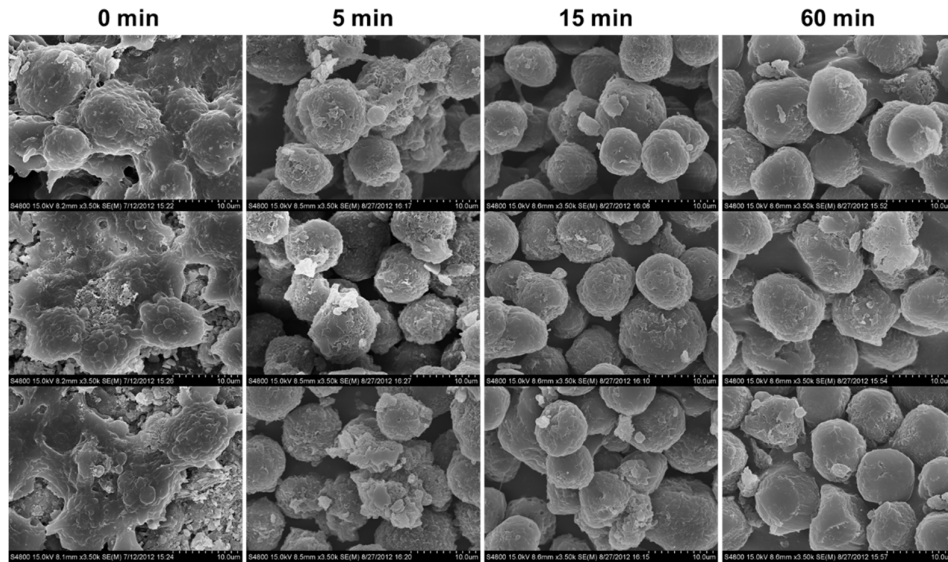
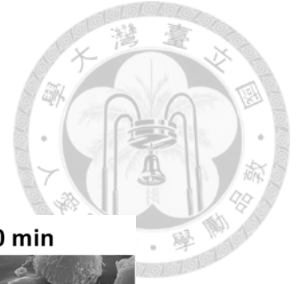


Fig. 33. The SEM images showed the cells following fixation at 0, 5, 15, and 60 min after receiving HV (1600 V, 10 ms, 3 pulses) electric stimulation.

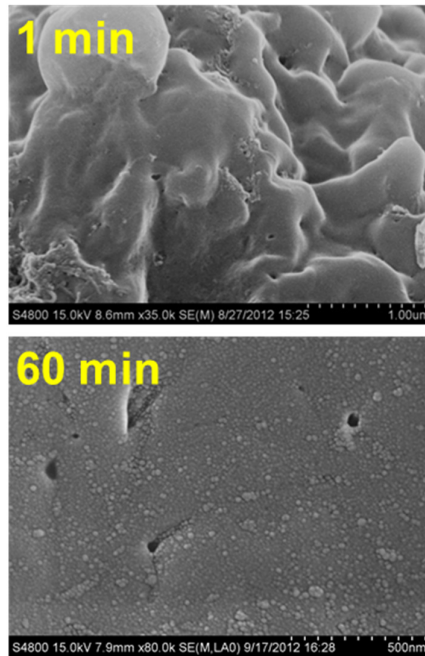


Fig. 34. Scanning electron microscope images of the cells. Cell membrane appearances at 1 and 60 min after exposing to LV/SWNT electrical stimulation. Pores were easily identified within the surface of cells at 1 min after EP. However, the pore numbers were decreased at 60 min after EP. Green arrows showed the pores distributed numerously on the cell membrane.

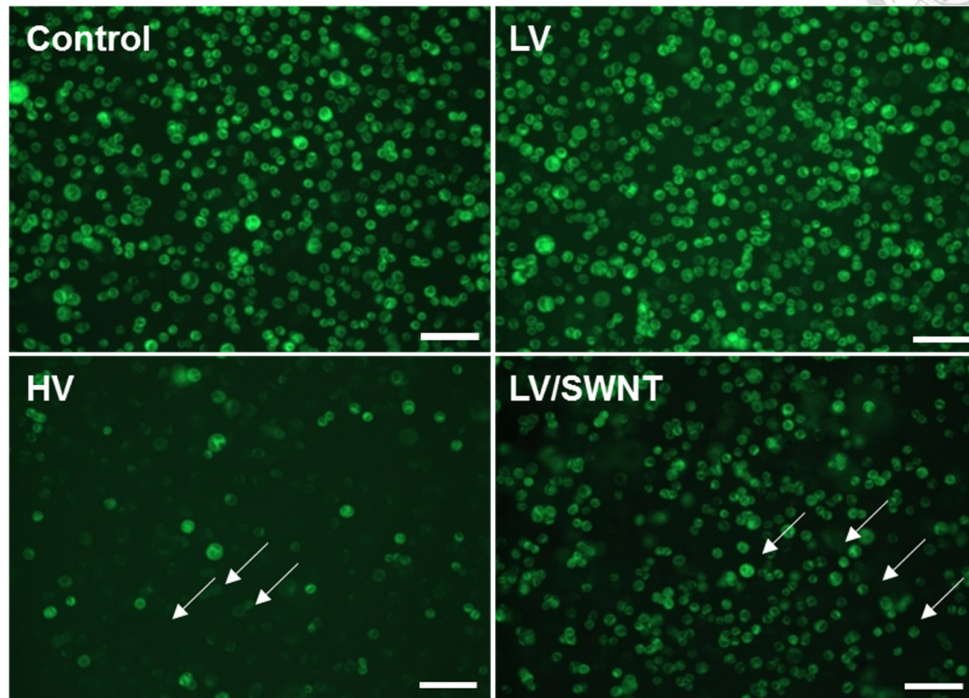
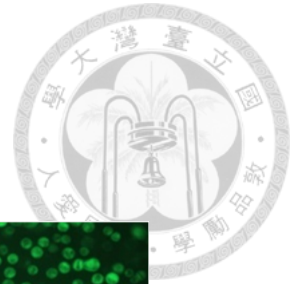


Fig. 35. Investigation of the transmembrane potential of HT-29 cells by the membrane potential probe. (A) Fluorescence images showed DIOC₆-highlighted changes in the membrane potential immediately after EP. White arrows showed the decrease in fluorescence intensity (scale bar = 50 μ m).

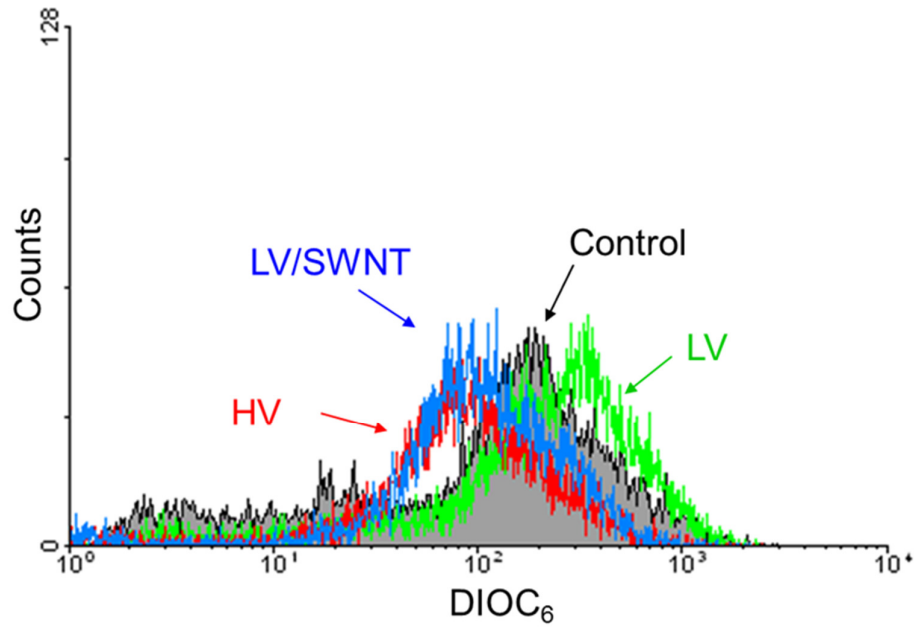


Fig. 36. Flow cytometry of HT-29 cells. Conditions were the same as in **Fig. 35**.

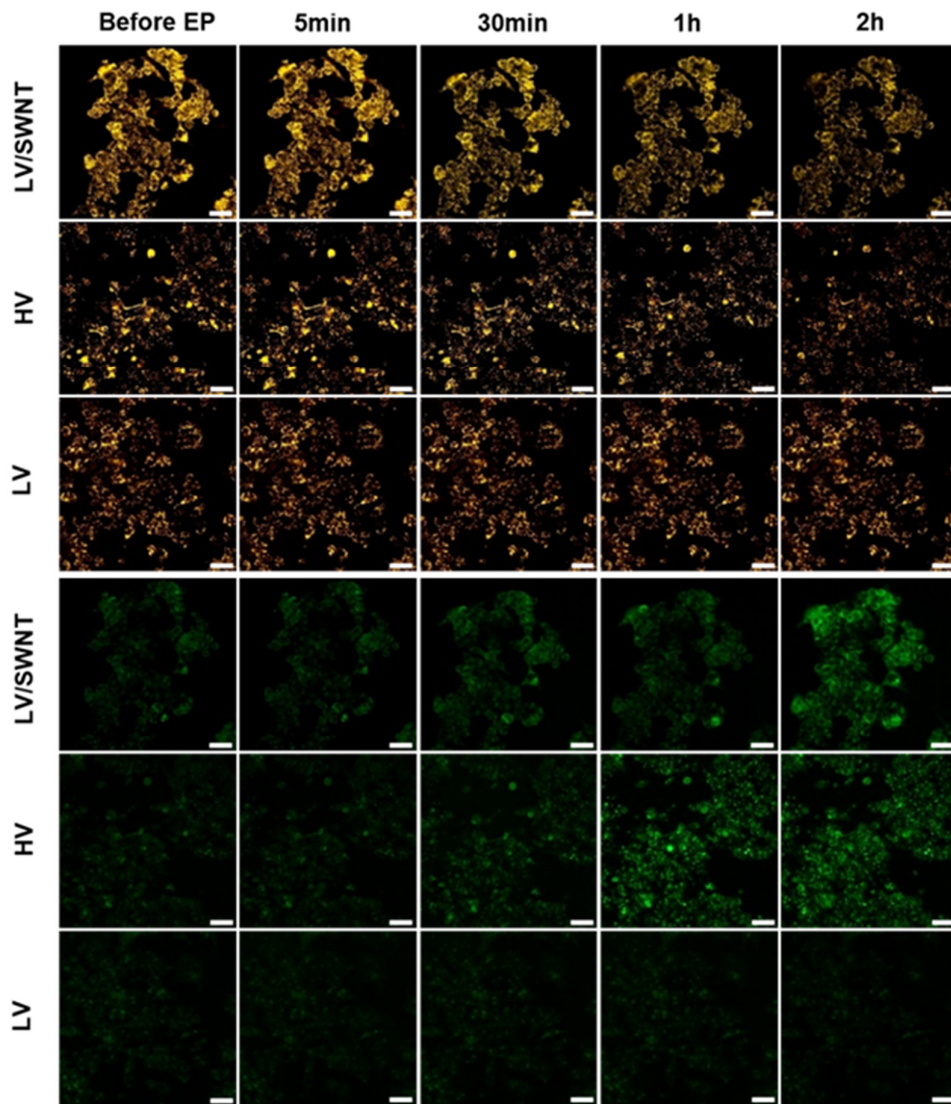
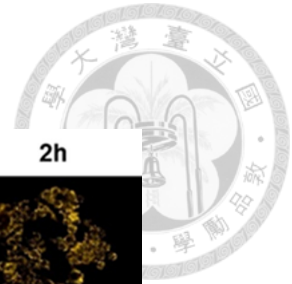


Fig. 37. Membrane potential monitored by JC-1 dye at 5, 30, 60, and 120 min after EP.

The results showed the same fields of view of cells, before and after electro-pulsation.

The loss of orange J-aggregate fluorescence and cytoplasmic diffusion of green monomer fluorescence occurred after the exposure of electro-stimulation in the HV and LV/SWNT groups (scale bar = 50 μm).

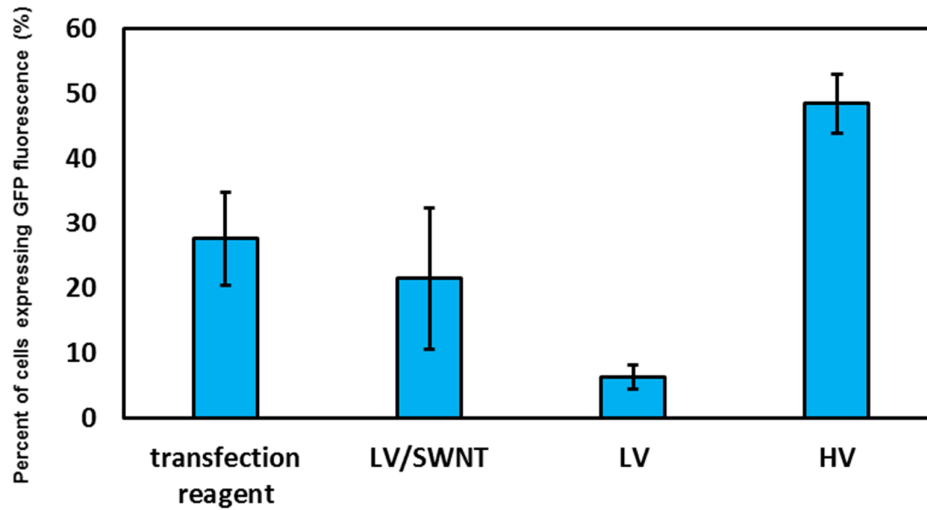


Fig. 38. HT-29 cells transfected with minicircle DNA encoding GFP by using transfection reagent or exposing to LV (50 V, 40 ms, 100 pulses) and HV (1600 V, 10 ms, 3 pulses) pulses. Histogram data analysis by flow cytometry showed the fluorescence intensity of GFP expressed in HT-29 cells at 48 h after transfection (SWNT pulsing buffer = LV/SWNT group, pulsing buffer without SWNT = HV and LV group).

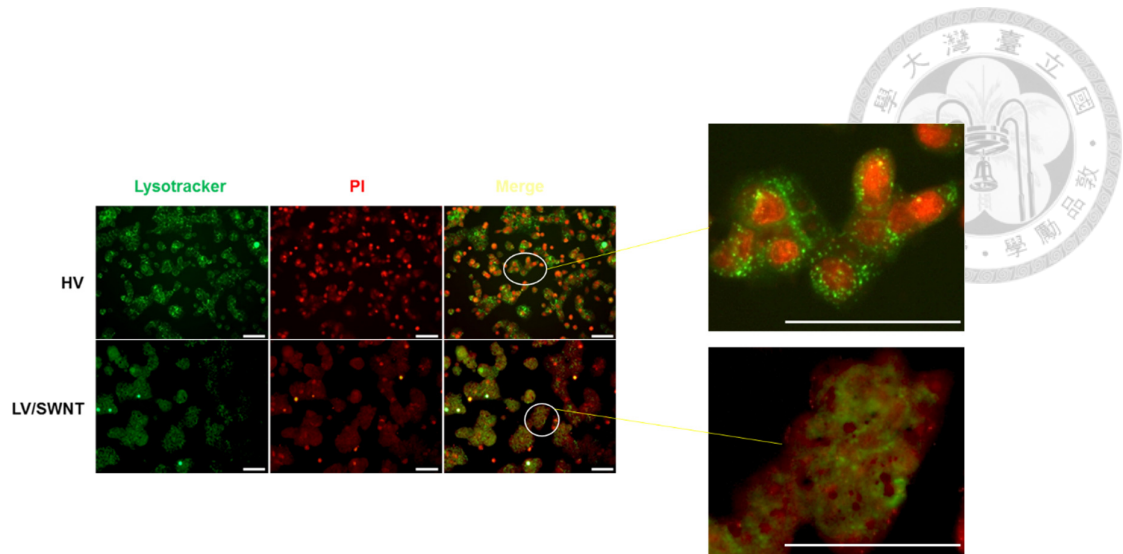


Fig. 39. PI dye transferred into cells at 3 h after EP. Fluorescence images: Lysotracker (green), PI (red), and Merge (yellow). High magnification showing the different modes of entrance of PI for HV compared with the LV/SWNT group (Scale bar = 100 μm).

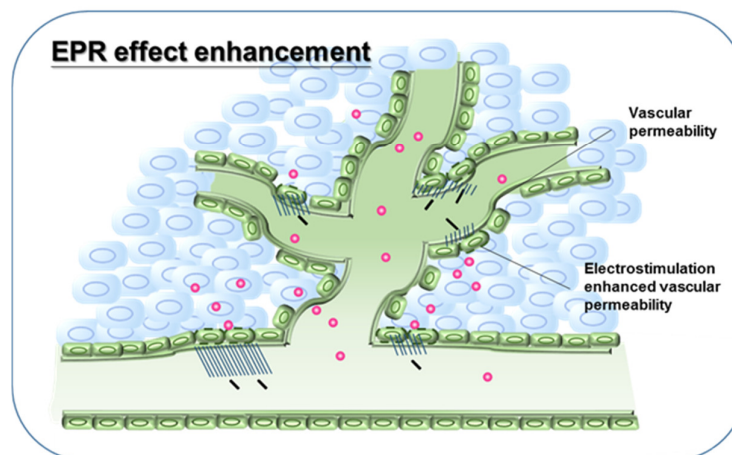
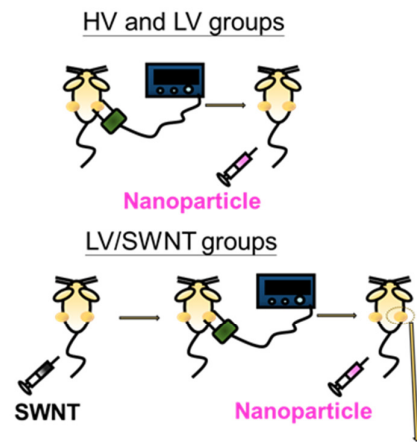


Fig. 40. EPR effect enhancement following low-intensity electric stimulation enlarged due to CNTs. The accumulation of nanoparticles in the tumor tissue occurred due to not only the original intercellular space between the endothelial cells but also the tumor vascular permeability increased by the electric stimulation effect.

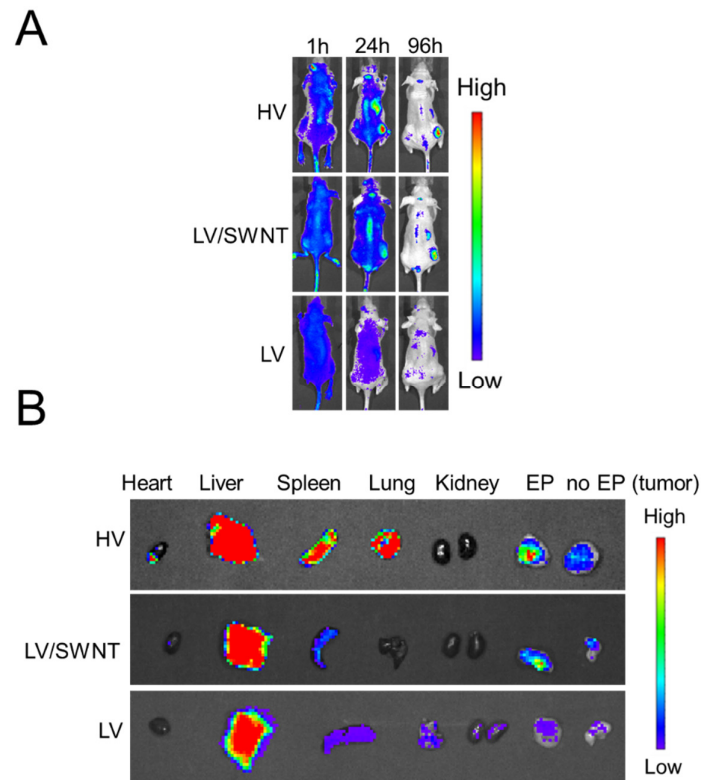


Fig. 41. (A) *In vivo* IVIS images of the mice bearing HT-29 tumors at 1, 24, and 96 h after injection with nanoparticles, respectively. Accumulation of nanoparticles in the tumors was different between the different EP conditions. The treatment methods demonstrated are from (A) (HV = 700 V, 20 ms, 3 pulses, LV = 50 V, 40 ms, 10 pulses). (B) *Ex vivo* imaging of nanoparticles in the heart, liver, spleen, lung, kidney, and tumor of mice at 96 h after the same treatments as in (A).

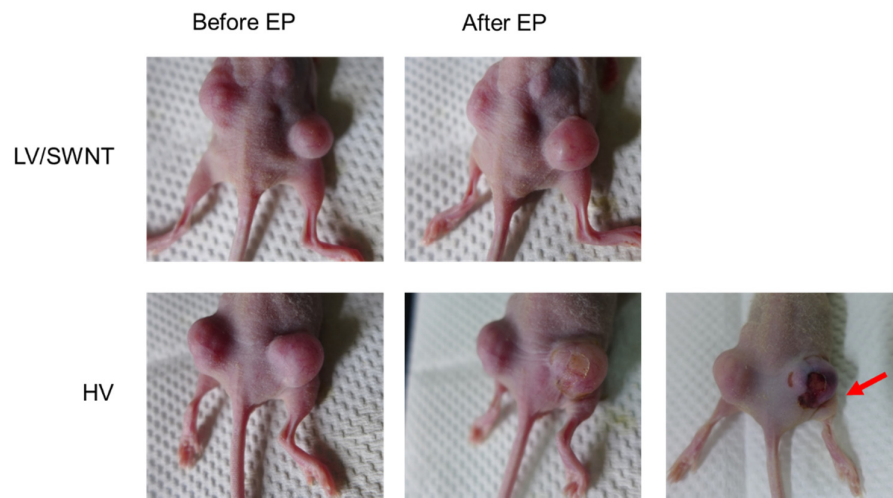


Fig. 42. Comparison of the tumor surface (right side tumor) after treating with different EP conditions. The mice with the SWNT post-injection treated with LV pulse stimulation (LV/SWNT) showed no harmful effect of the tumor. However, an obvious ablation was observed on the tumor treated with HV pulses (HV). (The red arrow indicated the tumor treated by HV after 1 h with severe blood stasis).

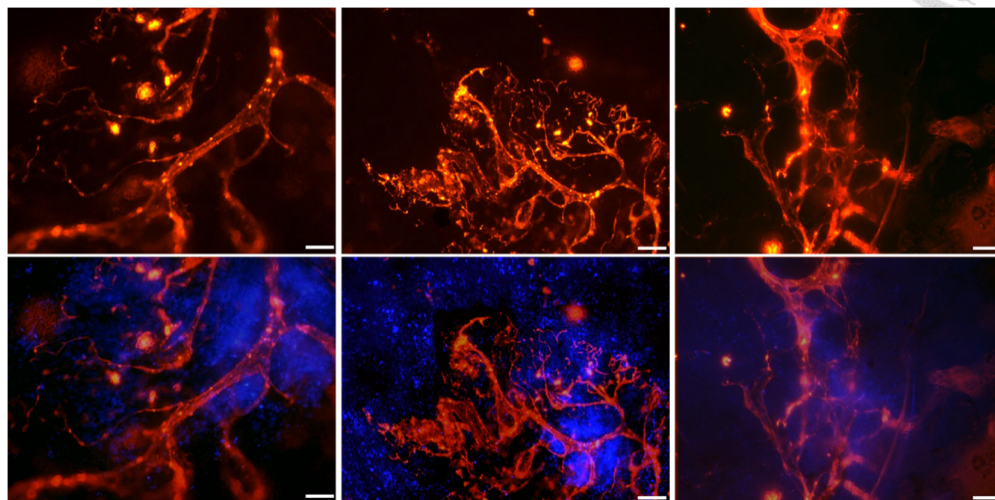


Fig. 43. Different regions of tumors were imaged using fluorescence microscopy for 10 min post-injection. Nanoparticles (red), tumor cells (Hoechst, blue). (Scale bar = 100 μm).

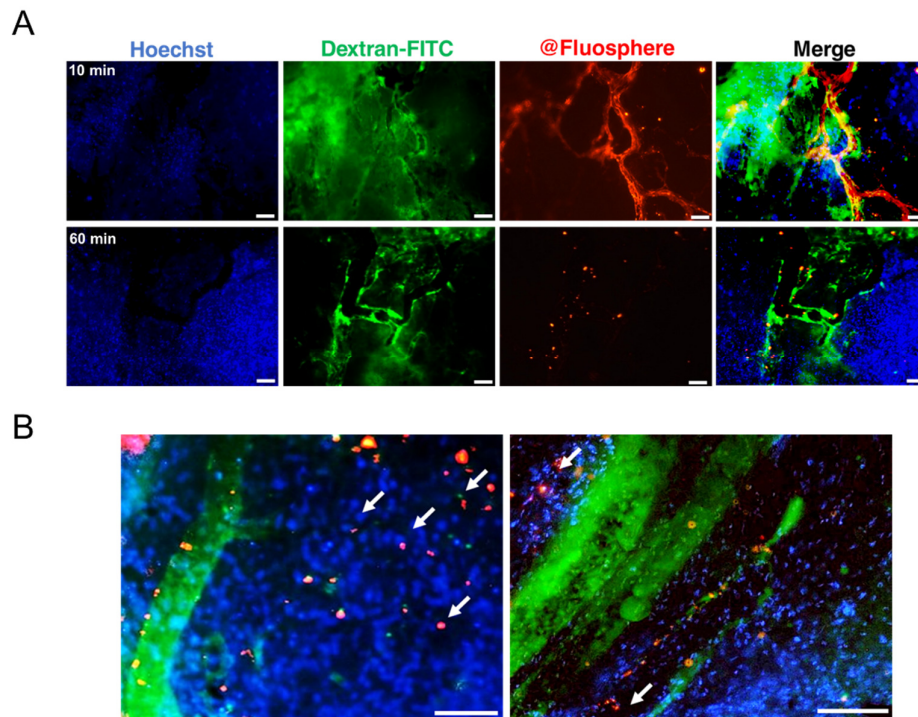
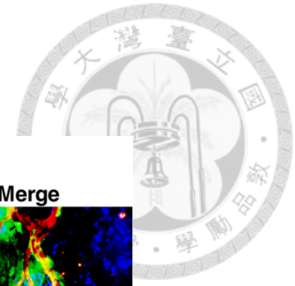


Fig. 44. (A) Typical intravital micrograph of tumors treated without electro-stimulation after injecting nanoparticles. The nanoparticles were completely filled inside the tumor vessels at 10 min after injection. At 60 min, the nanoparticles aggregated along the tumor vessels without obvious appearance in the tumor tissue. Tumor cells (blue), blood vessels (green), and nanoparticles (red) (scale bar = 100 μm). (B) Tumor treated with LV pulses after SWNT injection, followed by intravenous administration of nanoparticles. White arrows indicated the leakage of nanoparticles into the tumor interstitial tissue at 60 min after EP. Tumor cells (blue), blood vessels (green), and nanoparticles (red) (scale bar = 100 μm).

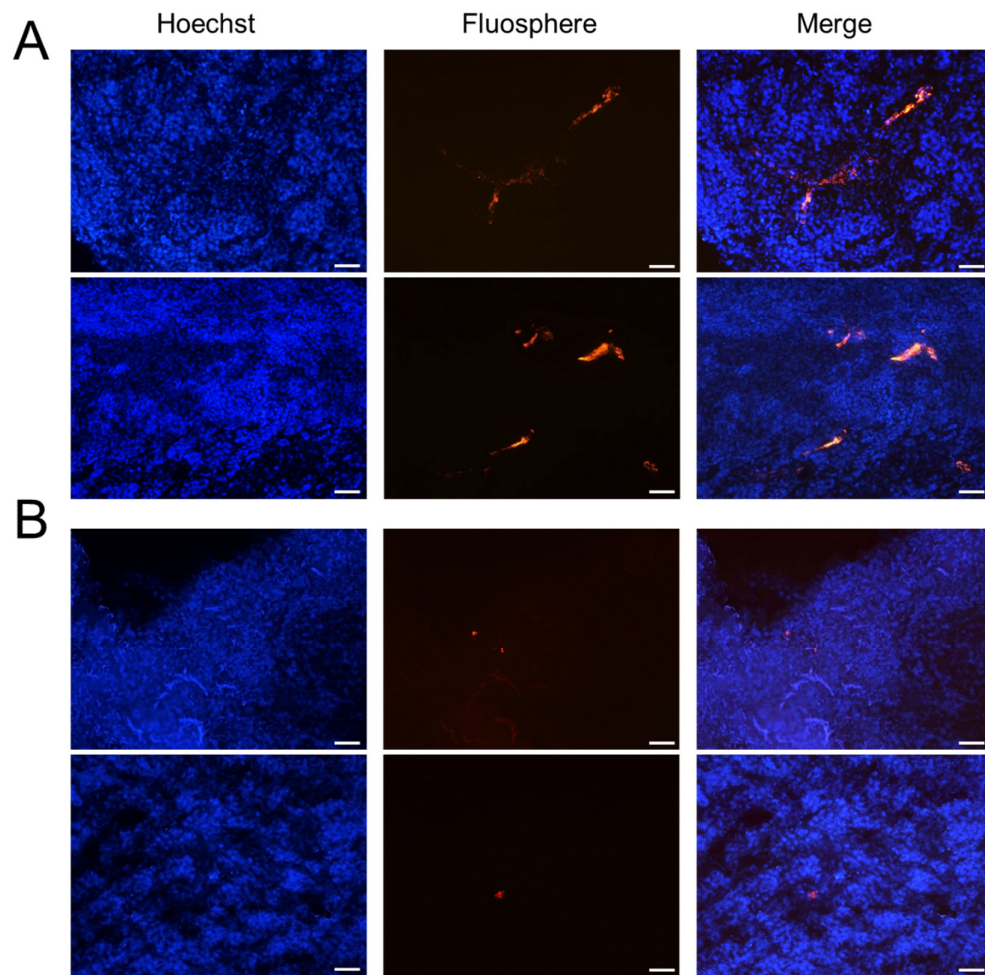
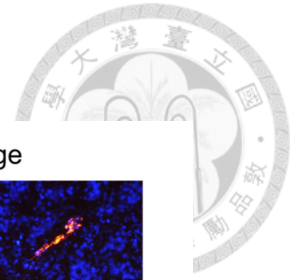


Fig. 45. Comparison of LV/SWNT with LV groups by enhancement of nanoparticle accumulation. Tumor sections were extracted at 3 h after administering nanoparticle injection. (A) The tumor treated with SWNT post-injection showed an apparent aggregation of nanoparticles in the tumor region. Nanoparticles (red), tumor cell (Hoechst, blue). (Scale bar = 50 μm). (B) The tumor treated without SWNT showed less aggregation of nanoparticles compared to (A). Nanoparticles (red), tumor cell (Hoechst, blue). (Scale bar = 50 μm).

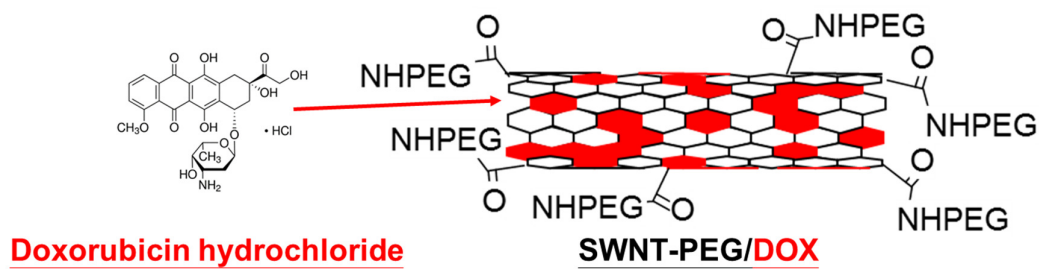
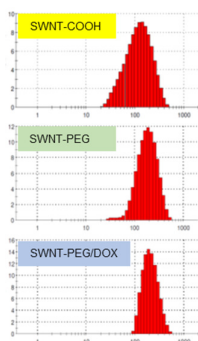
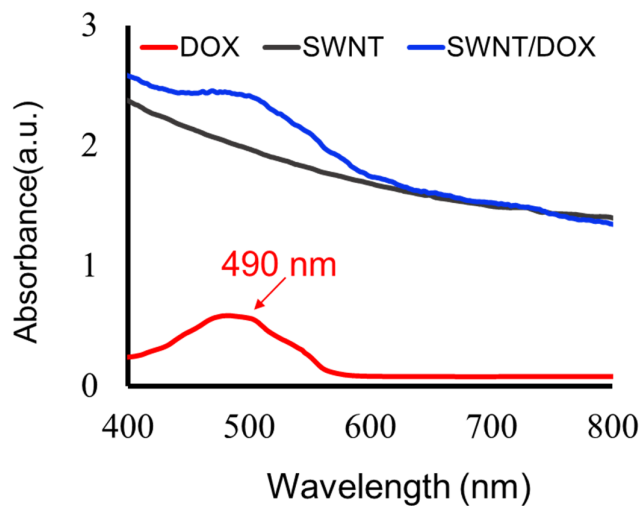


Fig. 46. SWNT-PEG was loaded with doxorubicin non-covalently by π - π stacking.



	Size (nm)	Zeta potential (mV)
SWNT-COOH	100.7	-49.4
SWNT-PEG	179.0	-31.7
SWNT-PEG/DOX	248.0	-12.6

Fig. 47. Particle size and zeta potential analyses of SWNT-COOH, SWNT-PEG, and SWNT/DOX by DLS. SWNT with much more modification showed a larger size. Zeta potentials of the SWNT showed that SWNT-PEG had negative charges. Loading DOX increased the zeta potentials of SWNT-PEG.



Ratio (W/W= 1:10) SWNT-PEG/DOX

DOX 75.2ug

SWNT 133.3ug

Loading efficiency 56.4%

* Loading efficiency = $\text{DOXug}/\text{SWNTug} * 100 \%$

Fig. 48. UV-visible absorbance spectra of SWNT/DOX (blue), DOX (red), and SWNT-PEG (black). The drug loading efficiency was 56.4%.

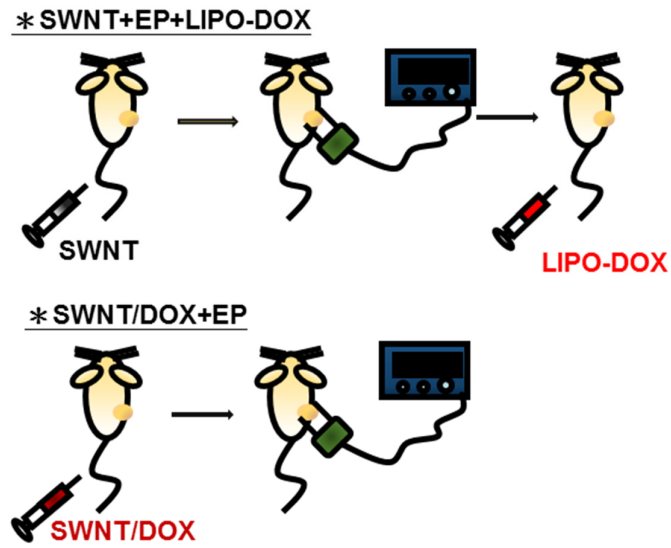


Fig. 49. SWNT combined with LV pulses for improving the tumor therapy efficacy by nanomedicine. Schematic representation of ECT in a HT-29 human colon cancer xenograft model.

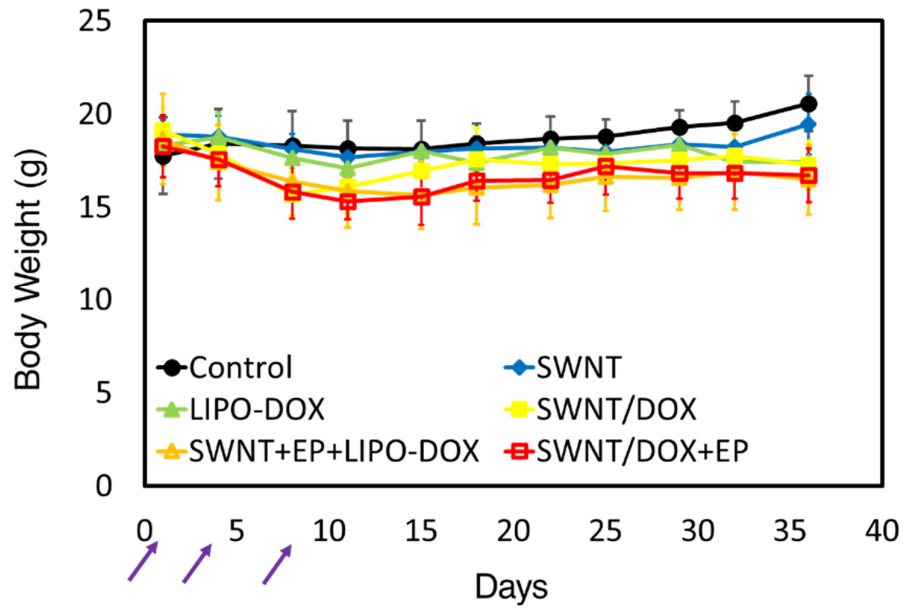


Fig. 50. Body weights of all the groups showed no notable changes.

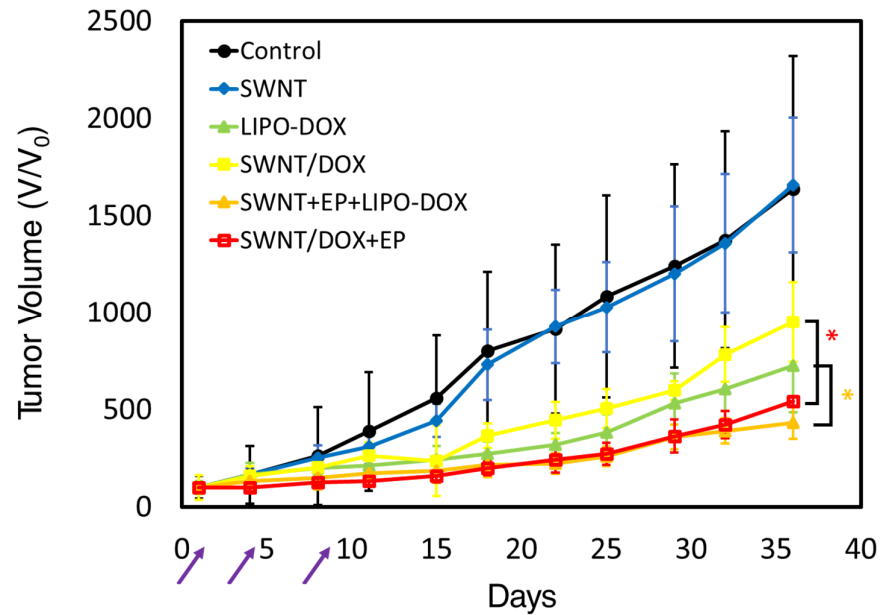


Fig. 51. Tumor volume ratio of HT-29-bearing mice among the various groups. Animals that received a combination of pulses and nanomedicine showed significant tumor growth suppression (SWNT/DOX + EP vs SWNT/DOX, $*p < 0.05$; SWNT + EP + LIPO-DOX vs LIPO-DOX, $*p < 0.05$).

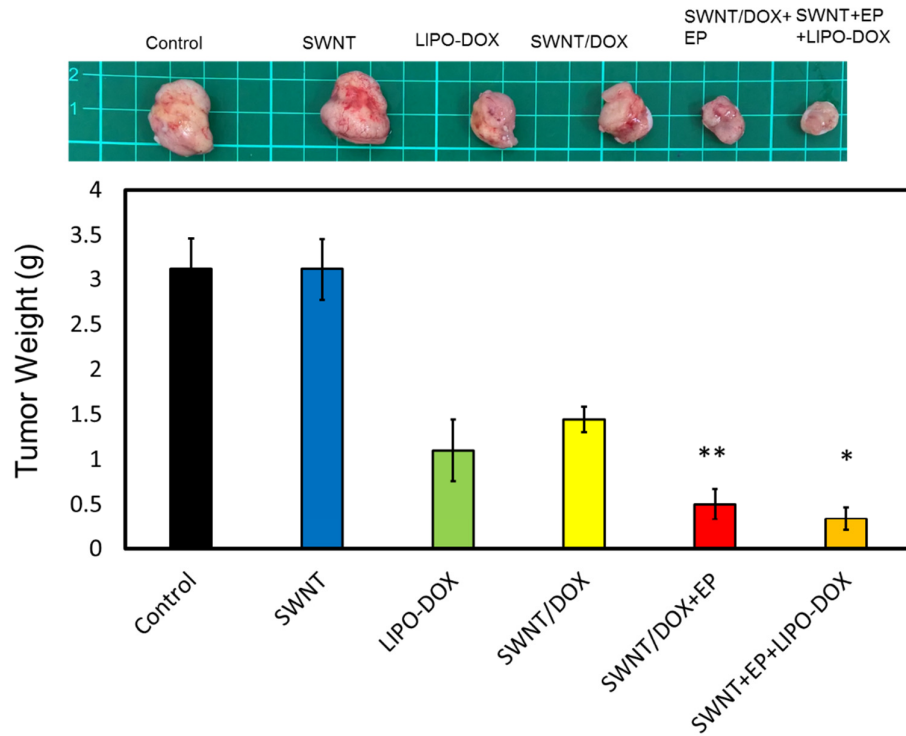


Fig. 52. Photographs of dissected tumors. Measurement of tumor weight for each group after 36 days. The effective EP combined with nanomedicine revealed a high reduction in the tumor weights (SWNT/DOX + EP vs SWNT/DOX, $**p < 0.01$; SWNT+ EP + LIPO-DOX vs LIPO-DOX, $*p < 0.05$).

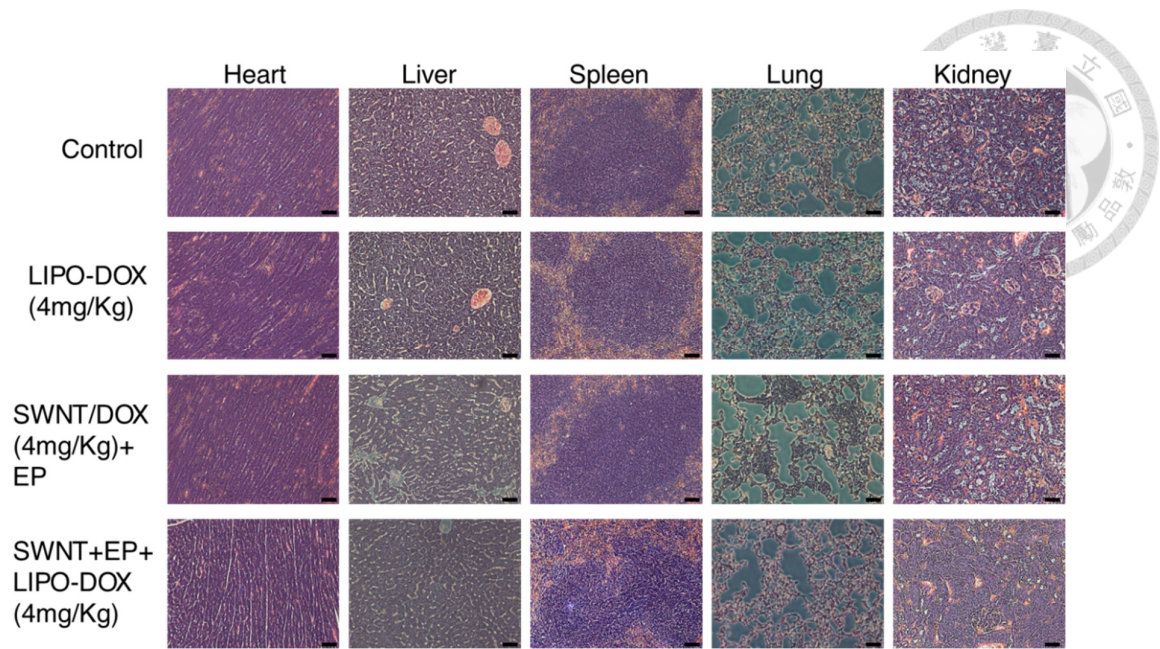


Fig. 53. Hematoxylin and eosin (H&E) staining of organs of HT-29 tumor xenograft-bearing mice treated with PBS (control), LIPO-DOX, SWNT/DOX, and SWNT + EP + LIPO-DOX. Scale bar = 50 μ m.

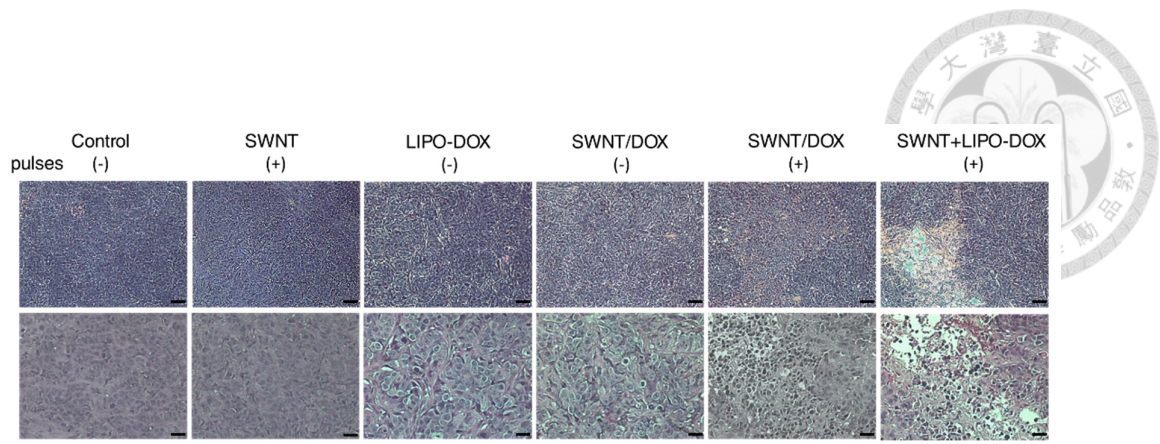


Fig. 54. H&E-stained images revealed severe damage in the tumor tissues of SWNT/DOX + EP and SWNT + EP + LIPO-DOX groups. No notable damage was observed in the PBS and SWNT + EP groups. Scale bar = 50 μm and 25 μm .

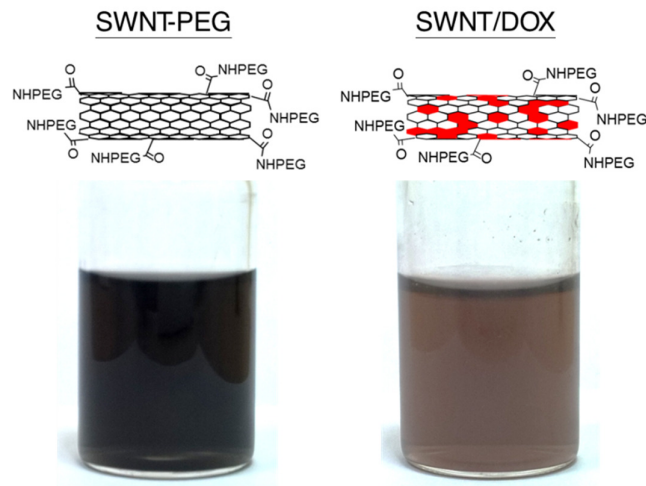


Fig. 55. Photograph of SWNT-PEG and SWNT/DOX suspended in PBS lasting for a month. The solutions were stored at 4°C.



Fig. 56. Images of livers extracted from mice at 1 and 8 weeks after injecting with PBS

(control), SWNT, and SWNT/DOX.

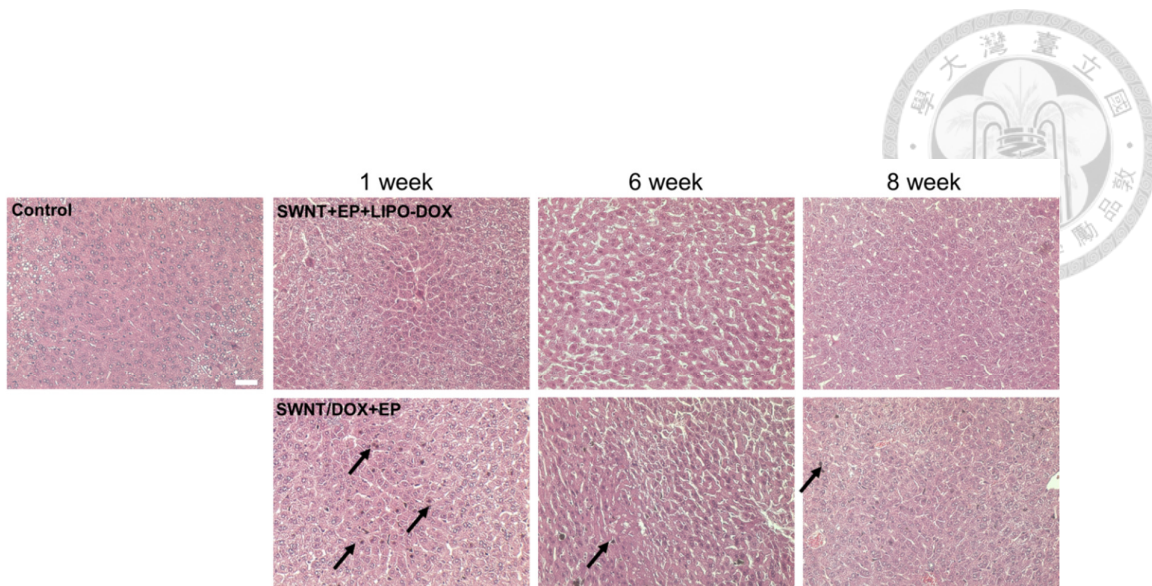


Fig. 57. Hematoxylin and eosin (H&E)–stained images of livers extracted from mice injected at 1, 6, and 8 weeks after injecting with PBS (control), SWNT, and SWNT/DOX.

Black arrows showed the aggregation of SWNT/DOX. Scale bar = 50 μ m.